THERMAL PERFORMANCE OF A NOVEL HEAT TRANSFER FLUID CONTAINING MULTIWALLED CARBON NANOTUBES AND MICROENCAPSULATED PHASE CHANGE MATERIALS

A Thesis

by

KALPANA TUMULURI

Submitted to the Office of Graduate Studies of
Texas A&M University
in partial fulfillment of the requirements for the degree of

MASTER OF SCIENCE

May 2010

Major Subject: Mechanical Engineering

THERMAL PERFORMANCE OF A NOVEL HEAT TRANSFER FLUID CONTAINING MULTIWALLED CARBON NANOTUBES AND MICROENCAPSULATED PHASE CHANGE MATERIALS

A Thesis

by

KALPANA TUMULURI

Submitted to the Office of Graduate Studies of
Texas A&M University
in partial fulfillment of the requirements for the degree of

MASTER OF SCIENCE

Approved by:

Chair of Committee,	Jorge L. Alvarado
Committee Members,	Yassin A Hassan
	Debjyoti Banerjee
	Hessam Taherian
Head of Department,	Dennis O'Neal

May 2010

Major Subject: Mechanical Engineering

ABSTRACT

Thermal Performance of a Novel Heat Transfer Fluid Containing Multiwalled Carbon Nanotubes and Microencapsulated Phase Change Materials.

(May 2010)

Kalpana Tumuluri, B.E., Osmania University

Chair of Advisory Committee: Dr. Jorge L. Alvarado

The present research work aims to develop a new heat transfer fluid by combining multiwalled carbon nanotubes (MWCNT) and microencapsulated phase change materials (MPCMs). Stable nanofluids have been prepared using different sizes of multiwalled carbon nanotubes and their properties like thermal conductivity and viscosity have been measured. Microencapsulated phase change material slurries containing microcapsules of octadecane have been purchased from Thies Technology Inc. Tests have been conducted to determine the durability and viscosity of the MPCM slurries. Heat transfer experiments have been conducted to determine the heat transfer coefficients and pressure drop of the MWCNT nanofluids and MPCM slurries under turbulent flow and constant heat flux conditions.

The MPCM slurry and the MWCNT nanofluid have been combined to form a new heat transfer fluid. Heat transfer tests have been conducted to determine the heat transfer coefficient and the pressure drop of the new fluid under turbulent flow and

constant heat flux conditions. The potential use of this fluid in convective heat transfer applications has also been discussed.

The heat transfer results of the MPCM slurry containing octadecane microcapsules was in good agreement with the published literature. The thermal conductivity enhancement obtained for MWCNTs with diameter (60-100 nm) and length (0.5-40μm) was 8.11%. The maximum percentage enhancement (compared to water) obtained in the heat transfer coefficient of the MWCNT nanofluid was in the range of 20-25%. The blend of MPCMs and MWCNTs was highly viscous and displayed a shear thinning behavior. Due to its high viscosity, the flow became laminar and the heat transfer performance was lowered. It was interesting to observe that the value of the maximum local heat transfer coefficient achieved in the case of the blend (laminar flow), was comparable to that obtained in the case of the MPCM slurry (turbulent flow). The pressure drop of the blend was lower than that of the MWCNT nanofluid.

DEDICATION

I dedicate my thesis to my loving parents and sister.

ACKNOWLEDGEMENTS

I would like to thank my advisor Dr. Jorge L. Alvarado for his constant guidance, help, and support extended to me for the entire duration of the research project. His constant encouragement and patient approach helped me complete this project successfully. I would like to thank him for giving me the opportunity to do this research project.

I would like to thank Dr. Hessam Taherian who gave me very valuable input during both experimental and analysis stages of the project. He has designed and built some of the equipment and instrumentation required for the successful completion of this project. I have learnt a lot of things from him and he has been a great source of inspiration to me.

I would like to thank my committee members, Dr. Debjyoti Banerjee and Dr. Yassin A. Hassan, for their support and co-operation during the course of this project.

I would like to thank my lab mates Mansuck Kim and Chan Hyun Park for their valuable time and help provided during the course of experiments. I would like to thank Guillermo Soriano for his help and guidance, particularly during the initial stages of the project. I would like to thank the entire staff at Energy Systems Laboratory, Riverside Campus, Texas A&M University for their help and support.

I would like to thank all my colleagues and friends who have helped me and supported me. Finally, I would like to thank my parents and my sister for their love and constant encouragement.

TABLE OF CONTENTS

CHAPTER Page

CHAPTER Page

LIST OF FIGURES

Page

Page

Page

Page

LIST OF TABLES

Page

CHAPTER I

INTRODUCTION

Heat transfer processes play a vital role in many industrial, biological and natural systems. Heat transfer processes come into play using the mechanisms of conduction, convection and radiation. Convective heat transfer has a huge application in processing and power industries, district cooling, HVAC, refrigeration and microelectronics cooling applications. The main objective in all the above applications is to maximize heat transfer with minimum input power and size of equipment. The choice of a heat transfer fluid and the system design are the key important factors that determine the realization of the above goal. Heat transfer enhancement can be obtained either by using an improved heat transfer fluid or by using enhanced surfaces in the equipment.

Enhanced surfaces such as fins and micro channels have been found to increase heat transfer rates significantly [1]. Enhanced surfaces increase the effective heat transfer area without increasing the overall volume of the equipment significantly. Increasing surface roughness or using specially treated surfaces is also another method of improving the heat transfer rate. Roughness can be introduced on the surface in the form of ridge like protrusions perpendicular to the fluid flow [2]. This can increase the

---

This thesis follows the style of ASME Journal of Heat Transfer.

convective mechanism and hence the heat transfer coefficient can be enhanced. Tube inserts and swirl flow devices are also useful for increasing the heat transfer rate as well. These devices are used under forced flow conditions and they increase the heat transfer rate by increasing the path length of the flow and by generating secondary flows inside the tube.

Though an enhancement in the heat transfer coefficient is obtained using the above mentioned techniques, it is usually obtained at the expense of increasing pressure drop which implies higher input pumping power and thus higher operational costs. Thus the other alternative of using improved heat transfer fluids to obtain enhanced heat transfer rates is gaining more importance day by day.

Commonly used heat transfer fluids are water, glycol water mixtures, poly alkylene glycols, hydrocarbon oils, refrigerants (phase change fluids) and silicones. Though a variety of heat transfer fluids are available today that can cater to the needs of the industry, problems like limited heat transfer, high pressure drop, limited temperature range, safety and suitability for a specific application still persist. This forms the motivation factor for research in improving existing heat transfer fluids. An improved heat transfer fluid should be able to carry and transfer greater amounts of heat effectively, without causing a significant increase in pumping power. The nature of the fluid in terms of its stability, operating temperature range and safety is equally important for its use in commercial applications.

Before we delve into the techniques for improving heat transfer fluids, some of the desirable characteristics of a heat transfer fluid are summarized as follows: a) High

heat transfer coefficient – provides greater heat transfer through the process of convection; b) High heat capacity - enables more heat to be carried across c) High thermal conductivity - provides higher heat transfer rate across the surfaces in heat exchangers and pipes; d) Low viscosity – Requires less pumping power which means operational costs are lowered; e) Non toxic and chemically inert – enables the fluid to be used in a wider range of applications like food processing and refrigeration, and eliminates the need for specially designed equipment and piping, which in turn lowers the total cost; f) The fluid should be stable.

There are several ways in which one can improve the heat transfer characteristics of a fluid. The following techniques describe some of the ways to improve a fluid's heat transfer characteristics by enhancing any one or a combination of the above mentioned properties.

Increase in thermal conductivity

This can be achieved by suspending solid (nano) particles of metals and other highly thermally conductive materials in fluids. Suspending solids of high thermal conductivity in liquids is expected to improve the thermal conductivity of the base fluid. This concept is not new and has been in use for more than a century. Different kinds of particles have been used to increase the thermal conductivity of the base fluid. But the problem in their usage was the size of the particles being used. Initially, micrometer sized particles were used that caused problems like clogging in pipes and heat

exchangers, adverse effect of the particles on the surfaces like erosion, settling out of the particles from the suspensions and increase in pressure drop [3].

In the early nineties at Argonne national lab, Dr. Choi's team [4] developed the novel concept of nanofluids. These nanofluids were formed by dispersing nanometer sized particles in conventional heat transfer fluids. Since the size of the particles was 1000 times lesser than the particles used previously, problems of clogging and erosion were minimized. Also, since the surface areas to volume ratios were higher in the case of nanofluids, they were expected to display higher thermal conductivities [4]. Stability and lower pressure drop were additional attractive features of nanofluids. Active research has been taking place since then to develop new nanofluids with improved thermal conductivity values.

Different kinds of nanofluids have been developed using different kinds of nanoparticles and base fluids. The base fluids tested were water, ethylene glycol, epoxy, transformer oil, engine oil and toluene [5]. Different kinds of nanoparticles like ceramic, metallic and carbon nanotubes have been tested. Ceramic particles include Al_2O_3, CuO, TiO_2, SiC, and SiO_2, the metallic particles include Cu, Fe, Au and Ag and in the area of carbon nanotubes, single walled double walled and multiwalled carbon nanotubes have been tested [6]. The concentrations of the particles were also varied from 0.3 to 5% by volume fraction. The thermal conductivity enhancement obtained from the nanofluids ranged from less than 10% to values greater than 100 %; however, results to date indicate that such thermal conductivity enhancements are unreasonable and not fully understood when considering current physical models [7]. There are many parameters to

be taken into account before we can compare the results of different researchers. The type and size of the nanoparticles, the base fluid being used, the surfactants or dispersants used, the processing technique (i.e. ultrasonication), ultrasonication time involved (if ultrasonication was used), and the type of methods used to measure thermal conductivity are some of the important factors that influence the thermal conductivity values [7-9].

Many results have been published so far reporting anomalous increases in thermal conductivities of the nanofluids (when compared to that of the base fluid) [5-6], although a recent research by a team at MIT disproves the fact that nanofluids can actually have higher thermal conductivities than predicted by theory [7]. There are several challenges being encountered in the development of nanofluids. Initially, nanofluids containing spherical nanoparticles (i.e. alumina) were prepared in our laboratory using micro fluidization and ultrasonication to disperse nanoparticles and avoid the formation of nano clusters (i.e. 260 nm). Both methods resulted in the formation of nanofluid with poor thermal performance indicating that nano clusters were still present in the fluid (i.e. 125 nm). Therefore, nanofluids were made with multiwalled carbon nanotubes. Both experimental and computational research were undertaken extensively to understand and overcome the problems faced in the development and use of nanofluids in heat transfer including nanofluid stability and repeatability of the published results.

Increase in heat capacity

The heat capacity or the amount of heat that a fluid can carry is dependent on the specific heat of the fluid in single-phase flow heating. Higher the specific heat, higher is the amount of heat that can be carried away by the fluid. One can improve the heat transfer rate by making a substance undergo phase change during heat transfer. During the process of phase transformation, temperature does not increase and the fluid can absorb heat equivalent to its latent heat capacity, thus enhancing the heat capacity.

Refrigerants make use of this concept in air conditioning and refrigeration applications. But the operating temperature range is quite low and they would not be suitable for medium to high temperature ranges normally found in industrial processes. Furthermore, the risk of dry-out spot in certain heat transfer applications requires a constant wetting of all heat transfer surfaces. Instead of making heat transfer fluids undergo phase change, it is more practical in many applications to add phase change materials to the heat transfer fluid. These phase change materials can be chosen appropriately to match the temperature range and nature of the bulk fluid. These phase change materials can be made to undergo phase change (solid to liquid) in the operating conditions, resulting in enhancements in heat capacity and local heat transfer rates as well as making sure all heat transfer areas remain wet.

There are different types of phase change materials like organic ones which include paraffins and fatty acids, and salt hydrates which are inorganic and eutectic materials which are compounds of organic and inorganic substances [10]. The selection of appropriate phase change materials depends on factors like melting point, latent heat

of fusion, volume changes on phase transformation, no super cooling behavior and chemical stability. Other factors like non toxic nature, low cost and large scale availability are essential for the phase change materials to be used in commercial applications.

Phase change materials have been in use for quite some time now, but their use has been limited due to problems such as clogging and stickiness in pipes and heat exchangers. To overcome these problems, microencapsulated phase change materials have been developed. In these types of materials, the phase change material is separated from the bulk fluid by encapsulation of the phase change material in small capsules which then prevents clogging and stickiness. The phase change material inside the capsule is referred to as the core and the wall of the capsule is called the shell. A suspension of MPCMs (microencapsulated phase change materials) in a carrier fluid is referred to as MPCM slurry. There are still major challenges involved in the making of MPCMs, like making durable capsules that can withstand several pumping cycles and prevention of the super cooling phenomena [1, 11]. Super cooling phenomena can be successfully suppressed by the use of adequate nucleating agents [11].

Many researchers have proposed MPCM slurries as heat transfer fluids due to an increase in heat capacity [1, 12]. The heat transfer coefficient also increases when the phase change process takes place. One of the important factors affecting the heat transfer performance of MPCM slurries is the flow regime in which the fluid operates [12]. Turbulent flows are more beneficial for increased heat transfer rates, though the associated pressure drop is higher. The MPCM concentration is also an important factor

that determines the increase in heat transfer rate [1, 12, 13]. Heat transfer of MPCM slurries using enhanced surfaces was also investigated [1] and was found to be beneficial at low mass fractions.

The present research work aims to combine the benefits of nanofluids and MPCM slurries by developing a novel heat transfer fluid using both multiwalled carbon nanotubes and MPCMs, and test it as a heat transfer fluid. De-ionized water was used as the base fluid and multiwalled carbon nanotubes and MPCMs were added to it. Different types of carbon nanotubes and MPCMs were tested for determining the right type and concentration of each constituent for the proposed fluid. Heat transfer experiments were conducted to determine the heat transfer coefficient and pressure drop for the proposed fluid under constant heat flux and turbulent flow conditions.

CHAPTER II

THESIS OBJECTIVES AND PROPOSED APPROACH

The main aim of this thesis work was to determine the feasibility of combining MPCMs (Microencapsulated phase change materials) and multiwalled carbon nanotubes (MWCNTs) in de-ionized water and to experimentally examine the heat transfer potential of the developed fluid. To meet these overall objectives, there are several sub-tasks or objectives that needed to be completed. These objectives are summarized below.

1. Microencapsulated phase change materials (MPCMs)
    a. Microencapsulated phase change materials should be prepared by Thies Technology Inc. and tested for durability and super cooling behavior. Different batches needed to be tested, and the best batch in terms of durability of the microcapsules, and with the minimum level of super cooling should be identified.
    b. Viscosity measurements and heat transfer experiments for the best batch identified in step (a) should be conducted. A heat transfer loop was assembled at the Energy Systems Laboratory (ESL) at the Riverside Campus of Texas A&M University where durability and heat transfer tests were conducted. The loop was calibrated using DI water to ensure accurate results with other heat transfer fluids. Viscosity tests were conducted at different temperatures and shear rates using a Brookfield's

rotary viscometer. An air-cooled chiller will be used to obtain different temperatures for the fluid.

2. Multiwalled carbon nanotubes (MWCNTs)

    a. Different sizes of MWCNTs should be purchased from Helix Materials Solutions. MWCNTs of different diameters and lengths should be tested for.

    b. Nanofluids should be prepared by dispersing multiwalled carbon nanotubes in de-ionized water using gum Arabic as dispersant (surfactant). Ultrasonication was used to prepare well dispersed and homogeneous nanofluid samples. Different samples were prepared using different periods of ultrasonication time to study the effect of ultrasonication time on thermal conductivity enhancement. All the samples were tested for stability.

    c. Thermal conductivity of the MWCNT-based nanofluids should be measured at different temperatures using a transient hot wire apparatus.

    d. Viscosity and heat transfer tests should be conducted to determine the best type of MWCNTs in terms of thermal conductivity enhancement, heat transfer coefficient increase, stability and pressure drop. An ultrasonic probe was used to make well dispersed and homogeneous nanofluids. A transient hot wire apparatus was used for measuring thermal conductivity of the prepared nanofluids at different temperatures.

Viscosity and heat transfer tests were conducted using the same apparatus that was used in the case of MPCMs.

3. Development of the heat transfer fluid
    a. A blend of MPCM and MWCNT was made with the objective of making and testing a fluid with estimated high thermal conductivity and heat capacity. The best batch of MPCMs and MWCNTs identified in steps 1 and 2 were combined with de ionized water in appropriate concentrations to form the proposed heat transfer fluid.
    b. Viscosity data was obtained using a rotary-type viscometer.
    c. Heat transfer tests were conducted to determine the heat transfer coefficient and pressure drop of the fluid under constant heat flux and turbulent flow conditions.
4. Examination of the heat transfer potential of the developed fluid
    a. The heat transfer experiment results obtained are discussed in detail to examine the potential of the proposed heat transfer fluid.

CHAPTER III

LITERATURE REVIEW

There has been little research done in the past on the potential use of microencapsulated phase change materials and carbon nanotubes in heat transfer. While the microencapsulated phase change materials (MPCMs) have shown to improve the heat capacity of the base fluid, carbon nanotubes (CNTs) have been found to be useful in enhancing the thermal conductivity of the base fluid. Although the degree of enhancement in thermal conductivity continues to be a matter of contention among different research groups, research on potential benefits of CNTs continues to be conducted. There has been basically very little research conducted on the combined benefits of MPCMs and CNTs. There is no literature available on heat transfer fluids which contain both MPCMs and MWCNTs.

The literature review in this chapter is divided into three parts. 1) Microencapsulated phase change materials. 2) Multiwalled carbon nanofluids. 3) Blend of MPCMs and MWCNTs. The main aspects that will be discussed with respect to MPCMs are durability, super cooling, viscosity, pressure drop and the heat transfer performance of MPCM slurries. Though literature available on nanofluids is large and varied, only those aspects relevant to the use of multiwalled carbon nanotubes in the present research project are discussed. Thermal conductivity, viscosity, pressure drop and heat transfer performance of aqueous multiwalled carbon nanotube fluids are

discussed. Results of an international nanofluid property benchmark exercise, conducted by 34 organizations around the world are also discussed. Only two papers have been found in the literature that discuss about the blends of MPCMs and nanoparticles. They are discussed in the third part of the chapter.

Microencapsulated phase change materials

Yamagishi et al. [12] conducted heat transfer experiments on MPCM slurries containing microencapsulated octadecane. The microcapsules varied in size between 2 and 10 μm, and were suspended in pure water. An anionic surfactant of less than 1 wt. % was added to the slurry. Newtonian behavior was exhibited by the slurries containing up to 30% of MPCMs by weight. The relative viscosity of the slurries remained constant with temperature. When particle volume fractions were increased, the slurry flow structure changed from turbulent to laminar. Pressure drop of MPCM slurries increased with increase in velocity and particle volume fraction. The pressure drop of the MPCM slurry (30% conc. by wt) was less than that of water under similar conditions.

Heat transfer experiments were conducted in a circular tube under constant heat flux and turbulent flow conditions. Increase in local heat transfer coefficients at bulk fluid temperatures equal to the melting point of octadecane was attributed to the phase change of MPCMs. Local heat transfer coefficient decreased with increase in heating rate, other conditions being same. For cases with same Reynolds number, slurries with a higher concentration of MPCMs had a higher maximum value of local heat transfer coefficient. But in cases with similar velocities, higher particle volume fractions reduced

the maximum value of local heat transfer coefficient obtained. Incomplete melting of solid MPCMs happened in the case where the flow structure changed into laminar flow. For similar particle volume fractions in laminar and turbulent flow, heat transfer in turbulent flow was found to be more effective than in laminar flow.

Mulligan et al. [13] conducted research on different types of microencapsulated paraffins slurried with both water as well as silicone oil. The microcapsule sizes varied between 10 and 30 μm. Different kinds of phase change materials were studied which included n-octadecane, n-eicosane, n-heptadecane and n-nonadecane. The capsules were made of 83% core material and 17% wall material. The wall was constructed of polymer material by phase separation techniques. Each type of phase change material had its own set of optimum operating condition in which maximum phase change was observed. This depended on the melting point of the MPCMs, heating and flow rates. The effective specific heat affected the fluid Prandtl number which indirectly influenced the entry region effect and the suspension heat transfer coefficient. Though effective specific heat improved even with a small amount of PCM, the full improvement was seen only at concentrations 25% or above. Heat transfer coefficients improved significantly at higher concentrations but not much at lower concentrations.

Alvarado et al. [1] determined the thermal performance of microencapsulated phase change material slurries containing n-tetradecane. The MPCMs used in this study were made by microencapsulating 99% n-tetradecane with gelatin through the process of coacervation. The diameter of the capsules was in the range of 2-260 μm. After several

tests, it was found that MPCMs made of 94% tetradecane and 6% tetradecanol with a capsule size of 4.4 μm had minimum super cooling and better durability characteristics.

Viscosity results of the MPCM slurry at different temperatures and shear rates confirmed the Newtonian fluid behavior of the slurry at least up to concentrations of 17.7%. Relative viscosity of the MPCM slurry was independent of temperature. . Pressure drop of MPCM slurries increased slightly when compared to that of water, but not high enough to affect pumping power. Thermal capacity enhancement of 40% was obtained with MPCM slurry (7% conc. by wt). At higher mass fractions experimental heat capacity enhancement increased to 70%.

An increase in local heat transfer coefficient was observed when the bulk fluid temperature reached the melting point of tetradecane. Heat transfer coefficient increased with increase in fluid velocity because of greater momentum transfer. Though the local transfer coefficients showed an increase during phase change, the absolute values were still lesser than that of water under similar conditions of heat flux and flow rates. At lower mass fractions, the ratio of heat transfer coefficients of MPCM slurry to that of water was 0.6 whereas at higher mass fractions, it decreased to 0.4 suggesting lower turbulence at higher mass fractions. Enhanced tubing was found to be more beneficial at lower mass fractions. Increase in flow rate had a more significant impact on the percentage of particles undergoing phase change rather than an increase in heat flux value.

Zeng et al [14] adopted experimental and numerical methods to analyze the forced convective heat transfer of MPCM slurry in laminar flow in a circular tube under

constant heat flux conditions. The core of MPCMs was 1-bromohexadecane while the shell was made of amino plastics. The average diameter of particles was 8.2 μm. A 6% thermal conductivity enhancement was obtained when the MPCMs were dispersed in water and had no phase change. An enthalpy model was developed to simulate the forced convective heat. Stephan number and dimensionless phase change temperature range are two important parameters that influenced the Nu fluctuation profile and the dimensionless wall temperature increase in the phase change region. Volume concentration, particle diameter, and Reynolds number affected the local heat transfer coefficient enhancement profile.

Roy and Avanic [15] developed an effective specific heat capacity model for turbulent heat transfer in PCM suspensions in a circular tube with constant wall heat flux. The results showed that the bulk Stefan number, the non dimensional melt temperature range and degree of sub cooling are three most important parameters. Considerable reductions of wall temperatures of the order of 50% or more were obtained at low to moderate Stefan numbers. In cases where high wall heat fluxes were present, Ste and degree of sub cooling determined the location of phase change.

Goel et al. [16] investigated the heat transfer characteristics of n-eicosane microcapsules in water for laminar flows in a circular duct with constant wall heat flux. The wall of the capsule was made of amino formaldehyde resin. The important parameters in the study were bulk Stephan number and volumetric concentration. Phase change material suspensions were found to reduce the wall temperatures by 50% in comparison to single phase heat transfer fluids. Increase in particle diameter by a factor

of 2.5 reduced the wall temperature rise by 15%. Another important factor that affected the heat transfer characteristics was the initial subcooling of the incoming liquid.

Zhang et al. [17] analyzed the convective heat transfer mechanism of MPCM slurries based on the analogy between convective heat transfer and conduction heat transfer with thermal sources. Laminar flow in a circular tube with constant wall temperature was analyzed using an effective specific heat capacity model.

Inaba et al. [18] obtained the heat transfer characteristics of plural microencapsulated phase change material slurry containing different sizes of MPCMs in a circular tube under constant heat flux conditions. Both laminar and turbulent flows were investigated experimentally. Microcapsules of n-docosane of size 17 μm were combined with capsules of n-tetradecane of size 1.5 μm. Concentration of particles was 20%. In the turbulent flow region the friction factor of plural MPCM slurry was found to be lower than that of water due to drag reducing effects. The heat transfer coefficient was increased by both the effects of latent heat evolved during phase change and due to micro convection around plural microcapsules with different diameters. Experimental results showed a 2 to 2.8 times increase of heat transfer coefficient when compared to that of water.

Multiwalled carbon nanotubes

Assael et al. [19] investigated the thermal conductivity enhancement in MWCNT nanofluids prepared using sodium dodecyl sulfate (SDS) as a dispersant. It was concluded that SDS interacted with the carbon nanotubes and changed only the outer

structure while preserving the basic structure of nanotubes. The maximum thermal conductivity enhancement was 38%. Increasing the amount of ultrasonication time reduced the thermal conductivity enhancement in MWCNT nanofluids. Increase in ultrasonication time broke the CNTs length wise. Thus the length of carbon nanotubes or the length to diameter ratio of MWCNTs was an important parameter that affected the thermal conductivity enhancement in MWCNT nanofluids.

Wen and Ding [9] conducted thermal conductivity experiments on aqueous MWCNT nanofluids. Thermal conductivity enhancement was found to increase with increase in particle concentration and temperature. At 0.84% concentration, the maximum enhancement at 20 ℃ was 23.7% and at 30°C was 31%. The dependence of normalized thermal conductivity on CNT concentration was found to be non linear even at low concentrations. This was a major difference from the results for metal/metal oxide nanofluids. The temperature dependence of thermal conductivity was approximately linear at lower temperatures (< 30°C) and the dependence tended to level off at higher temperatures. De stabilization of the dispersant at higher temperatures (70 ℃) was observed.

Xie et al.[20] measured thermal conductivities of different nanofluids containing multiwalled carbon nanotubes. The base fluids used were DI water, ethylene glycol and decene. For nanofluids with base fluid as DI water, the maximum enhancement in thermal conductivity obtained was around 7% for 1% concentration by volume of MWCNTs. The thermal conductivity increased linearly with increase in the concentration of MWCNTs. The thermal conductivity enhancement reduced with an

increase in the thermal conductivity of the base fluid. The thermal conductivity enhancement was larger when compared to that of alumina nanoparticle suspensions at the same volume fraction. A mechanism based on liquid layering was proposed to explain the thermal conductivity enhancement obtained.

Paritosh et al.[8] measured the thermal conductivity, viscosity and heat transfer coefficient (under laminar flow conditions) of MWCNTs dispersed in de-ionized water. Gum Arabic was used as the dispersant. TEM imaging results showed that the length of nanotubes reduced with increase in ultrasonication time. The viscosity experiments conducted on the nanofluids showed a shear thinning behavior that was explained by the possible de-agglomeration of the bundled carbon nanotubes. A maximum of 20% increase in thermal conductivity was obtained at 35 °C.

Convective heat transfer tests were conducted for the prepared nanofluids under laminar conditions. Maximum enhancement of heat transfer coefficient was found for sample B and the increase was 32% at Re ~600. Convective effects in the radial direction were proposed as one of the mechanisms to explain the enhancement in heat transfer coefficient. Non Newtonian behavior of CNT fluids was proposed to be another major factor behind heat transfer enhancement as compared to thermal conductivity enhancement.

Ding et al. [21] measured the heat transfer performance of aqueous CNT nanofluids. Effective thermal conductivity of the nanofluid increased with increasing temperature and concentration. The maximum enhancement in thermal conductivity was 80% at 30 °C for 1% wt. of CNTs. From viscosity measurements it was concluded that

the CNT fluid displayed a shear thinning behavior under all conditions. Viscosity increased with increasing concentration and decreasing temperature for a given shear rate.

Heat transfer tests were conducted on CNT fluids for different Re, concentrations and pH values. At Re~800, the maximum enhancement in heat transfer coefficient was found to be approximately 380% for 0.5% MWCNTs (conc. by wt) and 0.25% gum Arabic at a x/D =110. Enhancement in heat transfer coefficient increased with increase in concentration of CNTs. The heat transfer coefficient decreased with axial distance. Heat transfer coefficient increased with increase in Re number.

Chen et al. [22] determined the thermal conductivity enhancement of multiwalled carbon nanotubes in water, ethylene glycol and glycerol. The thermal conductivity enhancement increased with increase in particle concentration and decreased with an increase in the thermal conductivity of the base fluid. At 1% conc. by volume of CNTs, the maximum enhancements reported for DI water, ethylene glycol and glycerol were 12%, 17.5% and 16% respectively. The thermal conductivity enhancement of ethylene glycol based nanofluids showed weak temperature dependence. For water based nanofluids, it was found that the viscosity of nanofluid was less than that of the base fluid for concentrations less than 0.004 (conc. by volume), but increased with increase in particle loading for higher concentrations, with substantial increases seen at temperatures greater than 55°C.

Hwang et al. [23] measured the thermal conductivity of different nanofluids containing MWCNTs, fullerenes, copper oxide and silicon dioxide in different base

fluids like water, ethylene glycol and oil. MWCNT nanofluids had the maximum thermal conductivity enhancement among water based nanofluids. Higher thermal conductivity enhancement was obtained for base fluid with lower thermal conductivity. Thermal conductivities of water based MWCNT nanofluids increased with increasing particle concentration and a maximum of 7% enhancement was obtained at a volume fraction of 1%. The experimental results were validated with Jang and Choi model.

Glory et al. [24] measured the thermal and electrical conductivities of suspensions of MWCNTs in water as a function of temperature, nanotube weight content and nanotube length. The thermal conductivity enhancement increased with increase in MWCNT content and a maximum of 64% was achieved at a concentration of 3% by weight at 60 °C. Thermal conductivity enhancement was temperature independent up to a concentration of 2% by weight. The thermal conductivity enhancement increased by a factor of 3 with an increase in length of nanotubes from 0.5-5 μm. The behavior of thermal conductivity enhancement follows a power law as a function of nanotube length with exponent of 1/3. The thermal conductivity enhancement follows the Hamilton Crosser model but is increased by a factor of 5.

Wensel et al. [25] measured the thermal conductivity of heat transfer fluids containing metal oxide nano particles (Fe_2O_3 and MgO) and single walled carbon nanotubes. Approximately 10% increase in thermal conductivity was obtained at very low percentage loading (0.02% wt) of these two nano materials. The fluids were very stable and the viscosity was similar to that of water. The enhancement was attributed to the aggregation of metal oxide particles on the carbon nanotube surface by electrostatic

attraction and formation of aggregation chains along the nanotube. It has been shown that under the influence of a strong outside magnetic field, the thermal conductivity value decreases. It also decreases when the pH is shifted from 7 to 11.45.

As a part of the International Nanofluid Property Benchmark exercise or INPBE, 34 organizations world over, participated in the thermal conductivity measurement of identical samples of colloidally stable dispersions of nanoparticles. This exercise was spearheaded by Jacopo Buongiorno [7] at MIT. The nanofluids tested in the exercise consisted of aqueous and non base fluids, metal and metal oxide particles, near-spherical and elongated particles at low and high particle concentrations. The measurement techniques were grouped into four categories: the KD2 thermal properties analyzer, custom THW, steady state parallel plate and other techniques (which included thermal comparator, hot disk, forced Rayleigh scattering and coaxial cylinders).

For all the water based samples, the data from most organizations deviated from the sample average by +/- 5% and for PAO (Poly Alpha Olefins) based samples the deviation was +/- 10%. The classic effective medium theory for well dispersed particles accurately reproduced the INPBE experimental data, thus suggesting no anomalous enhancement of thermal conductivity in the given sample range. Though systematic differences in thermal conductivity measurements were seen for different measurement techniques, they disappeared when the data was normalized to the measured thermal conductivity of the base fluid.

Literature on experimental heat transfer performance of MWCNT fluids under turbulent flow conditions was not available. Similarly there has been no literature found

on the combined effects of MPCMs and MWCNTs. This formed an additional motivation for the current research project apart from the original objective of producing a new heat transfer fluid with better heat transfer properties. An international exercise conducted on thermal conductivity measurement of nanofluids which was concluded recently is discussed below. This provides valuable insights into the thermal conductivity measurements and enhancements obtained in the case of nanofluids.

Blend of MPCMs and MWCNTs

Taherian and Alvarado [26] developed a computer simulation code that revealed that the best composition for the MPCM and MWCNT blend depended on the actual percentage of phase change that took place in the process. It was concluded that better heat transfer rates could be achieved when high quantity of MPCMs underwent phase change. A concentric tube exchanger was considered as the heat transfer device for the simulations.

Wang et al. [27] investigated the thermal performance of nanoparticle enhanced latent functionally thermal fluids in a vertical circular tube in the laminar regime. The results showed that slurries containing 0.5% TiO_2 nanoparticles by mass and 5%-20% MPCMs by mass showed improved heat transfer rates in comparison with the conventional latent functionally thermal fluid. The enhancement increased with increasing MPCM concentration and dimensionless temperatures showed a reduction of 18.9%.

CHAPTER IV

DESIGN OF THE HEAT TRANSFER LOOP

A heat transfer loop was built at Riverside campus of Texas A&M University for measuring heat transfer coefficient and pressure drop of different fluids under turbulent flow and constant heat flux conditions. The heat transfer loop mainly consisted of copper piping, variable voltage transformer, heat exchanger, water chiller, pump and motor. Other equipment like flow meter, data acquisition units, thermocouples and pressure transducers were installed to collect and store data during experiments. Figure 4.1 below shows a photograph of the experimental setup at the Riverside campus laboratory.

Figure 4.1: Heat transfer loop at Riverside campus

Copper sections

The heat transfer loop comprises **seven** sections made of copper pipes. They are connected to one another by PVC couplings to minimize axial heat conduction. The total length of the heat transfer loop is 12.5 m and is sufficient to ensure fully developed turbulent flow. The boundary layer development of the flow takes place in the first section and from section 2 onwards the flow is assumed to be fully developed. Usually, the first section is long enough for complete development of both hydrodynamic and thermal boundary layers of the fluid.

Each copper pipe is uniformly heated by means of three nichrome coils connected to one another in parallel. The bare copper pipe is coated with a fine spray of insulation paint before the nichrome wire is wound around it to minimize electrical conduction. The nichrome wire is insulated with fiberglass sleeve to avoid any electrical contact with the copper tube. Surface and bulk thermocouples were soldered onto the copper pipe before the heating coils were wound around the copper pipe. The entire copper pipe is covered with fiberglass insulation and aluminum tape to avoid heat losses. Additional details of the copper pipe are as follows:

1. Inner diameter of the copper pipe: 0.011 m
2. Outer diameter of the copper pipe: 0.013 m
3. Length of each section: 1.50 m
4. Surface roughness of copper pipe: 0.0000032 m

A schematic representation of the copper pipe sections is shown in Figure 4.2.

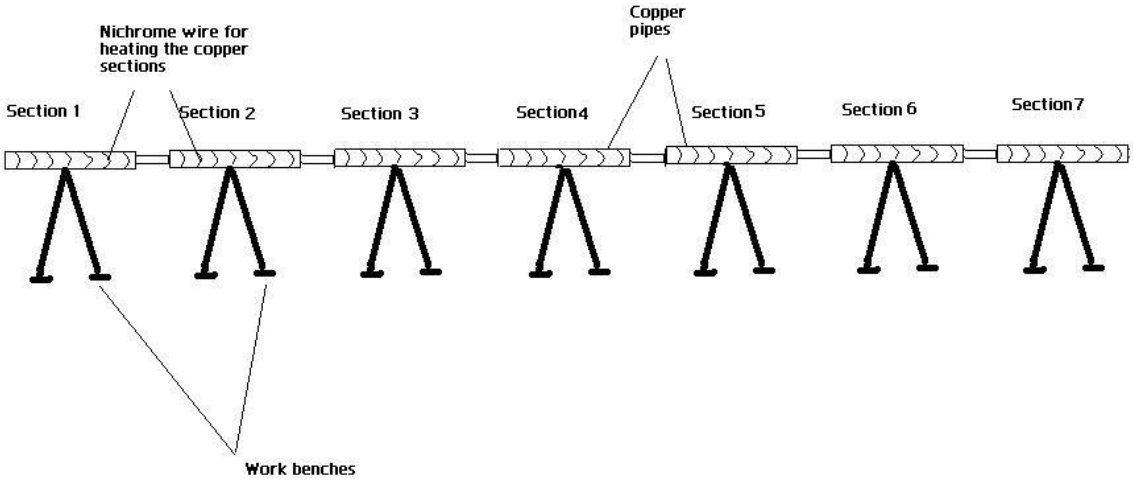

Figure 4.2: Schematic of copper pipe sections

Nichrome heating coils and their resistances

Nichrome wire of 24 Gauge (AWG) type 675 Nickel Chrome Alloy (NiCr60) was used for heating the copper pipes. The diameter of nichrome wire is 0.00051 m (0.0201”) and its resistance is 1.671 ohms per foot length of wire at 68 deg F (20℃). The nichrome wire was insulated with fiberglass sleeve to avoid electrical contact with the copper pipe. This wire was wound on the copper section for the entire length leaving no gaps between the windings. Figure 4.3 below shows the nichrome wire winding on the copper pipe.

Figure 4.3: Nichrome wire winding on copper pipe

This was done for all the sections to achieve the constant heat flux condition everywhere in the heat transfer loop. Though all the sections are of same length approximately, slight differences in their lengths leads to variation in the length of nichrome wire wound on them and thus gives rise to different pipe resistances. To achieve the constant heat flux condition, these resistances must be well balanced by external resistances. These external resistances are nothing but nichrome wire placed in ceramic tubes and connected to the pipe resistances through ceramic connectors. Ceramic tubes prevent the accidental contact of nichrome wire with other materials. The ceramic tubes also act as a hot sink during the heating of Ni wire and thus prevent breakage of nichrome wire at high temperatures. A brief description of different resistances of the heat transfer loop is provided below.

1. Total Resistance (R_t): The total resistance of each coil includes the pipe resistance and the external resistance.
2. Pipe Resistance (R_p): The resistance of the nichrome wire wound on the pipe.
3. External Resistance (R_e) = R_t - R_p .

Since all the sections do not have exactly the same length of nichrome wire wound around them, the small differences in the pipe resistances need to be adjusted for achieving the constant heat flux condition. The extra nichrome wire added to the pipe resistance is known as the external resistance. Figure 4.4 below explains the different resistances in a copper section.

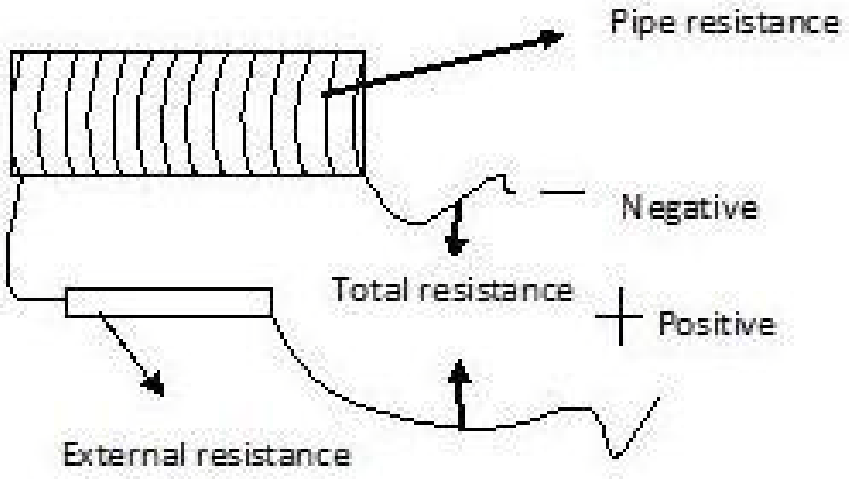

Figure 4.4: Different resistances in a copper section

Section 1 forms the entry length region of the heat transfer loop and calculations for full developed flow did not take into account the readings of the first section. The fully developed regime begins from section 2. Constant heat flux condition was satisfied in every coil of every section. Each section had 3 heating coils. Figure 4.5 below shows a schematic of a copper section with heating coils.

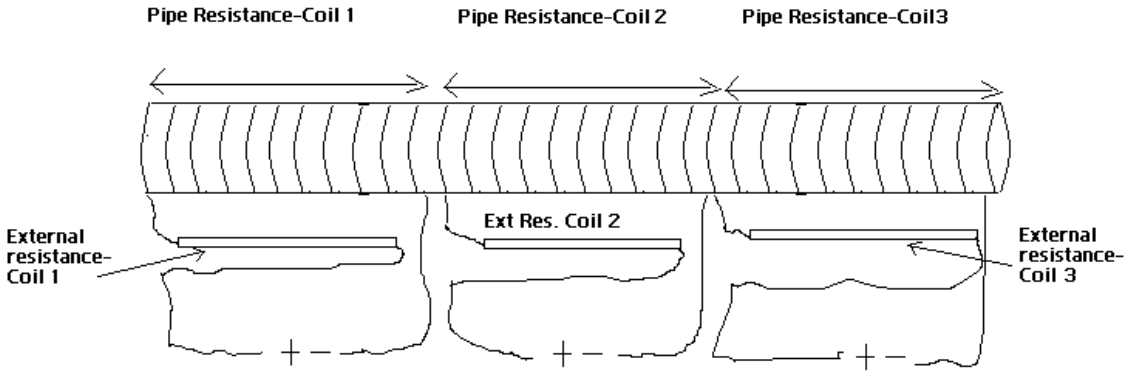

Figure 4.5: Copper section having 3 coils of heating wire

As we can see from Figure 4.5, the pipe resistance and the external resistances of a coil are connected in series and their combined set of resistances is connected in parallel with the other sets of coils. The electrical circuit diagram of the heat transfer loop is show in Figure 4.6 below.

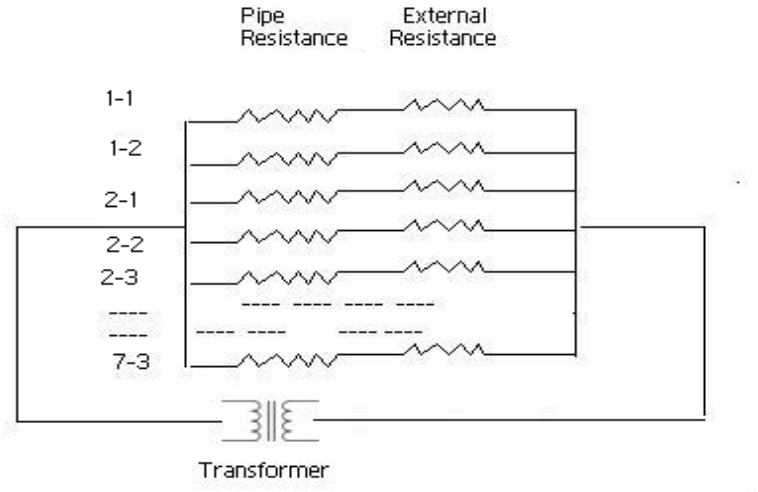

Figure 4.6: Electrical circuit diagram of the heating coils of the heat transfer loop

Each coil of the heat transfer loop is connected to the positive and negative terminals of a variable voltage transformer. Two transformers were used to supply power to all the coils of the heat transfer loop. The naming of coils was as follows: Coil 2-3 stands for the third coil of section 2. Power to coils 1-1 to 4-2 was provided by one transformer and the second transformer supplies power to the remaining coils.

Thermocouples on the heat transfer loop

Thermocouples of type T have been soldered onto the surface of the copper pipe before the nichrome heating wire was wound around it. Five thermocouples were soldered onto the surface of each section in order to measure the surface temperature of the copper pipe. These thermocouples were soldered onto the surface of the copper pipe at distances of 0.28, 0.58, 0.74, 0.89 and 1.12 m from the start of the section. Small

copper pipes were placed between the main sections and were connected to them by PVC couplings. Two thermocouples were soldered onto each of these copper pipes. A strip of twisted copper sheet was inserted in each of these small copper pipes to ensure mixing cup temperature conditions. These small copper pipes have no heating wire on them. Although these thermocouples actually measure the surface temperatures, the surface temperature measured closely matches with the bulk or fluid temperature at that place after the system reached steady state. This is due to the mixing cup conditions achieved at that place and also because of high thermal conductivity of the copper tubing and copper strip. A schematic of the thermocouple layout on the copper tubing is shown in Figure 4.7 below.

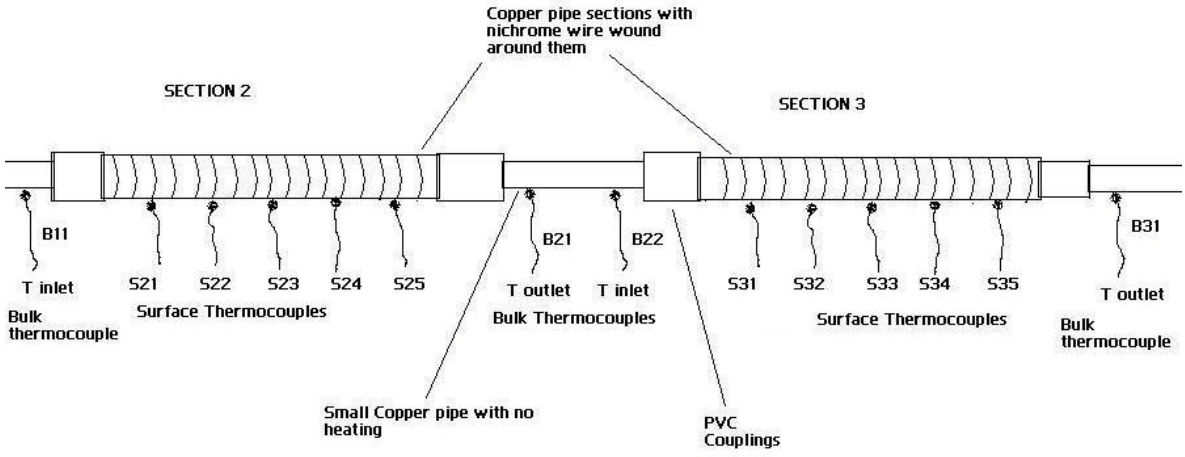

Figure 4.7: Thermocouple layout on the copper sections

The naming of thermocouples is as follows:

Surface thermocouple – For example S32, where the first digit denotes the section number (section 3) and the second digit denotes the number of the thermocouple on that particular section (in this case second thermocouple on section 3).

Bulk thermocouple – For example B21, where the first number denotes the section after which it has been placed (section 2 in this case) and the second digit denotes the number of the thermocouple on the small copper pipe. So B21 is the thermocouple immediately after the end of section 2 and it represents the fluid temperature at the outlet of section 2. B22 gives the inlet bulk fluid temperature of section 3 and B31 is the outlet bulk fluid temperature of section 3. There is only one thermocouple after section 1 that measures the bulk inlet temperature of the fluid for section 2.

Data from the thermocouples was recorded by two Agilent data acquisition units (Agilent 34970 A). Thermocouples starting from S11 to S63 were recorded by one Agilent and the remaining thermocouple data were recorded by the second Agilent unit. Two Agilent units were used to eliminate noise associated with longer thermocouple wires.

Calibration of thermocouples has been done based on the data gathered from the heat transfer tests conducted using DI water at two different voltages and five different flow rates. The tests have been repeated at other voltages for DI water and the results were found to be satisfactory thus confirming the accuracy of calibration. The calibration procedure will be explained in detail in the following pages.

Other devices and instruments

a) Pump

A Moyno progressing cavity pump is used to pump the fluid in the heat transfer loop. This pump has been found to be suitable for viscous slurries and solid laden fluids without causing damage to the solid particles in the slurry [1]. The capacity of the pump is 57 liters per minute and the maximum operating pressure is 1 MPa. The pump is capable of withstanding high temperature fluids up to 100 °C. Figure 4.8 [28] below shows the inner view of the pump.

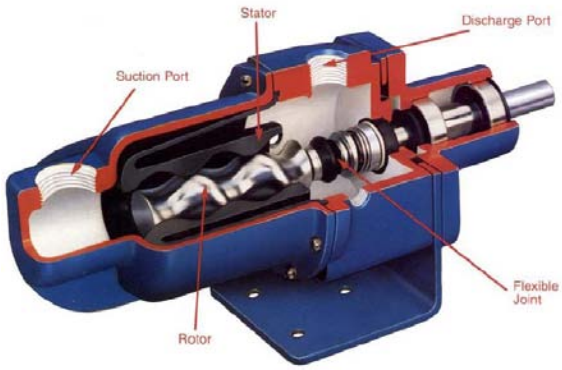

Figure 4.8: Moyno progressive cavity pump (Source: Moyno®500 Progressing Cavity Pumps::Bulletin 90 M) [28]

b) Air cooled water chiller

To control the inlet temperature of the heat transfer fluid entering the heat transfer loop, an air cooled water chiller was used along with a shell-and-coil heat exchanger. The chilled water from the chiller enters the shell and coil heat exchanger

and cools the hot heat transfer fluid entering it. The hot fluid enters the coil side of the heat exchanger and the chilled water is on the shell side. The capacity of the chiller is 5 tones. The chiller uses the R22 refrigerant. A tube – fin condenser and a tube – in – shell evaporator in the chiller ensure that there is effective heat transfer between the refrigerant and the chilled water. Figure 4.9 below shows the air cooled water chiller used.

Figure 4.9: Air cooled water chiller

c) Variable speed drive

A variable speed drive is used to adjust the speed of the pump over a range of speeds. The variable speed drive operates on 1 phase input power supply with voltage 200-240 V.

d) Electromagnetic flow meter

An electromagnetic flow meter from Omega was used to measure the flow rate and flow speed of the heat transfer fluid flowing in the heat transfer loop. The electromagnetic flow meter measures the volumetric flow rates of electrically conductive materials on the basis of Faraday's Law of Electromagnetic induction. The device consists of two units: the detector, through which the fluid to be measured flows and the converter, which receives the electromotive force signals from the detector, then converts the signals into the 4-20 milli amps DC signal. The accuracy of the measurement is +/- 0.5%. The maximum fluid pressure that can be sustained by the flow meter is 2 MPa. The operating fluid temperature can range from -10 to 120 °C. The flow meter is suitable to measure the flow rate of slurries without compromising on the accuracy of the measurement. Figure 4.10 shows the electromagnetic flow meter.

Figure 4.10: Electromagnetic flow meter

e) Shell and coil heat exchanger

A shell and coil heat exchanger was designed by Dr. Hessam Taherian to replace the existing compact heat exchanger. The existing plate heat exchanger did not provide sufficient heat exchange capacity. The newly designed heat exchanger was used along with the water chiller to cool the hot fluid exiting the heat transfer loop. The chilled water from the water chiller enters the shell side of the heat exchanger and the hot fluid from the heat transfer loop enters the tube side of the heat exchanger. The specifications of the shell and coil heat exchanger are given below:

1. Shell diameter: 0.15 m
2. Shell height: 0.61 m
3. Tube diameter: 0.00635 m (nominal)
4. Total length of tubes: 28.96 m
5. Number of coils: 3
6. Total heat transfer area: 0.864 m^2

Figure 4.11 below shows the designed shell and coil heat exchanger.

Figure 4.11: Shell-and-coil heat exchanger before insulation

The heat exchanger is insulated properly **using thick rubber like insulation sheets.**

f) Variable transformers

Two Staco variable voltage transformers were used to provide power to the nichrome heating coils. One transformer provides power to heating coils 1-1 to 4-2 and the other one provides power to coils 4-3 to 7-3. The variable transformers were selected to provide variable output voltage that can be adjusted from 0 to 117% of the unit's input voltage. The transformer consists of a copper winding on a toroidal core of laminated, grain oriented, and silicon steel. A carbon brush connected to an output terminal was rotated over the length of a precision-ground, precious metal-plated

commutator track to tap off voltage at any turn from zero volts to the maximum output voltage of the winding. It operates on 240 V single phase supply and the output ranges from 0-280 V.

g) Power meter

A power meter was purchased from Brand Electronics which measured and displayed different parameters of the variable transformer like voltage, current and power. One meter is a multi channel digital power meter which was used for data acquisition and display from multiple electrical circuits and analog inputs.

h) Data acquisition unit

Two Agilent data acquisition units were utilized to record data from thermocouples, pressure transducers, and flow meter. Agilent units of type 34970 A were used. The Agilent 34970 A consists of a three slot mainframe with a built-in 6 ½ digit multimeter. It is configured with a 20-channel relay multiplexer. The 34970 A measures and converts 11 different input signals like temperature of thermocouples, RTDs, thermistors, DC and AC volts, 2 and 4-wire resistance, frequency, period and DC and AC current. Each channel can be independently configured on the same module. Agilent Bench Link Data Logger software was used with the 34970 A for configuration and data analysis. The switching, conversion and reference junction errors of thermocouples were already taken into account by the unit.

i) Dual range DC power supply for pressure transducers

The dual range DC power supply provides voltage in two ranges: 0-18V DC at 0-7A and 0-36V DC at 0-3.5A. This device was required to provide power to the three pressure transducers in the heat transfer loop.

j) Eplus motor

A premium efficient squirrel cage severe duty motor was bought from Century Motors. This is used to power the Moyno progressing cavity pump. It is made of cast iron, operates at 1200 rpm and it is a 1 HP motor. The service factor of the motor is 1.15.

k) Pressure transducers

Three Cole-Parmer Wet/Wet Differential Pressure Transmitters have been installed to measure the pressure drop of the heat transfer fluid across sections 2, 4 and 6 of the heat transfer loop. The range of differential pressures that can be recorded is 0 to 17.24 KPa. The output of the pressure transmitter ranges from 4 to 20 mA. The accuracy of the pressure transmitter is +/- 0.25% of the full scale. The operating temperature range is from -17.77 to 79.44 °C. The capacitance sensor inside the pressure transducer allows the ports to be wet/wet, wet/dry, or dry/dry. The differential pressure sensor measures the difference between two or more pressures introduced as inputs to the sensing unit. The capacitance sensor uses a diaphragm and pressure cavity to create a variable

capacitor to detect strain due to applied pressure. Figure 4.12 shows the pressure transducer used in this project.

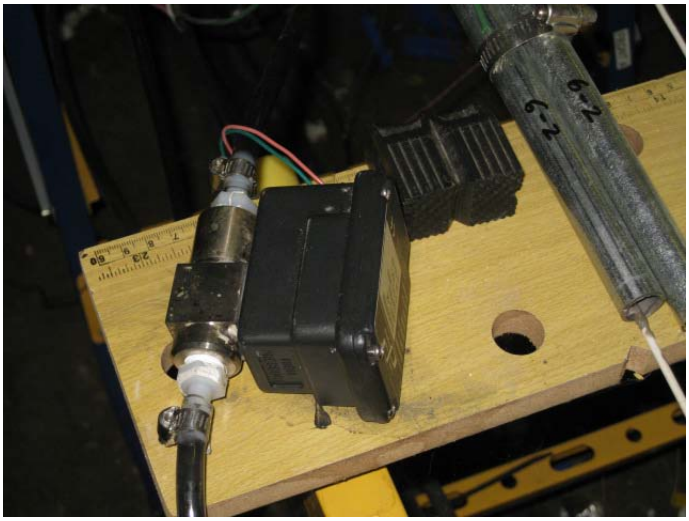

Figure 4.12: Cole Parmer differential pressure transducer

Durability testing loop

A durability testing loop has also been constructed in series with the heat transfer loop. This loop consists of copper piping of length 10 m. The diameter of the copper pipe is 10.5 mm. There are no heating coils on this copper piping. This loop is useful for testing the durability of MPCM capsules. The microcapsules were pumped through the durability loop for a fixed number of cycles and then a sample of the fluid was drawn out of the loop from the sample collecting station to inspect for any damage. For other heat transfer fluids, this loop also serves as a sample collecting station for mass fraction measurements. A schematic of the durability loop is shown in Figure 4.13 below.

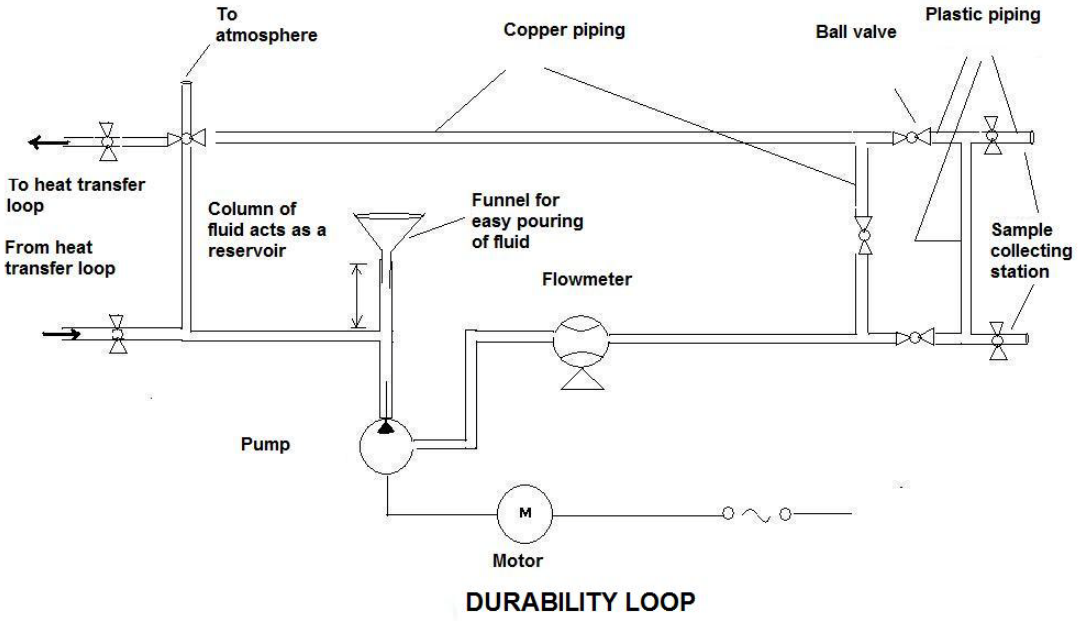

Figure 4.13: Durability loop

The detailed procedure of the calibration of the heat transfer loop can be found in Appendix A.

CHAPTER V

MEASUREMENT OF THERMAL CONDUCTIVITY AND VISCOSITY

Thermal conductivity measurement

Thermal conductivity of a fluid can be measured using two types of methods – 1) Steady State methods and 2) Transient methods. In the steady state method, the heat flux that is required to maintain a constant temperature difference between two surfaces immersed in a fluid is measured. Thus one can determine the thermal conductivity of the fluid sample using Fourier's law of heat conduction. Generally, the two surfaces used can be either parallel plates or concentric cylinders. Though the working equations of such devices are simple, difficulty lies in machining the surfaces and aligning them exactly parallel to one another.

In a transient thermal conductivity measurement, a time dependent perturbation, in the form of a heat flux is applied to a fluid in equilibrium and the response of the temperature of the fluid to this disturbance is measured. Using this response and appropriate working equations, one can calculate the thermal conductivity of the fluid very accurately. The transient method was used in this research work. The principle of the transient method [29] is presented in appendix B. Some of the advantages of transient thermal conductivity measurement are discussed below.

1) Exact working equation can be deduced after careful mathematical modeling of the transient hot wire apparatus and this can be used to obtain very high accurate values of thermal conductivity of the fluid.
2) Convective heat transfer effects can be eliminated to the maximum extent possible by adjusting the time scale of the measurement to be smaller than the time required for the onset of significant free convection for a given set of experimental conditions. Applying temperature gradients in a compressible fluid will inevitably create a state of motion due to the density differences created. But the characteristic time for the acceleration of the fluid by buoyancy forces is much longer than the propagation time of a temperature wave originated by a strong and localized temperature gradient. Success of transient techniques is based on this fact.
3) Transient hot wire technique can be used to determine thermal conductivity in most regions of the phase diagram except very close to the critical point where density fluctuations are very large.

For this research work, thermal conductivity of nanofluids was initially proposed to be measured by an instrument called KD2Pro Analyzer from Decagon Devices, Inc. The instrument worked on the principle of the transient hot wire apparatus. Despite making modifications to the instrument, measurement of thermal conductivity was inaccurate and was giving large errors. The working of KD2Pro, the difficulties faced during the measurement and the modifications made are explained in detail in Appendix B.

Transient hot wire apparatus

A new transient hot wire apparatus was designed and constructed by Dr. Hessam Taherian for the measurement of thermal conductivity of nanofluids. The single wire device was chosen because of its simplicity of construction, ease of operation and low cost. In this device, the line source of heat was thin Teflon coated Platinum wire. The Teflon coating avoided particles from sticking to the wire surface. The platinum wire diameter is 50 microns and the Teflon coating is 9 micron thick. The wire was thin enough to provide a fast temperature response. The length of the platinum wire is 20 cm.

The wire was soldered onto two copper lead wires supported by surface mount terminal blocks. Two polycarbonate rods of 1/8" in diameter are inserted through the blocks to form the supporting framework. This hot wire apparatus was inserted in a 100 ml graduated glass cylinder in which the fluid to be tested was filled. The cylinder was insulated properly to avoid any heat losses during the measurement. The transient hot wire designed is shown in Figure 5.1 below. The thin wire is stretched between the two terminal blocks shown in the figure.

Figure 5.1: Transient hot wire

Principle of measurement of thermal conductivity using Wheatstone bridge

The THW is connected as one of the arms in a Wheatstone bridge. Figure 5.2 shows the Wheatstone bridge circuit.

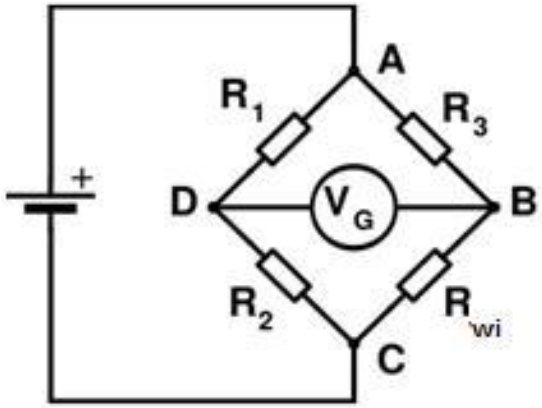

Figure 5.2: Wheatstone bridge circuit

R_1 and R_2 are standard 100Ω resistors, R_3 is the adjustable resistor (potentiometer) and R_{wi} is the resistance of the platinum wire at initial conditions or ambient conditions. The Wheat stone bridge is initially balanced and the bridge voltage is as close to zero as is practically possible (approximately 0.2 V). An Agilent unit (34970 A) is connected to the Wheatstone bridge to detect the change in voltage across the bridge. When the hot wire is heated, its resistance changes as a function of the temperature rise in the wire. This creates a voltage signal across the bridge (between the points B and D) which is detected by the multimeter. The digital voltmeter is equipped

with a data storage system that collects voltage data every 5 milliseconds. Based on the data collected by the acquisition system, an excel program is utilized to plot ΔT vs. ln(t).

The value of ΔT and thus thermal conductivity of the fluid can be deduced from the bridge output voltage using the Wheatstone bridge resistance balance equation, which is written below.

$$\frac{R_2}{R_1} = \frac{R_{wi}}{R_3}$$

The resistance of hot wire can be written as follows.

$$R_{wi} = \frac{R_2}{R_1} R_3$$

Using Kirchoff's law the bridge voltage output signal is written below.

$$V_G = \left(\frac{R_{wi} + \Delta R_w}{R_3 + R_{wi} + \Delta R_w} - \frac{R_2}{R_1 + R_2}\right) V_s$$

As temperature changes the resistance of the hot wire changes and ΔR_{wi} is the change in the resistance of the hot wire after time t. In the above equation, V_s is the supply voltage and V_G is the voltage output across the bridge.

Since $\Delta R_w = R_{wt} - R_{wi}$, by substituting ΔR_w in the equation for V_G, we get

$$V_G = \left(\frac{R_{wt}}{R_3 + R_{wt}} - \frac{R_2}{R_1 + R_2}\right) V_s$$

Temperature change of hot wire can be written as follows:

$$\Delta T = \frac{R_{wt\,2} - R_{wt\,1}}{\alpha(R_{wi})} = \frac{\Delta R_w}{\alpha R_{wi}}$$

where α is the temperature coefficient of resistance.

Voltage drop across the hot wire can be given as follows:

$$V_w = \frac{V_s R_{wt}}{R_{wt} + R_3}$$

Rewriting equation for V_G in terms of V_w, we get

$$V_G = V_w - \frac{V_s R_2}{R_1 + R_2}$$

By measuring V_G we can find out V_w, since $V_{s,} R_2$ and R_1 are known. From the value of V_w, we can find the value of R_{wt}. From the value of ΔR_w we can find the value of ΔT.

$$\Delta T = \frac{q}{4\pi\lambda} \ln\left(\frac{4at}{r_o^2 C}\right)$$

$$\Delta T = A \ln(t) + B$$

where

$$A = \frac{q}{4\pi\lambda}$$

and

$$B = \frac{q}{4\pi\lambda} \ln\left(\frac{4a}{r_o^2 C}\right)$$

The heat flux per unit length at time t can be given as:

$$q = \frac{V_w^2}{L_w R_{wt}}$$

The value of ΔT can be plotted as a function of ln(t) and from the slope of the graph we can find the value of thermal conductivity. Thermal diffusivity can be found from constant B. Alternatively we can also find thermal conductivity by plotting V_G as a function of ln(t). This was the procedure that was followed during the thermal conductivity measurements. A sample plot of V_G vs. ln(t) is shown in Figure 5.3 below.

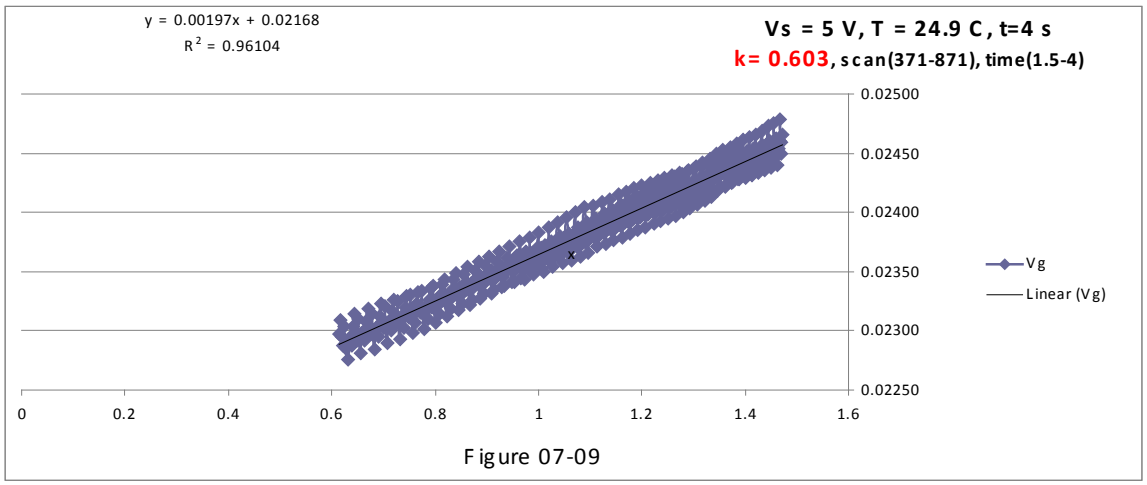

Figure 5.3: Sample plot of V_G vs. ln(t) for DI water

Calibration of THW

The calibration procedure for THW is taken from the THW manual. The THW is calibrated with DI water. The optimum voltage supply is set to 5V and the optimum time span for data collection is 4s or since the scan rate is 200 scans per second, it is 800 scans. A total of 2000 scans is collected by the data acquisition system. The optimum range of 800 scans out of a total of 2000 should be selected by calculating the thermal conductivity from each range and comparing it with the NIST [30] values. For obtaining a value of thermal conductivity of DI water at a particular temperature at least 10 measurements are taken. Measurements should have a gap of at least 5 minutes between one another so that the temperature of the Pt wire regains its original temperature. Thermal conductivity of DI water is measured at different temperatures When the fluid is getting heated or cooled by a chiller, it is essential to wait for at least 15 minutes to ensure that fluid is uniformly heated or cooled and is in thermal equilibrium with the chiller fluid. The temperature of the liquid was monitored using a thermocouple wire and

a digital thermometer. After calibration with DI water, the error of the THW measurements when compared to NIST [30] values was found to be -0.016%. Table 5.1 below tabulates the thermal conductivity measurements for DI water at room temperature.

Table 5.1: Thermal conductivity measurements of DI water at room temperature using THW

Test no.	Room temperature (° C)	Thermal conductivity measured (W/m-K)	Thermal conductivity of DI water (NIST) (W/m-K)	Error (%) w.r.t. NIST values	Last scan number	R^2 value
1	25.0	0.610	0.607	0%	872	0.960
2	25.1	0.620	0.607	2%	875	0.958
3	25.0	0.613	0.607	1%	865	0.960
4	24.9	0.603	0.607	-1%	871	0.961
5	24.9	0.599	0.607	-1%	879	0.960
6	24.8	0.610	0.607	0%	877	0.958
7	24.7	0.599	0.607	-1%	872	0.960
8	24.7	0.598	0.607	-1%	871	0.960
9	24.7	0.609	0.607	0%	868	0.959
10	24.7	0.608	0.607	0%	886	0.959
Average	**24.9**	**0.607**	**0.607**	**-0.016%**	**874**	**0.960**
Std dev	**0.151**	**0.007**	**0.000**	**0.012**	**5.97**	**0.001**
Relative dev	**1%**	**1%**	**0%**		**1%**	**0%**

A sample plot of V_G vs. ln(t) has been shown in Figure 5.3. A linear curve fit is applied to the measured data. R^2 (correlation coefficient) value in each case has been tabulated in Table 5.1.

Measurement of nanofluid thermal conductivity

The thermal conductivity of the nanofluid is measured at room temperature at least 10 times with the scan range obtained from DI water calibration. Care should be taken to prevent CNT-nanofluid from evaporation. Thermal conductivity of CNT fluid is also measured at other temperatures in the same way as was done in the case of DI water. Equilibrium between CNT-nanofluid and the fluid in chiller should be also attained while controlling the temperature of the CNT fluid with a chiller.

Viscosity measurement

For this research work, the DV-I Prime Viscometer model from Brookfield Engineering Laboratories Inc. was used to measure viscosity of different heat transfer fluids. The DV-I Prime is a rotary digital viscometer which displays the viscosity of the fluids on its LCD display. This viscometer is capable of continuous sensing and display without requiring any attention by the user. This instrument can be connected to a PC or a printer for recording and storage of data. Figure 5.4 below shows the DV-I Prime Viscometer.

Figure 5.4: Brookfield DV-I Prime Viscometer

The viscometer measures the torque required to rotate an immersed element (the spindle) in a fluid. The spindle is driven by a motor through a calibrated spring. Deflection of the spring is indicated on the digital display. The viscous drag or resistance to flow (degree to which the spring deflects) is proportional to the spindle's speed of rotation and is related to the spindle size and shape. As the rotational speed increases, the drag increases. For a particular test fluid, the speed of the spindle is varied to determine the change in viscosity with respect to rotational speed. Different kinds of spindles may be used to obtain different viscosity ranges. The viscometer used in this research work belongs to the LV series of viscometers from Brookfield. The maximum torque that can be measured by this series of instruments is 673.7 dyne-cm or 0.063 milli-Newton-m.

The type of spindle selected for this research work is the UL adapter. The UL adapter is suitable for accurate measurements on low viscosity materials. Viscosities of both Newtonian and Non Newtonian type of fluids can be measured using this kind of spindle. This spindle is most commonly used with the LV series of viscometers. The UL adapter consists of a precision cylindrical spindle rotating inside an accurately machined tube. Due to its rheologically correct cylindrical geometry, extremely accurate viscosity measurements can be obtained. The capacity of the UL adapter is 16 ml. The tube of the UL adapter has a removable end cap which allows the open ended tube to be used in a beaker or a tank. With the cap in place, the closed tube can be immersed in a temperature bath for precise temperature control. The working temperature range of the UL adapter is -15°C to 100°C. The range of viscosity measured by the combination of LV series of viscometers and UL adapter is 1-2000 cP (mPa.s). The entry code for the UL adapter is S00. The various dimensions of the UL adapter are shown in Figure 5.5 [31] below.

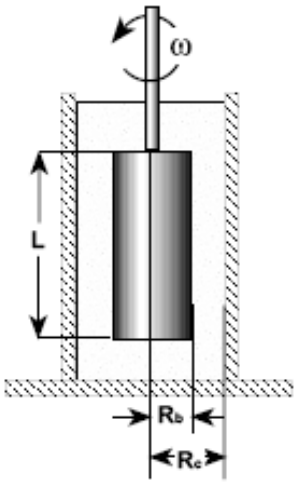

Figure 5.5: UL adapter (Source: Brookfield's *More Solutions To Sticky Problems*) [31]

The basic equations applicable for coaxial cylindrical geometries as found in the case of UL adapter are presented below. These equations are valid for any Brookfield viscometer.

The shear rate (sec^{-1}) of the fluid is given as follows.

$$\gamma = \frac{2\dot{\omega} R_{C^2}}{(R_{C^2} - R_{b^2})}$$

where ω=angular velocity of spindle (rad/sec) = 2πN/60 where N=spindle speed in RPM.

R_b=radius of spindle (cm);

R_c=radius of container (cm);

And $\dot{\gamma}$ is the shear rate at surface of spindle.

The shear stress ($dynes/cm^2$) in the fluid is given as follows.

$$\tau = \frac{M}{2\pi R_{b^2} L}$$

where M=torque input by instrument (dyne-cm)

L= effective length of spindle (cm)

The viscosity (poise) of the fluid can be obtained by using the following relation.

$$\eta = \frac{\tau}{\dot{\gamma}}$$

For UL adapter, the values of different dimensions are given as follows:

1. L= 90.74 mm (including corrections for end effects)
2. R_b= 25.15/2= 12.575 mm
3. R_c=27.62/2= 13.81 mm

Shear rate for UL adapter can be given as: 1.224 N where N is the rotational speed in rpm.

In a real concentric cylinder viscometer, the container is of finite size and therefore the top and base of the inner cylinder will also exert a torque. Near the ends, the torque per unit length will be reduced since the velocity gradient is no longer radial. But the torque will still be proportional to angular velocity. The end effects require corrections to the above formulas. But it is taken care of, if the calibration is performed accurately.

Important points in viscosity measurement

1) The following information should always be recorded when making a viscosity measurement; viscometer model, spindle type, rotational speed, container size, sample temperature, and time of measurement.
2) The spindle should be checked for any damage before each test. The spindle should be screwed firmly to the coupling of the viscometer and it should not hit the sides of the container as it may damage the shaft alignment.
3) Always immerse and position the spindle in the sample fluid before attaching it to the viscometer.

4) For any spindle and speed combination, the goal is to obtain a % torque reading between 10 and 100 for every measurement. The relative error of measurement improves as the reading approaches 100.
5) The sample fluid should be free from entrapped air. Air can be removed by gently tapping the container on a table top. The sample should be at a constant and uniform temperature. The sample and spindle must be of the same temperature. Agitation of the sample prior to each measurement can ensure uniform temperature.
6) Homogeneity of the sample is also important in the case of dispersed systems. In most cases, simple stirring prior to the test will ensure reasonable amount of homogeneity in the sample.
7) The spindle should be immersed up to middle of the shaft indentation.

Sensitivity and accuracy of the viscometer

The Brookfield viscometers are guaranteed to be accurate to within +/- 1% of the full scale range of the spindle /speed combination in use. Repeatability is within +/-0.2% of the full scale range. The relative error of a particular viscosity reading is dependent upon the actual display (%torque) reading. The relative error of the viscosity value should improve as the reading approaches 100.

The following steps form the procedure for taking viscometer readings on a Brookfield viscometer:

1) The viscometer should be securely attached to its stand and properly leveled. The spindle should be firmly attached to the coupling of the viscometer.
2) Select a spindle. Make sure it is not damaged.
3) After turning the viscometer on, disconnect the spindle and press any button for the viscometer to autozero its settings.
4) Connect the spindle and run the test. Wait for at least 5 minutes or till the reading appears relatively constant. Sometimes the reading may not come to equilibrium but will continue to oscillate. This happens due to the presence of elastic as well as a viscous component in the fluid. In such cases, median value of the range may be taken.

Viscometer calibration

The DV-I Prime viscometer has been calibrated with the calibration fluid supplied by the Brookfield Laboratories Inc. Its accuracy was found to be +/- 0.7%. It has also been tested with DI water and values are in very good agreement with the tabulated values of NIST [30].

CHAPTER VI

MICROENCAPSULATED PHASE CHANGE MATERIALS

MPCMs or microencapsulated phase change materials are small capsules in which the core is a phase change material surrounded by the wall of the encapsulant. The MPCMs are usually suspended in a carrier fluid like water and the suspension is referred to as MPCM slurry. Phase change materials are known to increase the heat capacity of the carrier fluid due to their high latent heat of fusion. Since phase change materials have problems like clogging in pipes, they are microencapsulated in order to separate the PCMs from the carrier fluid.

MPCMs are generally manufactured through the process of complex coacervation. The process involves three steps outlined as below:

1) Three immiscible chemical phases are formed which are i) liquid manufacturing vehicle phase ii) core material phase iii) coating material phase. The core material is dispersed in a solution of the coating polymer. The solvent for the polymer is the liquid manufacturing vehicle phase.
2) The liquid polymer coating is deposited on the core material when the polymer is adsorbed at the interface of the core material and the liquid vehicle phase.
3) The coating is then rigidized through processes like cross linking to form microcapsules.

Three most important aspects in selection of MPCMs are its particle size, durability and super cooling.

a) Particle size

It had been observed in previous studies [1] that larger capsules (greater than 100 μm) are prone to breakage under continuous pumping and hence ineffective for use in heat transfer fluids. Although a decrease in particle size results in more durable micro capsules smaller micro encapsulated phase change material also exhibits lower freezing point of the material which then results in an increase in the super cooling behavior. Super cooling is a highly undesirable feature since the MPCM slurry would need reheating. Thus a tradeoff should be obtained between super cooling and durability so the right particle size can be selected.

b) Durability of MPCMs

It is the ability of the particles to withstand continuous pumping for a long time without breakage. Durability (discussed later) can be tested for, by pumping the MPCMs continuously through a loop for a large number of cycles and then estimating the amount of broken capsules in the slurry. The amount of broken capsules should be less than 1% if the MPCMs are to be used as heat transfer fluids.

c) Super cooling

It is the difference in the solidification and melting temperatures of the material. This will pose problems in heat transfer fluid applications since the temperature of the

material would have to be decreased lower to the crystallization point for the PCMs to re solidify in the heat exchanger. The slurry would then have to be reheated before it enters the loop so that phase change can be observed in the loop. To prevent the super cooling phenomenon in MPCMs nucleating agents are added. The amount of nucleating agent added is important since too much of it can adversely impact the heat transfer coefficient value of the MPCMs.

DSC results

In our experiments we have used the MPCMs manufactured by Thies Technology Inc. These MPCMs have octadecane as the core material and gelatin for the shell or wall material. The nucleating agent is Octadecanol and its concentration is 5% by wt. The average particle size of the MPCMs used is 5 µm**.** The DSC data of unencapsulated and encapsulated octadecane is presented in Figures 6.1 and 6.2 respectively.

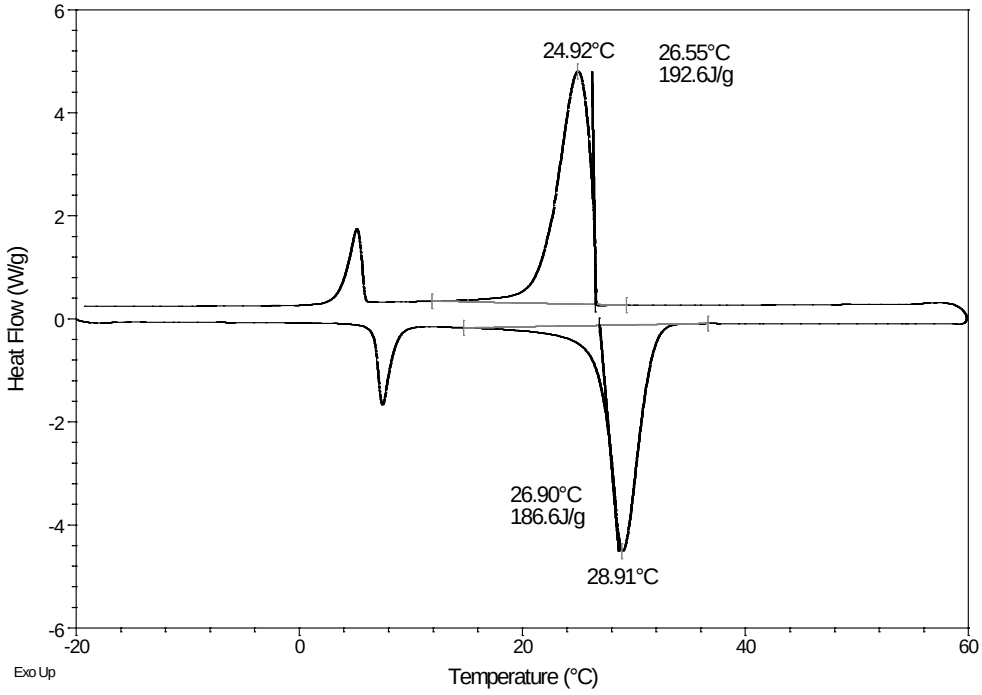

Figure 6.1: DSC data of unencapsulated octadecane/nucleating agent (95/5 w/w%)

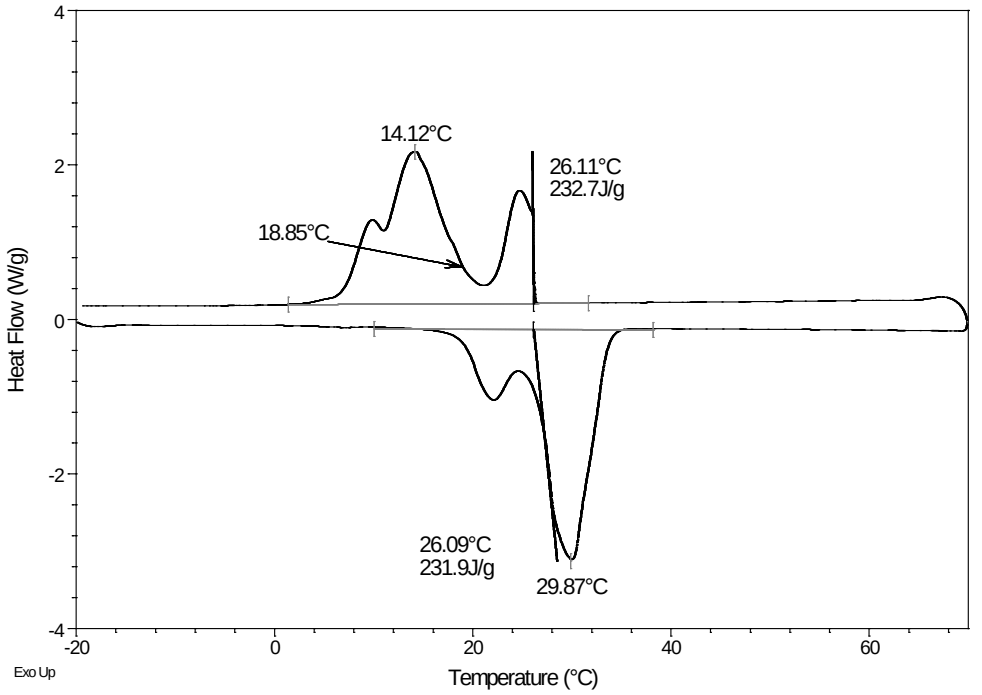

Figure 6.2: DSC data of encapsulated octadecane/nucleating agent (95/5 w/w%)

The observations from the DSC curves have been summarized into Table 6.1. As one can observe from the table, the super cooling behavior was less than 0.5 ℃ in both unencapsulated and encapsulated octadecane by the use of a nucleating agent. Thus this batch of MPCMs showed a very less amount of super cooling and had satisfied one of the major criteria in the selection of MPCMs. The next section deals with the durability of the MPCM capsules.

Table 6.1: Summary of DSC data for unencapsulated and encapsulated octadecane

Sno	Batch	Crystallization point(℃)	Latent heat of solidification (J/g)	Melting point (℃)	Latent heat of fusion (J/g)	Super cooling (℃)
1	unencapsulated octadecane/Nucleating Agent (95/5 w/w %) CT071209A (Gelatin shell)	26.55	192.6	26.9	188.6	0.35
Sno	Batch	Crystallization point(℃)	Latent heat of solidification (J/g)	Melting point (℃)	Latent heat of fusion (J/g)	Super cooling (℃)
2	encapsulated octadecane/Nucleating Agent (95/5 w/w %) CT071209A (Gelatin shell)	26.11	232.7	26.09	231.9	-0.02

Durability of MPCMs

The durability of MPCMs or the ability of MPCMs to withstand continuous pumping power and the turbulent flow conditions in the heat transfer loop was tested in this experiment. In this experiment the amount of breakage of MPCM capsules was determined after pumping them through a closed piping section for a fixed number of cycles at a particular speed. Usually when the capsules break, they release the core material and the core material being lighter (in this case it is octadecane), floats on the surface of the MPCM slurry. The durability loop was used to conduct the durability experiments of MPCMs. The loop has been described in detail in chapter IV.

The MPCM slurry received from Thies Technology Inc. had a concentration of 27.8% by weight. It had been concluded in earlier studies that particle size affected the durability of the microcapsules [1] and small microcapsules (2-10 μm in diameter) showed the least degree of damage. The sizes of MPCMs used in this experiment have a diameter in the range of 2-10 μm.

The MPCM slurry was diluted to a concentration of 14% by weight and was then filled in the loop ensuring that there were no air bubbles in the loop. It was then pumped at a particular velocity for a fixed number of cycles. After the required number of cycles was completed, a sample was collected from the bypass loop to examine the amount of MPCM capsules breakage. It was then repeated for different velocities. The different experimental conditions and the durability results for the experiment are summarized in Table 6.2 below.

Table 6.2: Results of the durability experiments on MPCMs

Batch No.	Velocity(m/s)	Volume flow rate Q (l/s)	No. of cycles	Total time of durability test (min)	Amount of free octadecane observed
1	0.409	0.071	200	85	Negligible
2	0.603	0.107	300	85	Negligible

The samples collected were inspected visually to check for free octadecane in the MPCM slurry. Though there was some free octadecane observed (looked like oil droplets on the free surface of the MPCM slurry), the amount of free octadecane as compared to the entire sample was negligible.

Viscosity of MPCMs

Viscosity of MPCMs was measured using a Brookfield viscometer. Viscosity was measured at four different temperatures and three different shear rates. Two MPCM slurries of 7% and 11% (concentration by weight) were tested. Following observations were made.

1) Viscosity increased with increase in concentration of MPCMs in the slurry.
2) Viscosity of the MPCM slurry reduced with increase in temperatures in a linear way
3) Viscosity of MPCM slurry did not change significantly with change in shear rate

4) All the above observations meant that the MPCM slurry was Newtonian up to a concentration of 11% by wt. of MPCMs.

Viscosity vs. temperature plots are shown in Figures 6.3 and 6.4 respectively.

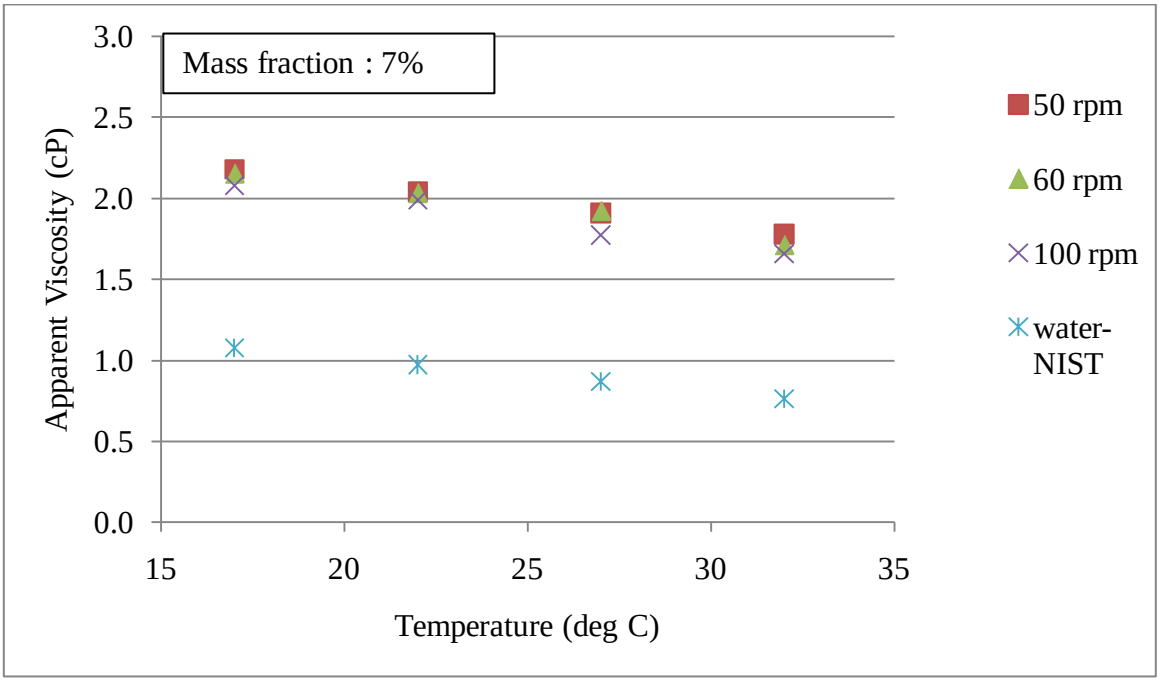

Figure 6.3: Viscosity vs. temperature plot for 7% (conc. by wt) MPCM slurry

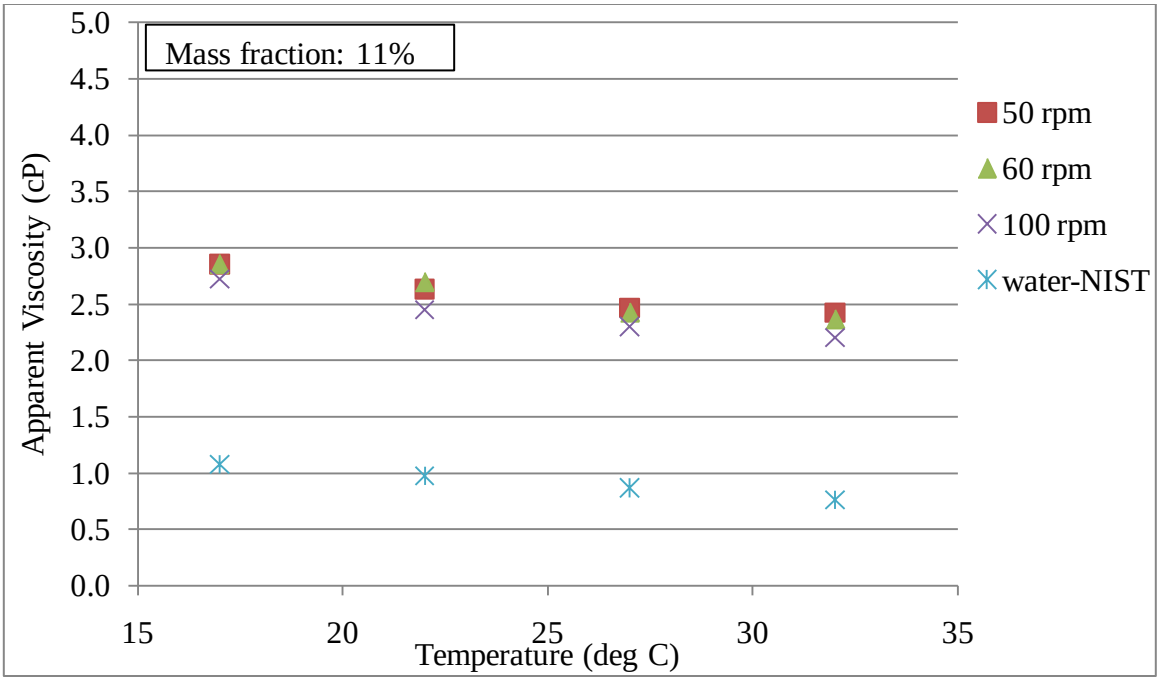

Figure 6.4 Viscosity vs. temperature for 11% (conc. by wt.) MPCM slurry

Relative viscosity vs. temperature plots of 7% and 11% MPCM slurries are shown in Figure 6.5 below. Relative viscosity is defined as the ratio between absolute viscosities of the MPCM slurry to that of DI water at same temperature. The relative viscosity remained almost constant with temperature.

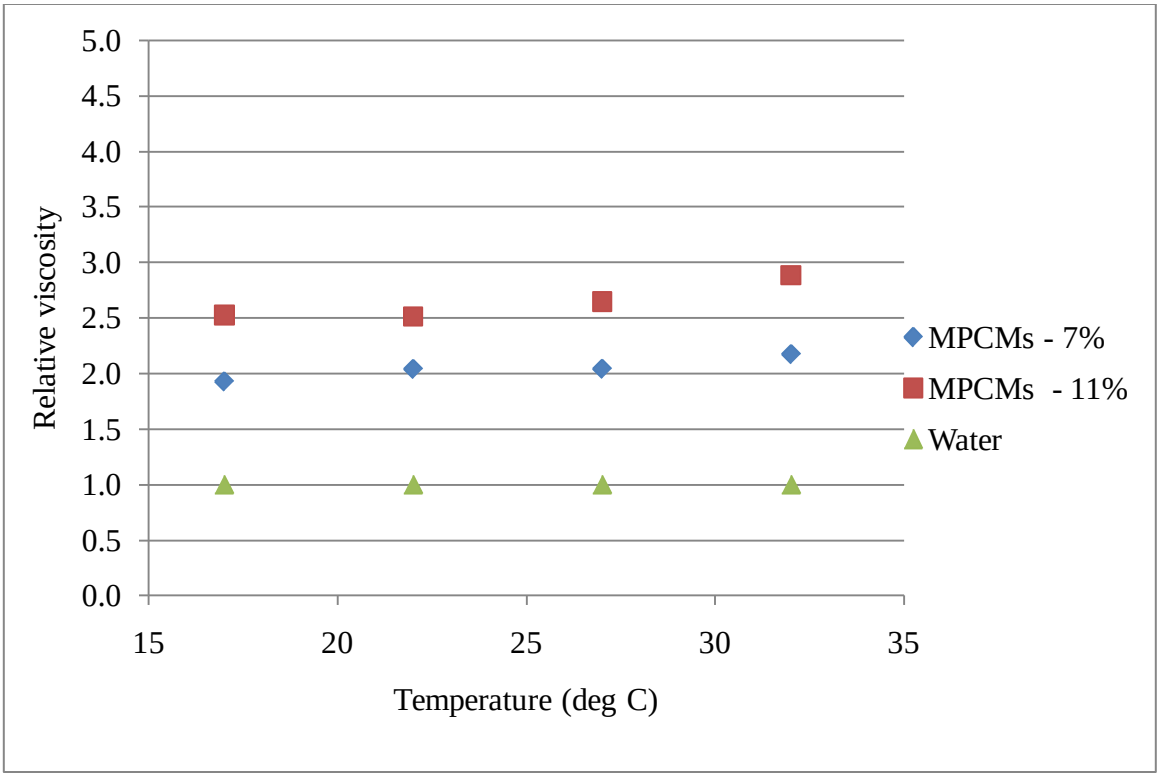

Figure 6.5: Relative viscosity vs. temperature for 7% and 11% (conc. by wt.) MPCM slurries

Thermal properties of MPCMs

The density of the MPCM slurry was evaluated using the following equation.

$$\rho_{slurry} = \frac{1}{\frac{MF_w}{\rho_w} + \frac{MF_{MPCM}}{\rho_{MPCM}}}$$

The specific heat of the slurry was evaluated as follows.

$$C_{p,slurry} = MF_w . C_{p,water} + MF_{MPCM} . C_{p,MPCM}$$

The thermal conductivity of the MPCM slurry was evaluated as follows.

$$k_{slurry} = k_w . \frac{2k_w + k_{MPCM} + 2MF_w(k_{MPCM} - k_w)}{2k_w + k_{MPCM} - MF_w(k_{MPCM} - k_w)}$$

Heat transfer results of MPCMs

Heat transfer tests were conducted on two different concentrations of MPCM slurries, one at 7% and the other at 11% by weight. The melting point of octadecane is 26.1 ℃.

a) Temperature and heat transfer coefficient plots of MPCMs

During the phase change of octadecane from solid to liquid, the input heat flux to the fluid contributed to the latent heat required for the phase change. The latent heat did not cause any significant increase in the bulk temperature of the fluid (theoretically phase change should occur at constant temperature but in actual experiments there was a slight increase in the bulk temperature of the fluid because all the MPCM capsules do not undergo phase change at the same time instantaneously). The temperature plots and the corresponding heat transfer coefficient plots have been plotted for both 7% and 11% (concentration by weight) MPCM slurries.

MPCM slurry (7 % concentration by weight)

Figures 6.6 and 6.7 show the temperature plots and the heat transfer coefficient plots of 7% MPCM slurry at heat flux q" = 12.1 kW/m^2 (155 V) and flow rate = 0.08 l/s.

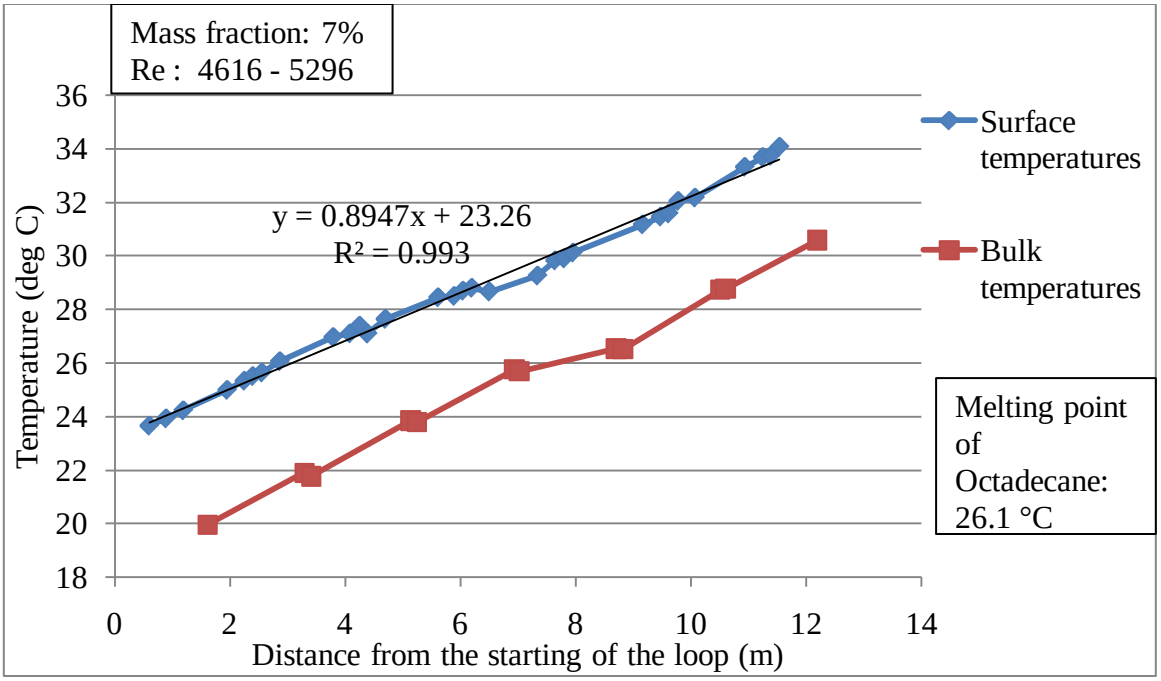

Figure 6.6: Temperature plots of 7% MPCM slurry at q" = 12.1 kW/m^2 (155 V) and flow rate = 0.08 l/s

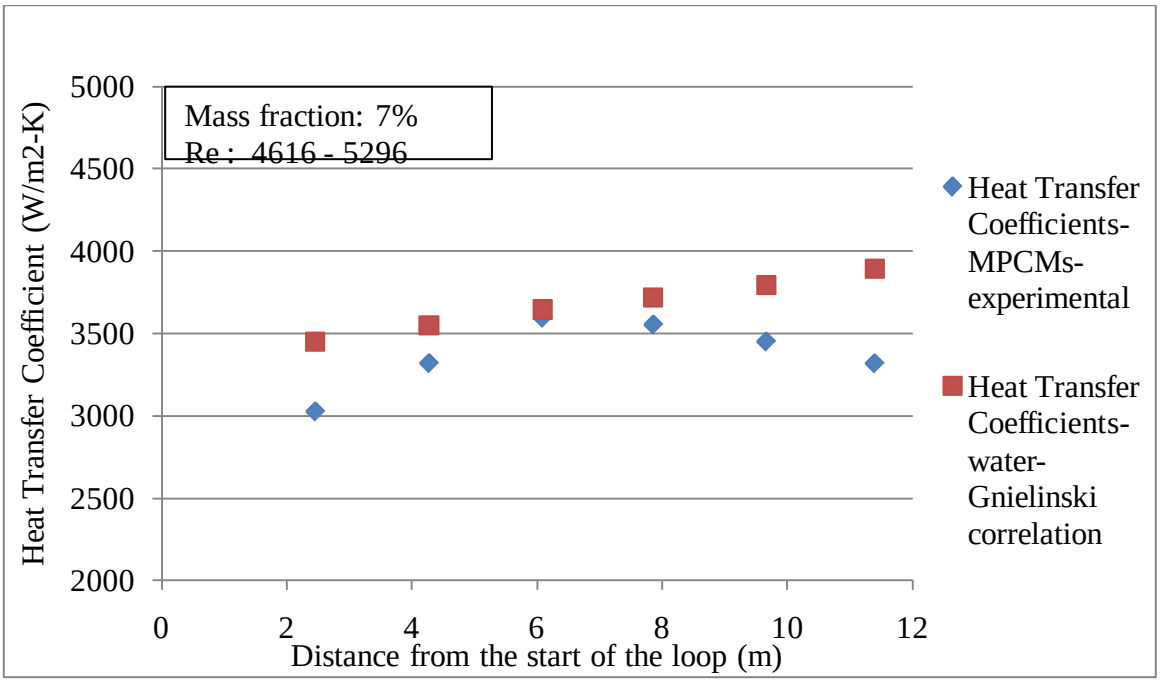

Figure 6.7: Comparison of heat transfer coefficients of water and MPCMs (7%) at q" = 12.1 kW/m^2 (155 V) and flow rate = 0.08 l/s

MPCM slurry (11% concentration by weight)

Figures 6.8 and 6.9 show the temperature plots and the heat transfer coefficient plots of 11% MPCM slurry at heat flux q" = 15.3 kW/m^2 (175 V) and v_{loop}=1.3 m/s.(0.12 l/s)

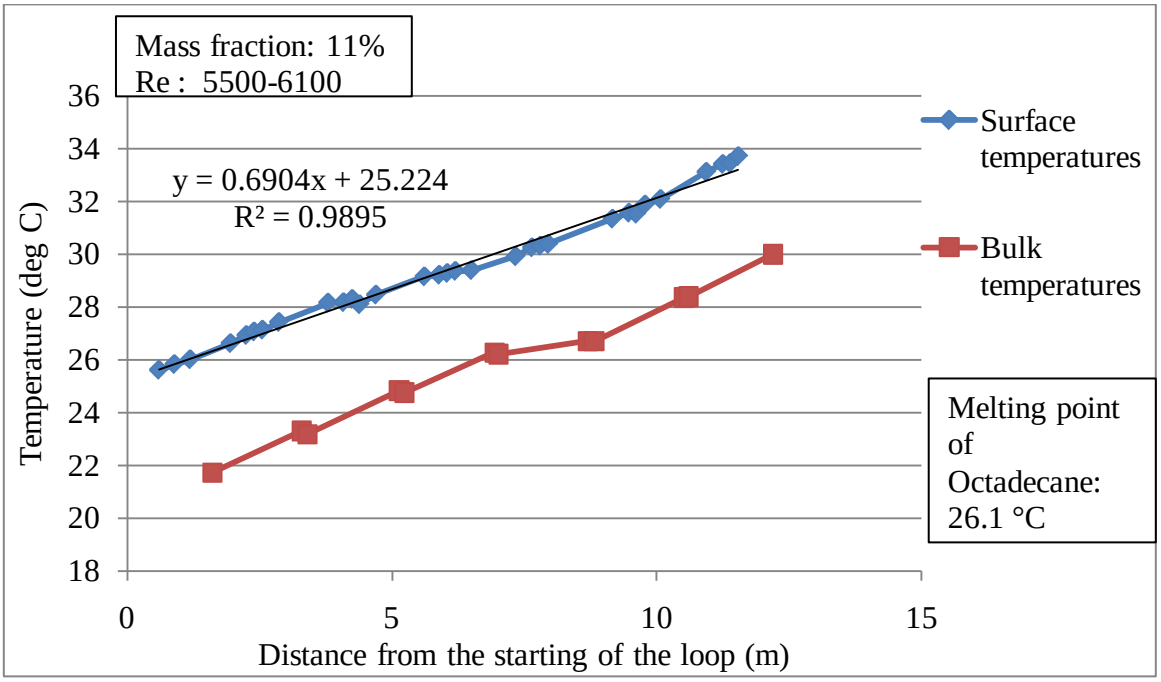

Figure 6.8: Thermocouple plots of 11% MPCM slurry at q" = 15.3 kW/m^2 (175 V) and flow rate = 0.12 l/s

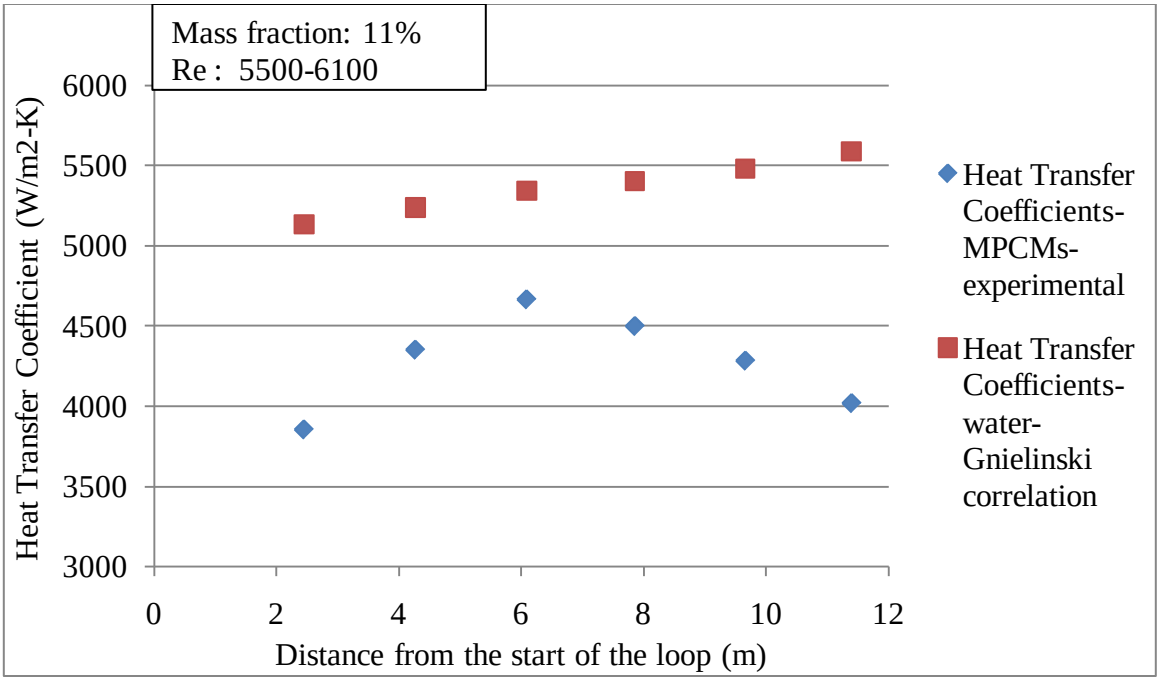

Figure 6.9: Comparison of heat transfer coefficients of water and MPCMs (11 %) at q" = 15.3 kW/m^2 (175 V) and flow rate = 0.12 l/s

From the above plots following observations can be made:

1) Phase change is clearly seen from the temperature plots. The bulk fluid temperature changes its slope when the phase change takes place.

2) A clear increase in local heat transfer coefficient occurs due to phase change. This occurs due to the increase in the effective (apparent) specific heat of the MPCM slurry during phase change.

3) Though the local heat transfer coefficient increases due to phase change, it is still below the heat transfer coefficient value of water.

These observations are in good agreement with the published results [1, 12-13].

b) Comparison of heat transfer coefficients of MPCM slurry under constant heat flux and varying flow rates condition

Heat transfer coefficients of MPCM slurry of (7% and 11% concentration by weight) at constant heat flux and varying flow rates condition are plotted in Figures 6.10 and 6.11 respectively.

MPCM slurry (7% concentration by weight)

Figure 6.10 shows the comparison of heat transfer coefficients of MPCM slurry (7% concentration by wt.) at q"=15.3 kW/m^2 (175 V) for different flow rates.

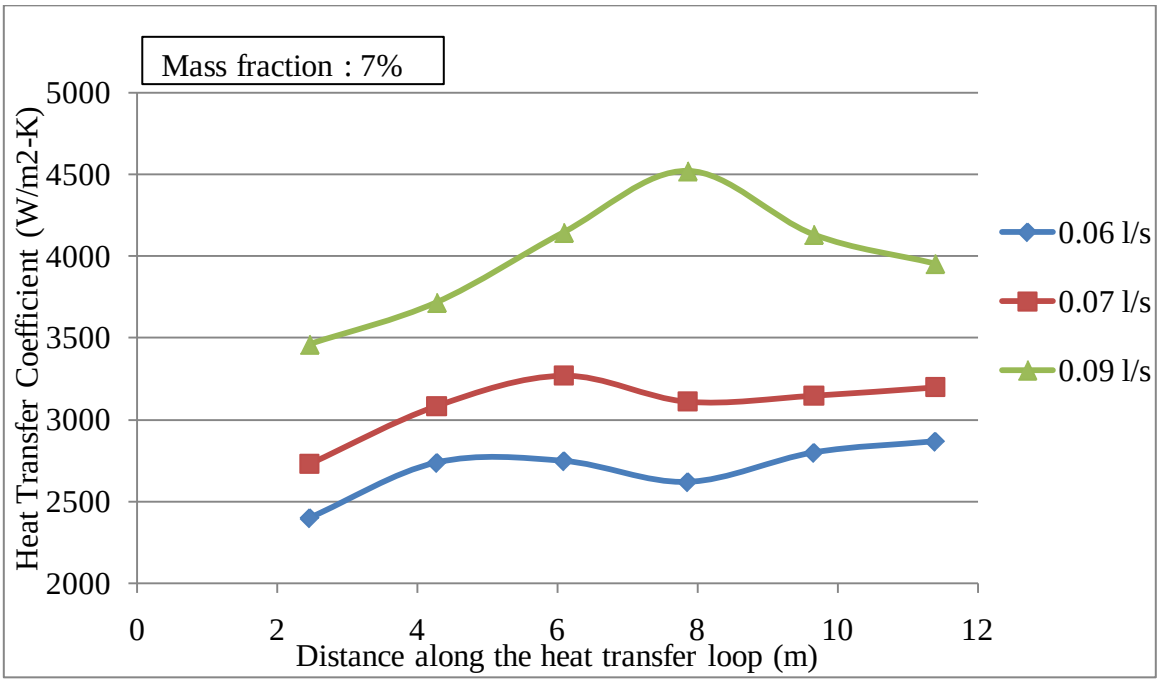

Figure 6.10: Comparison of heat transfer coefficients of MPCM slurry (7% concentration by wt.) at q"=15.3 kW/m^2 (175 V) for different flow rates

MPCM slurry (11% concentration by weight)

Figure 6.11 shows the comparison of heat transfer coefficients of MPCM slurry (11% concentration by wt.) at q"=15.3 kW/m^2 (175 V) for different flow rates.

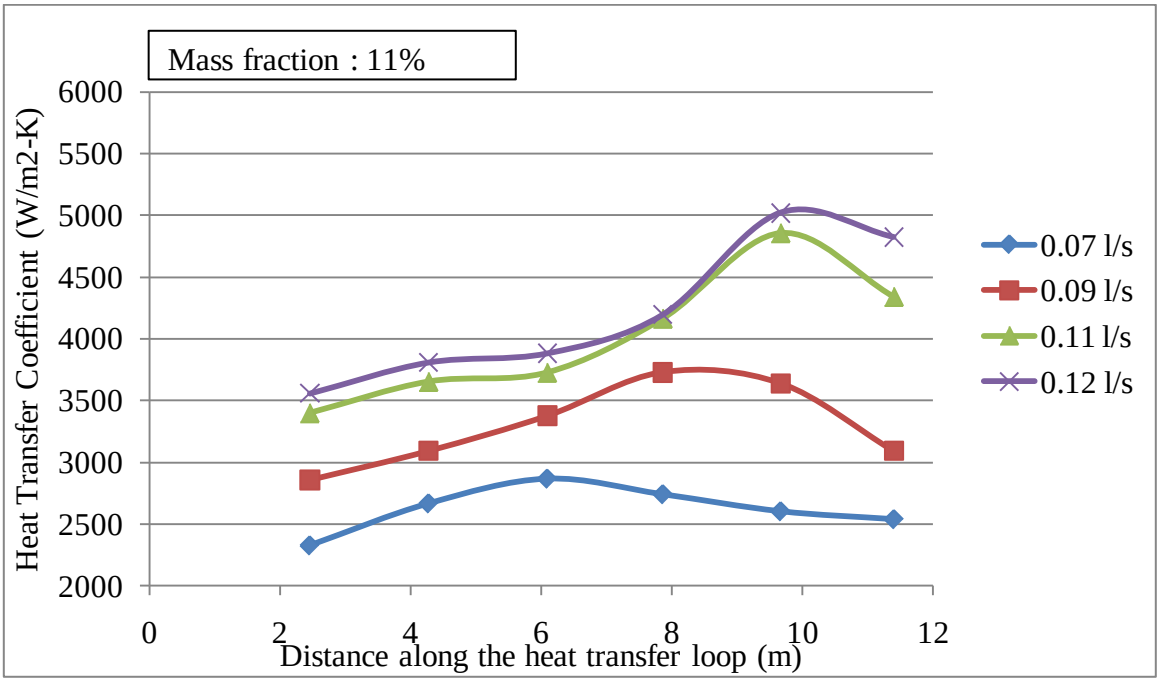

Figure 6.11: Comparison of heat transfer coefficients of MPCM slurry (11% concentration by wt.) at q"=15.3 kW/m^2 (175 V) for different flow rates

From the above plots it can be inferred that

1) Heat transfer coefficient increases with increase in velocity due to increase in turbulence and momentum transfer.

2) As the flow rate increases, the region of phase change moves farther from the start of the loop as expected.

3) The increase in local heat transfer coefficient is slightly higher in the case of higher flow rate or greater velocity of the MPCM slurry.

c) Comparison of heat transfer coefficients of 7% and 11% (concentrations by weight) MPCM slurries under two different sets of same heat flux and different flow rate conditions.

In this case set 1 and set 2 have same heat flux values and different flow rates. Heat transfer coefficients of MPCM slurries of 7% and 11% concentrations by weight under two different sets of same heat flux and different flow rate conditions are plotted in Figure 6.12. The following are the two different sets of different heat flux and different flow rate conditions.

1. Set 1: q"=15.3 kW/m^2 (175 V) & flow rate = 0.07 l/s
2. Set 2: q"=15.3 kW/m^2 (175 V) & flow rate = 0.09 l/s

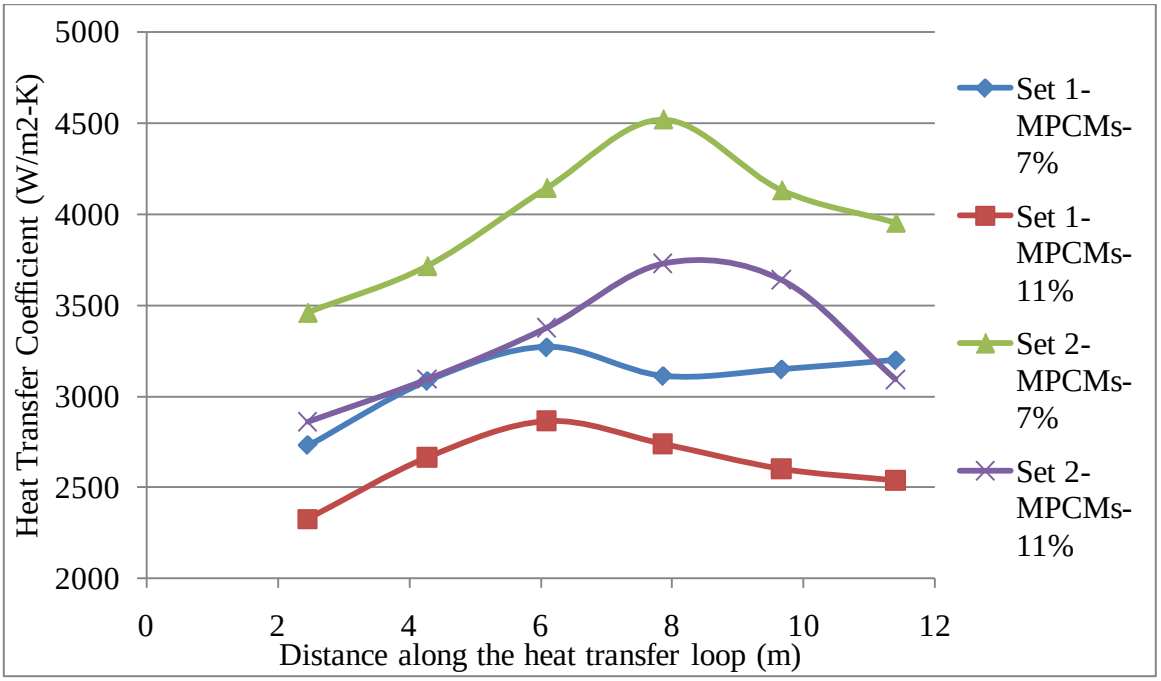

Figure 6.12: Comparison of heat transfer coefficients at q" =15.3 kW/m^2 (175 V) and different flow rates for 7% and 11% conc. of MPCMs

From the above plot it can be concluded that the heat transfer coefficient for 11% MPCM slurry is lower than that for 7% MPCM slurry for same heat flux and same flow rate conditions because at higher concentrations of MPCMs, the flow becomes more laminar due to viscous effects. Similar trends are observed in both sets of experiments.

d) Comparison of heat transfer coefficients of MPCM slurries (7% and 11% concentrations by weight) under four different sets of different heat flux and different flow rate conditions.

In this case all the sets have different heat flux values and different flow rates. Heat transfer coefficients of MPCM slurries of 7% and 11% concentrations by weight under four different sets of different heat flux and different flow rate conditions are plotted in Figure 6.13 and Figure 6.14 respectively.

MPCM slurry (7% concentration by weight)

The following are the four different sets of different heat flux and different flow rate conditions.

1. Set 1: q”=14.7 kW/m^2 (170 V) & flow rate = 0.06 l/s
2. Set 2: q”=14.7 kW/m^2 (170 V) & flow rate = 0.09 l/s
3. Set 3: q”=15.3 kW/m^2 (175 V) & flow rate = 0.06 l/s
4. Set 4: q”=15.3 kW/m^2 (175 V) & flow rate = 0.09 l/s

Figure 6.13 shows the comparison of heat transfer coefficients for 7% (concentration by weight). of MPCM slurry for the above four sets of experimental conditions.

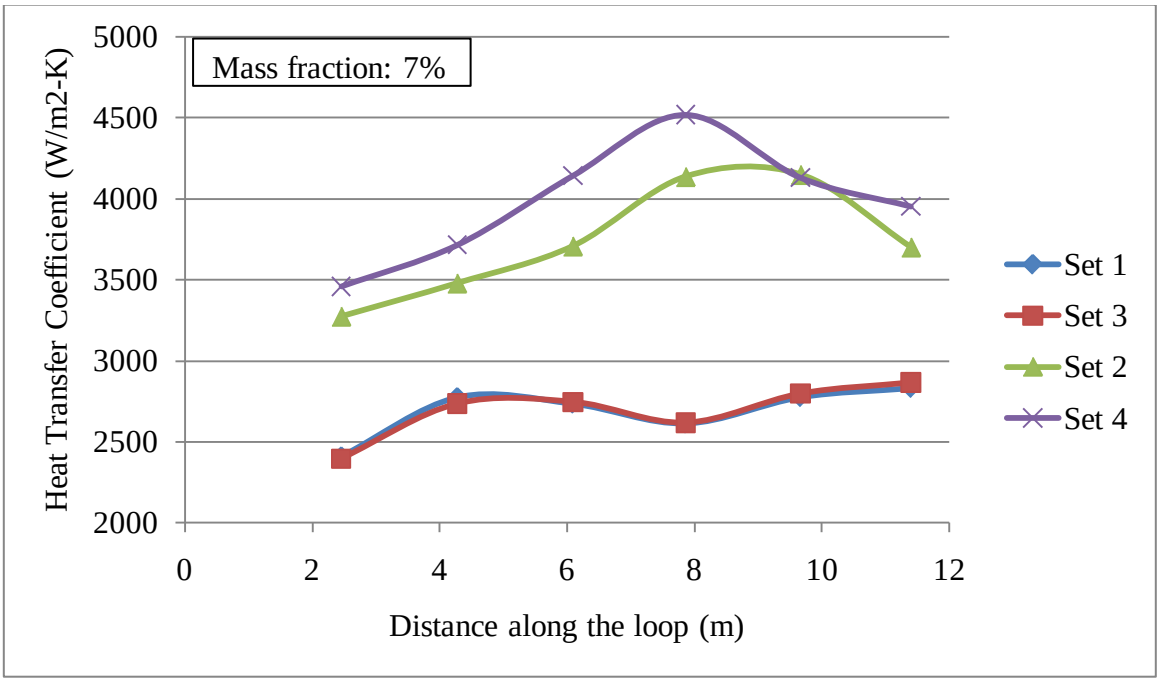

Figure 6.13: Comparison of heat transfer coefficients of MPCM slurry (7% concentration by weight) under four different sets of different heat flux and different flow rate conditions

MPCM slurry (11% concentration by weight)

The following are the four different sets of different heat flux and different flow rate conditions.

1. Set 1: q"=13.6 kW/m^2 (165 V) & flow rate = 0.07 l/s
2. Set 2: q"=13.6 kW/m^2 (165 V) & flow rate = 0.11 l/s

3. Set 3: q”=15.3 kW/m^2 (175 V) & flow rate = 0.07 l/s
4. Set 4: q”=15.3 kW/m^2 (175 V) & flow rate = 0.11 l/s

Figure 6.14 shows the comparison of heat transfer coefficients for 11% (concentration by weight). of MPCM slurry for the above four sets of experimental conditions.

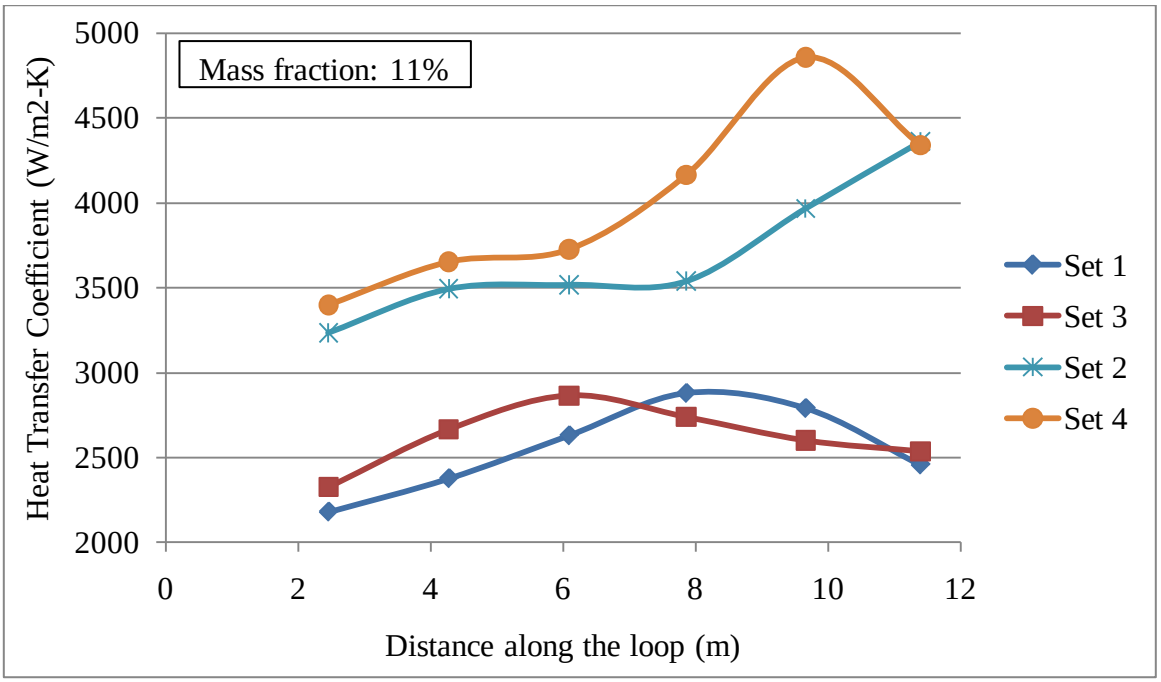

Figure 6.14: Comparison of heat transfer coefficients of MPCM slurry (11% concentration by weight) under four different sets of different heat flux and different flow rate conditions

From the above plots we can infer that

1) The heat transfer coefficients remain more or less constant with change in heat flux at lower flow rates. Impact of heat flux is clearly seen in the cases of higher flow rates.

2) At higher flow rates, a small increase in heat flux translates into a fairy large increase in the heat transfer coefficient when compared to the lower flow rates case

3) Similar trends are observed in both the MPCM slurry concentrations (7% and 11% concentrations by weight). Heat flux has a more significant impact at higher flow rates than at lower flow rates.

4) The effect of flow rate is more intense than the effect of heat flux.

e) Comparison of heat transfer coefficients of 7% and 11% (concentrations by weight) MPCM slurries under two different sets of same heat flux and different Reynolds numbers

Figure 6.15 shows the comparison of heat transfer coefficients of MPCM slurries - 7% and 11% (concentration by wt.) for two different sets of Reynolds numbers at q"=15.3 kW/m^2. The following are the two different sets of different heat flux and different flow rate conditions.

Set 1: q"=15.3 kW/m^2 (175 V) & Re = 3000-4500

Set 2: q"=15.3 kW/m^2 (175 V) & Re = 5000-6000

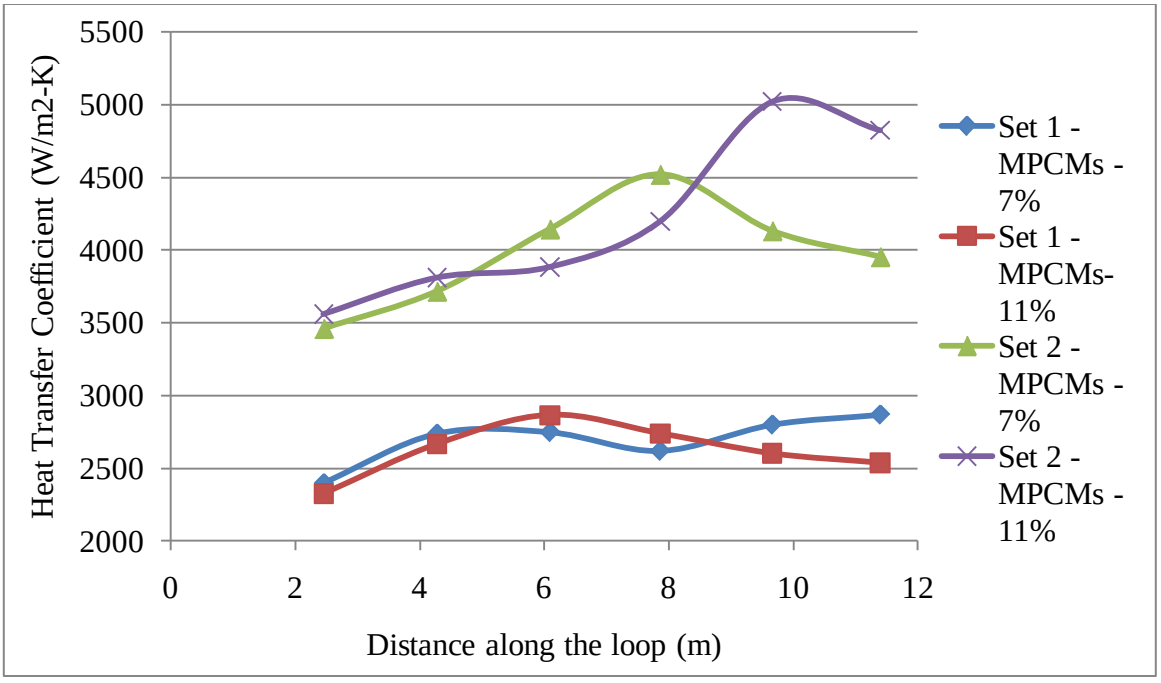

Figure 6.15: Comparison of heat transfer coefficients of MPCM slurries - 7% and 11% (concentration by wt.) for two different sets of Reynolds numbers at q"=15.3 kW/m^2

From the above plot it can be observed that:

1) At same Reynolds number (higher range: Re: 5000-6000) the MPCM slurry with higher concentration has higher heat transfer coefficient augmentation than the lower concentrated MPCM slurry. This is expected since at same Re both the slurries have same level of turbulence. The slurry with greater amount of MPCMs would have higher local heat transfer coefficient increase due to more phase change taking place.

2) At a lower range of Reynolds number (Re: 3000-4500) also, the MPCM slurry with higher concentration has a higher heat transfer coefficient increase, though the increase is not as large as was observed in the higher Reynolds number range.

3) Lower Reynolds number range (3000-4500) indicates the presence of a near laminar (intermediate) flow structure which translates into lower heat transfer coefficient when compared to higher Reynolds number range (5000-6000) results.

All the results obtained are in good agreement with the published results [1, 12-13].

Pressure drop results of MPCMs

The pressure drop of MPCM slurries at 7% and 11% (concentration by weight) are tabulated as shown in Table 6.3. The table also contains pressure drop of water under similar conditions obtained from Darcy-Weisbach equation.

Table 6.3: Comparison of pressure drop of MPCM slurries at 7% and 11% (concentration by wt.) with that of water

Velocity (m/s)	Water (kPa/m)	MPCM slurry (7% by wt) (kPa/m)	MPCM slurry (11% by wt) (kPa/m)
0.8	1.1	1.1	1.0
1.0	1.6	1.4	1.5
1.2	2.4	1.8	2.1
1.3	2.7	2.5	2.6

From the above table one can conclude that:

1) Pressure drop of MPCM slurries (both 7% and 11% conc. by wt.) are lower than that of water. This may be due to the lower density of MPCM slurry when compared with water or by a possible drag reducing effect [1].

2) The pressure drop of 11% conc. MPCM slurry is only slightly higher than that of the 7% conc. slurry.

CHAPTER VII

MULTIWALLED CARBON NANOTUBE FLUIDS

There has been considerable amount of research conducted in the past with different types of nanoparticles in different kinds of base fluids. Different techniques were utilized by different researchers to prepare stable nanofluids. Different measurement methods have been used for determination of various thermal and rheological properties of the nanofluids. Till date, there has been no consensus reached either on the values of thermal properties of nanofluids or their performance in heat transfer. This is due to the fact, that several factors can affect the measured values of the properties of nanofluids, some of which include, size and type of nanoparticles, base fluid used dispersants or surfactants used, mechanical or chemical alterations done on the fluid to achieve stability, measurement techniques and experimental errors associated with them.

Multiwalled carbon nanotubes

Multiwalled carbon nanotubes have been selected for this particular research work since multiwalled carbon nanotubes have high thermal conductivity, do not react with most base fluids, and are relatively inexpensive when compared to single walled carbon nanotubes. Multiwalled carbon nanotubes have been found to increase the thermal conductivity of the base fluid when they were homogeneously dispersed in it

[20-25]. Also since carbon nanotubes have a higher aspect ratio due to their cylindrical structure, they are expected to provide better thermal conductivity enhancement than their spherical counterparts. Spherical alumina particles were tried in earlier research works conducted at our lab, but neither micro fluidization nor ultrasonication techniques could produce stable nanofluids with improved thermal performance in thermal conductivity. Hence multiwalled carbon nanotubes were chosen for further research projects.

Multiwalled carbon nanotubes were purchased from Helix Material Solutions Inc. Different sizes of MWCNTs; both in terms of diameter and length of the nanotubes were purchased. These MWCNTs were dispersed in de ionized water, to produce different samples of nanofluids. DI water was chosen as the base fluid since it is abundantly available, does not react with the MWCNTs and is easy to handle. Gum Arabic was used as the dispersant. Stable carbon nanofluids were prepared using the ultrasonication technique. All the sample nanofluids prepared had 1% (conc. by wt) of MWCNTs, 0.25 % (conc. by wt) of gum Arabic and the rest of it was water. These nanofluids were tested for stability and thermal conductivity.

Stability of carbon nanofluids was determined based on visual inspection. All the prepared nanofluids were stable and there was no visible sedimentation of the nanotubes even after a week of preparation. To find out the best type of MWCNT suitable for this research project, thermal conductivity of the prepared nanofluids was measured in the temperature range of 26-30 °C. This is because our final objective was to combine MPCMs and MWCNTs, and the melting point of octadecane (core part of MPCM

capsule) is in the range of 26-28 ℃. Viscosity was measured only for the best type of MWCNT nanofluid identified from the thermal conductivity tests. Heat transfer tests were then conducted for that nanofluid under different operating conditions to determine the heat transfer coefficient and pressure drop. Before we discuss the thermal conductivity results of carbon nanofluids, the preparation method of carbon nanofluid is discussed.

Carbon nanofluid preparation

The nanofluid preparation technique followed for all types of MWCNTs was similar. The nanofluid preparation technique discussed below involves 60-100 nm diameter sized particles with length ranging from 0.5-40 μm and ultrasonication time of 10 minutes.

Carbon nanofluid preparation involves dispersing carbon nanotubes in a base fluid such as de ionized water, ethylene glycol, etc. To disperse carbon nanotubes in DI water, some kind of dispersant or surfactant is needed, since carbon nanotubes are non-polar and do not have any affinity towards polar substances like water. In this particular case, gum Arabic was used as the surfactant since it has been proved in earlier studies that gum Arabic produces highly stable suspensions with minimal adverse effect on the properties of carbon nanotubes.

a) Specifications of the constituents of Carbon nanofluid

High quality de ionized water of resistivity 18.2 mega ohms-cm is used as the base fluid in this carbon nanofluid preparation. Carbon nanotubes have been purchased from Helix Material Solutions. These CNTs have diameter in the range 60-100 nm and length in the range 0.5-40 micro meters. The purity of CNTs in the package is greater than 95%. Gum Arabic has been purchased from Fluka. It is in the form of a fine powder.

b) Determination of the weight of the constituents of Carbon nanofluid

Firstly, we had to determine the amount of CNTs and gum Arabic required for the carbon nano fluid. In this preparation, we dispersed 1% (by weight) CNTs using 0.25% gum Arabic (by weight) in DI water. To prepare a 300 gm sample of carbon nano fluid, the split up of the weights of the constituents is shown in Table 7.1 below.

Table 7.1: Constituents of MWCNT nanofluid

Sno.	**Constituent**	**% by weight**	**Actual weight in grams**
1	Carbon nanotubes	1.00	3.00 g
2	Gum Arabic	0.25	0.75 g
3	DI water (base fluid)	98.75	296.25 g

Using a highly sensitive weighing scale (accurate up to fourth decimal place), the individual components were weighed and kept aside.

c) Procedure for the dispersion of CNTs in the base fluid

Pour the measured amount of DI water into a cylindrical beaker of sufficient capacity. Add the measured amount of gum Arabic to the DI water. Using a magnetic stirrer, stir the mixture until the gum Arabic dissolves completely and nothing is visible to the naked eye. Gum Arabic is usually sticky and it might stick to the walls or the bottom of the beaker. In that case, use a clean glass stir rod to stir the mixture manually till the gum Arabic dissolves entirely. This process usually takes about 15-20 minutes to complete (depends on the amount of water and gum Arabic).

After the gum Arabic has been dissolved completely, the measured amount of CNTs is added to the solution. The mixture is stirred for 5 minutes using a magnetic stirrer. The mixture is then ultrasonicated for 5 minutes using an ultrasonic probe (VCX-130 PB, Sonics & Materials Inc.). The amount of energy that is delivered to the mixture can be controlled using the amplitude settings of the ultrasonic probe. For this particular preparation, the amplitude was set to 100%. The amount of energy delivered to the mixture during the 5 minutes of ultrasonication can be read from the display of the ultrasonic machine. Note down the amount of energy delivered in Joules.

If we need to ultrasonicate the mixture for more time, then we need to stir the mixture for 5 minutes using a magnetic stirrer before continuing with the ultrasonication process. This process of alternating magnetic stirring and ultrasonication (each for a time period of 5 minutes) must be continued till the desired amount of ultrasonication has been done on the mixture. The mixture is then stored in an air-tight glass bottle to prevent contamination and evaporation.

d) Ultrasonication

Ultrasonication is a process in which alternating low-pressure and high pressure waves are produced in the liquid mixture that causes formation and collapse of small vacuum bubbles. This produces high speed impinging liquid jets and strong hydro dynamic shear forces that is useful for de-agglomeration and milling of nanoparticles in the mixture. The process of ultrasonication disentangles the carbon nanotubes from their bundles and allows for uniform dispersion in the mixture. But ultrasonication also breaks the carbon nanotubes along their length which adversely affects the properties of the nanotubes. Also, the mixture gets heated up very quickly as a large amount of energy is dispersed in a very small area. Hence it is usually done for 5 minutes and then magnetically stirred for 5 minutes, so that the heat can be dissipated before continuing with further ultrasonication. Also it is important to determine the optimum duration of the total ultrasonication time so as to achieve a uniform dispersion with minimal adverse effect on the properties of CNTs.

e) Energy density of the mixture

The energy density of the mixture can be calculated by dividing the total energy supplied to the mixture during ultrasonication by the weight of the mixture. This parameter facilitates the determination of the optimum energy density for a carbon nanofluid (for a particular combination of base fluid and CNTs).

f) Precautions to be taken during the preparation of the carbon nanofluid

1. Care should be taken to prevent evaporation of DI water from the mixture during the magnetic stirring and ultrasonication processes.
2. Contamination of CNTs should be avoided. They should be handled under a fume hood if possible, so that their loss or contamination can be prevented.
3. It is advisable to use a face mask and gloves when handling CNTs, though no adverse health effects due to these particles have been reported in literature.

Thermal conductivity of nanofluids

Different diameters and lengths of CNTs were used to make different samples of nanofluids. These samples were ultrasonicated for different amounts of time to examine the effect of ultrasonication on the thermal conductivity. The transient hot wire apparatus was used to measure the thermal conductivity of carbon nanofluids. The description and the method of measurement of thermal conductivity using THW were discussed in the chapter – Measurement of thermal conductivity and viscosity. Thermal conductivity was measured at different temperatures using a chiller to control the temperature of the fluid. Each measurement was repeated several times. Though slight changes were observed in measurements every time, they were within the limits of the accuracy of the THW. The results of thermal conductivity are presented below.

Four different types of MWCNTs were initially tested. Two samples had 60-100 nm diameter CNTs and the other two samples had 10-30 nm diameter CNTs. The two 60-100 nm diameter samples had different lengths of CNTs, one had 1-2 μm long CNTs

and the other had 0.5-40 µm long CNTs. The two 10-30 nm diameter sized CNT samples also varied in the length of their CNTs as mentioned above. Table 7.2 below compares the thermal conductivity of CNT nanofluids with CNTs of different diameters and lengths.

Table 7.2: Comparison of thermal conductivity of CNT nanofluids with different diameters and lengths of CNTs

Sno.	Diameter of CNTs (nm)	Length of CNTs (µm)	Ultrasoni-cation time (min)	Mass fraction of CNTs (%)	Temper-ature (°C)	Thermal conductivity (W/m-K)	Enhance--ment in thermal conductivity (%)
1.	60-100	1-2	20	1.0	28	0.638	4.12
					30	0.646	5.00
					32	0.655	**5.80**
2.	60-100	0.5-40	20	1.12	28	0.631	2.85
					30	0.649	5.03
					32	0.677	**8.47**
3.	10-30	1-2	20	1.00	28	0.629	2.69
					33	0.641	**3.34**
4.	10-30	0.5-40	40	1.00	25	0.609	0.26
					31	0.636	3.05
					34	0.650	**4.49**
Note: 10-30 nm(dia) and 0.5-40 µm(length) type of CNTs had been tested earlier by Garg et al. [8] and it was found that 40 minutes of ultrasonication time (UST) was the optimum time for that particular type of CNTs. Hence the samples were ultrasonicated for 40 minutes instead of 20 min of UST used in other cases.							

It was observed that longer CNTs with larger diameter nanotubes yielded higher thermal conductivity in the range of 28-32 °C. Further thermal conductivity tests were

conducted for 60-100 nm (dia) and 0.5-40 µm (length) type of CNT nanofluids. Ultrasonication times of 10, 20, 30 and 40 minutes were chosen to determine the optimum ultrasonication time for this type of CNTs. Table 7.3 shows the thermal conductivity values of CNT fluids with 60-100 nm dia and 0.5-40 µm long CNTs for different ultrasonication times (10-40 min).

Table 7.3: Comparison of thermal conductivity of CNT nanofluids with 60-100 nm diameter and 0.5-40 µm long CNTs for different ultrasonication times (10-40 min)

Sno.	Diam--eter of CNTs (nm)	Length of CNTs (µm)	Ultrasonic--ation time (min)	Mass fraction of CNTs (%)	Temperature (°C)	Thermal conduct--ivity (W/m-K)	Enhance--ment in thermal conductivity (%)
1.	60-100	0.5-40	10	1.02	28	0.646	5.59
					30	0.662	7.54
					32	0.671	**8.45**
2.	60-100	0.5-40	20	1.12	28	0.631	2.85
					30	0.649	5.03
					32	0.677	**8.47**
3.	60-100	0.5-40	30	1.24	28	0.624	1.91
					30	0.635	3.04
					32	0.654	**5.28**
4.	60-100	0.5-40	40	1.16	28	0.618	1.01
					30	0.627	1.86
					32	0.639	**3.04**

Ultrasonication times of 5, 10, 15 and 20 minutes were chosen for the next set of experiments since the maximum k obtained was at 20 minutes of ultrasonication as seen from the results of the above set of experiments. Table 7.4 below shows the thermal conductivity values of CNT nanofluids with 60-100 nm diameter and 0.5-40 μm long CNTs for different ultrasonication times (5-20 min).

Table 7.4: Comparison of thermal conductivity of CNT nanofluids with 60-100 nm diameter and 0.5-40 μm long CNTs for different ultrasonication times (5-20 min)

Sno	Diameter of CNTs (nm)	Length of CNTs (μm)	Ultrasoni-cation time (min)	Mass fraction of CNTs (%)	Temper-ature (°C)	Thermal conductivity (W/m-K)	Enhancement in thermal conductivity (%)
1.	60-100	0.5-40	5	0.94	28	0.62	1.28
					30	0.633	2.65
					32	0.648	**4.51**
2.	60-100	0.5-40	10	1.1	28	0.634	3.49
					30	0.649	5.12
					32	0.676	**8.37**
3.	60-100	0.5-40	15	1.08	28	0.627	2.42
					30	0.642	4.06
					32	0.666	**7.07**
4.	60-100	0.5-40	20	1.14	28	0.632	3.19
					30	0.648	4.9
					32	0.664	**6.8**

The optimum ultrasonication time was found to be 10 minutes. Thermal conductivity was measured again for the sample with 10 minutes of ultrasonication time

to conclude that this was the optimum ultrasonication time for this particular batch of CNTs. These results are tabulated in Table 7.5 below.

Table 7.5: Measurement of thermal conductivity of 60-100 nm dia and 0.5-40 µm long CNT fluid at an ultrasonication time of 10 minutes

Sno	Diameter of CNTs (nm)	Length of CNTs (µm)	Ultrasoni-cation time (min)	Mass fraction of CNTs (%)	Tempera--ture (°C)	Thermal conductivity (W/m-K)	Enhancement in thermal conductivity (%)
1.	60-100	0.5-40	10	1.07	28	0.635	3.54
					30	0.653	5.59
					32	0.674	**8.11**

Viscosity of nanofluids

Viscosity has been measured for the 60-100 nm (dia) and 0.5-40 µm CNT fluid with ultrasonication time of 10 minutes because this was the batch that showed the greatest enhancement in thermal conductivity in the 28-32 °C range. The viscosity of the CNT fluid was measured at different shear rates and temperatures, the results of which are tabulated in Figure 7.6. Figure 7.1 shows the viscosity vs. shear rate plot of the CNT fluid at different temperatures and Figure 7.2 shows the viscosity vs. temperature plot of the CNT fluid at different shear rates.

Table 7.6: Comparison of viscosity of CNT fluid at different temperatures and shear rates

Diameter of CNTs (nm)	Length of CNTs (µm)	Mass fraction of CNTs (%)	Ultrasoni -cation time (min)	Temperature (°C)	Shear rate (rpm)	% Torque	Viscosity (cP)
60-100	0.5-40	1.07	10	28	50	13	1.57
					60	14.5	1.45
					100	22.2	1.33
				30	50	12.2	1.47
					60	13.8	1.38
					100	21.7	1.30
				32	50	12.6	1.52
					60	14.4	1.44
					100	22.1	1.33

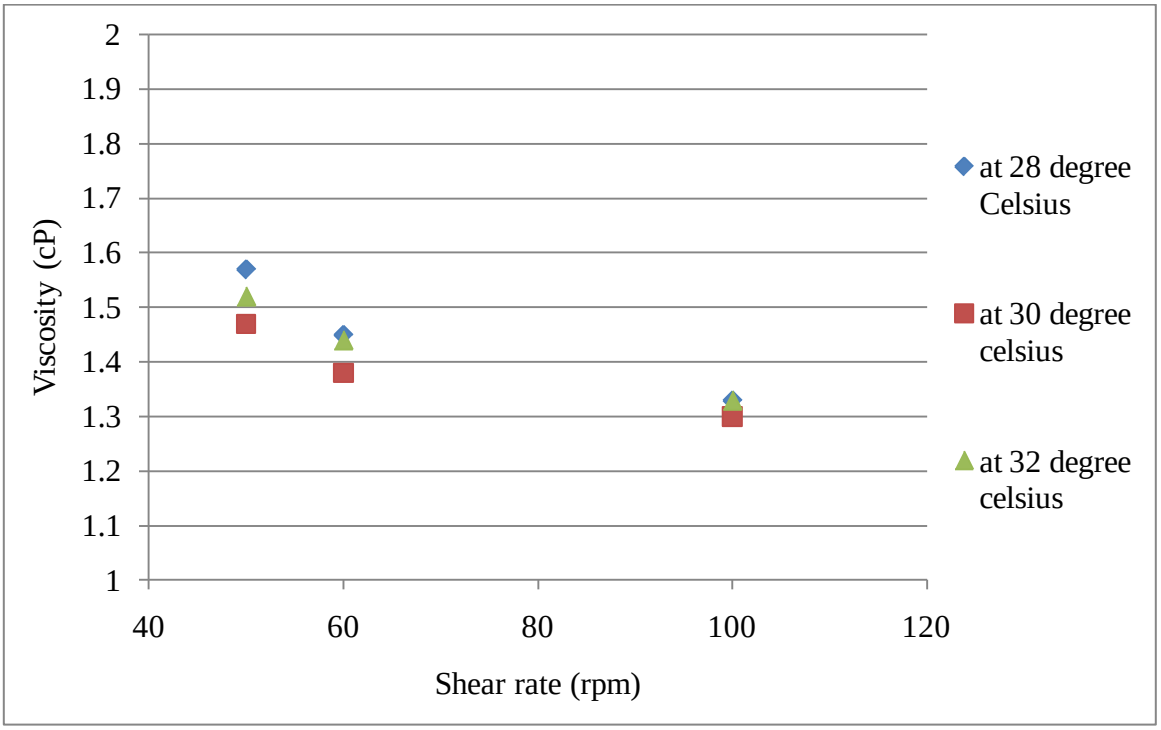

Figure 7.1: Viscosity vs. shear rate of CNT fluid at different temperatures

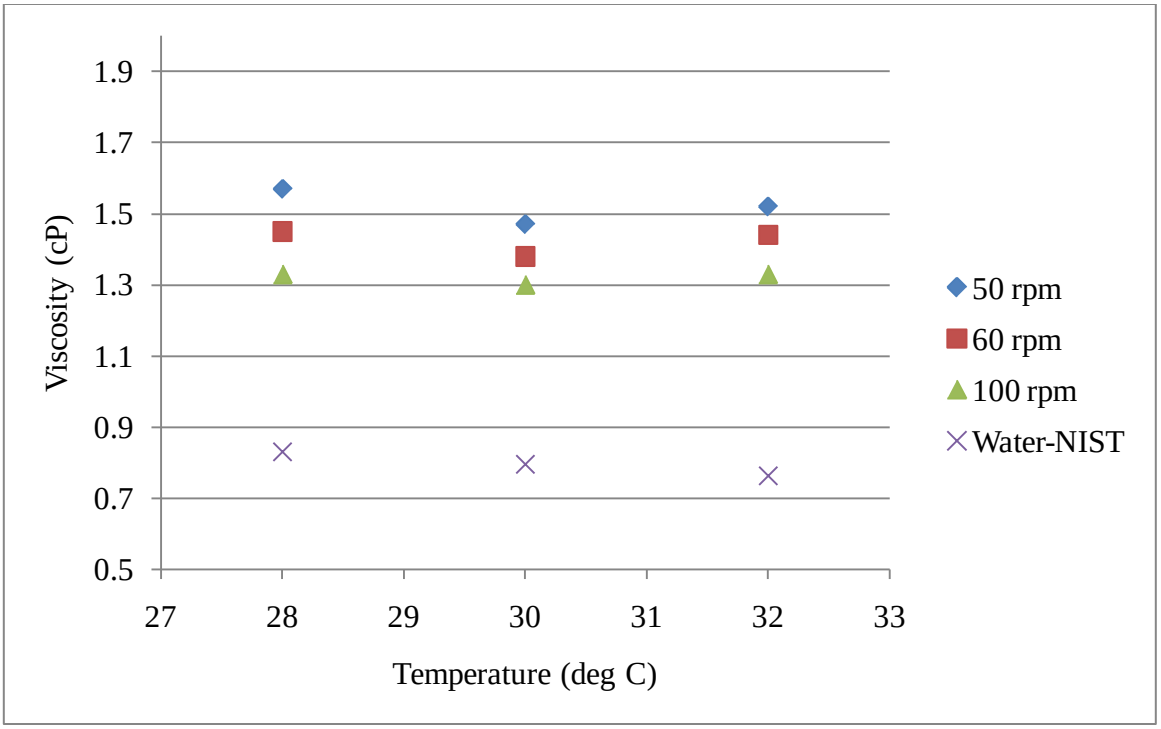

Figure 7.2: Viscosity vs. temperature plot of the CNT fluid at different shear rates.

From the above tests, it can be concluded that the CNT fluid shows a slight shear thinning (non-Newtonian) behavior, and the viscosity remains more or less constant in the selected temperature range. The viscosity of CNT fluid is higher than that of water (1 cP).

Heat transfer results of nanofluids

Heat transfer tests were conducted on two different concentrations of CNT fluid (0.5% and 1.1% by wt.) under turbulent flow and constant heat flux conditions. Tests were conducted at three different heat flux values and flow rates. The percentage

increase in heat transfer coefficients of the CNT fluid when compared to that of water, under similar conditions, (from Gnielinski correlation) are plotted.

a) Comparison of percentage increase in heat transfer coefficients of MWCNT fluids (0.5% and 1.1% concentration by wt.) to that of water under similar heat flux and flow rate conditions

MWCNT fluid (0.5% concentration by wt.)

Figure 7.3 below compares the % increase in *h* of 0.5% (by weight) MWCNT fluid compared to water at q" = 11.64 kW/m^2 (155 V) and flow rates = 0.07 l/s, 0.09 l/s and 0.11 l/s.

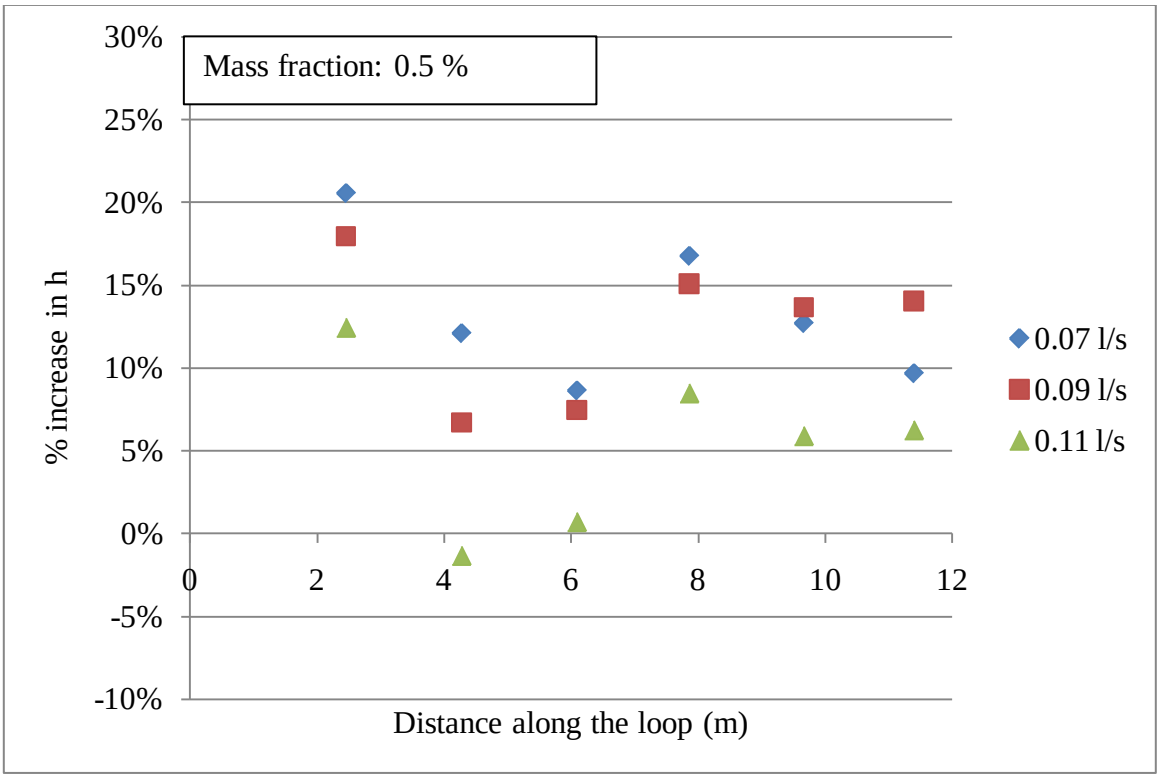

Figure 7.3: Comparison of % increase in *h* of 0.5% MWCNT fluid compared to water at q" = 11.64 kW/m^2 (155 V) and different flow rates

MWCNT fluid (1.1% concentration by wt.)

Figure 7.4 below compares the % increase in *h* of 1.1% (by weight) MWCNT fluid compared to water at q" = 11.64 kW/m^2 (155 V) and flow rates = 0.07 l/s, 0.09 l/s and 0.11 l/s.

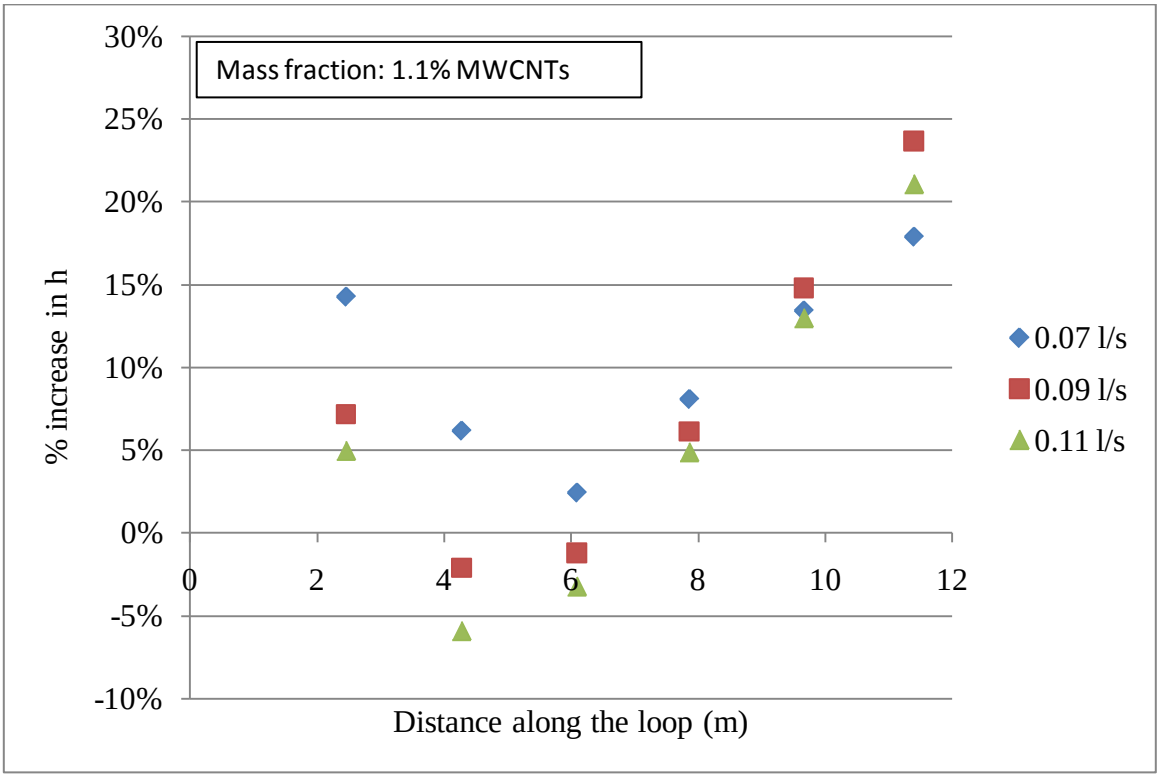

Figure 7.4: Comparison of % increase in *h* of 1.1% MWCNT fluid compared to water at q" = 11.64 KW/m^2 (155 V) and different flow rates

From the above plots we can observe that the maximum enhancement in the heat transfer coefficient for the case with 0.5% (by weight) MWCNTs is 20%, and the maximum enhancement for the case with 1.1% (by weight) MWCNTs is 25%. In the first case, the enhancement decreases until the middle of the loop and then stabilizes to a constant value. In the second case, the enhancement decreases until the middle of the

loop and then increases again. The final enhancement reached at the end of the loop is slightly lower in case of 0.5% CNTs and is higher in the case of 1.1% CNTs. % enhancement decreases with increase in flow rate.

b) Comparison of percentage increase heat transfer coefficients of MWCNT fluids (0.5% and 1.1% concentration by wt.) to that of water under similar heat flux and flow rate conditions

MWCNT fluid (0.5% concentration by wt.)

Figures 7.5 below compares the % increase in *h* of 0.5% (by weight) MWCNT fluid compared to water at q" = 13.4 kW/m^2 (165 V) and flow rates = 0.07 l/s, 0.09 l/s and 0.11 l/s.

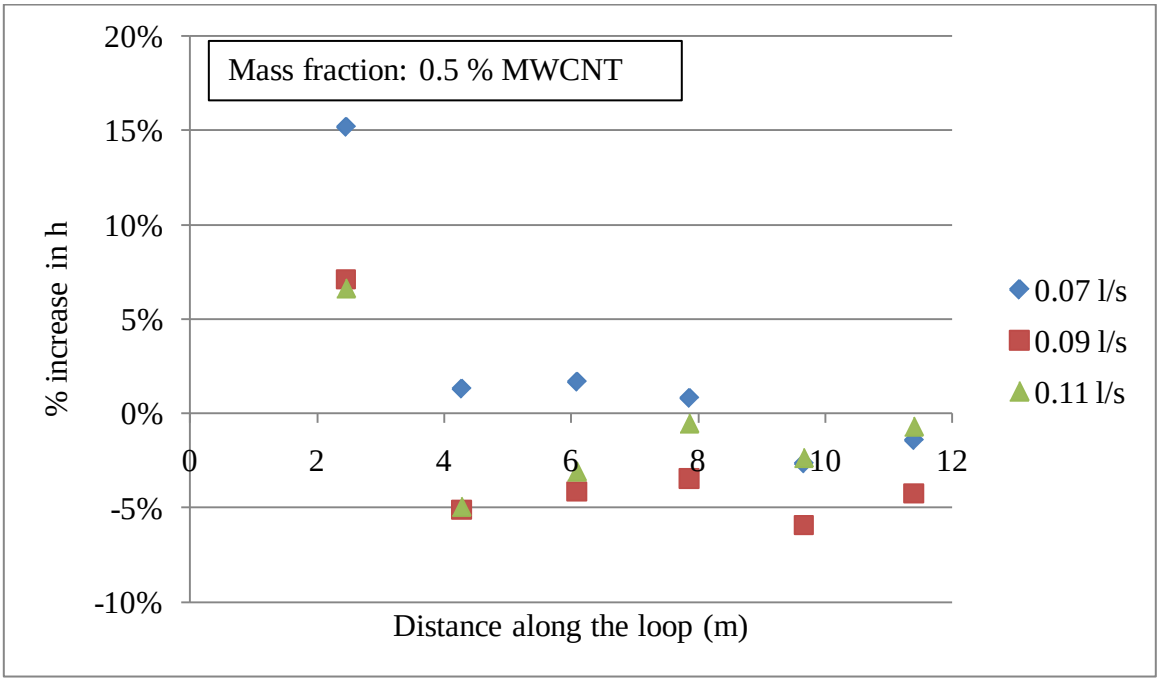

Figure 7.5: Comparison of % increase in *h* of 0.5% MWCNT fluid compared to water at q" = 13.4 KW/m^2 and different flow rates

MWCNT fluid (1.1% concentration by wt.)

Figures 7.6 below compares the % increase in *h* of 1.1% MWCNT fluid compared to water at q" = 13.4 kW/m^2 (165 V) and flow rates = 0.07 l/s, 0.09 l/s and 1.16 m/s.

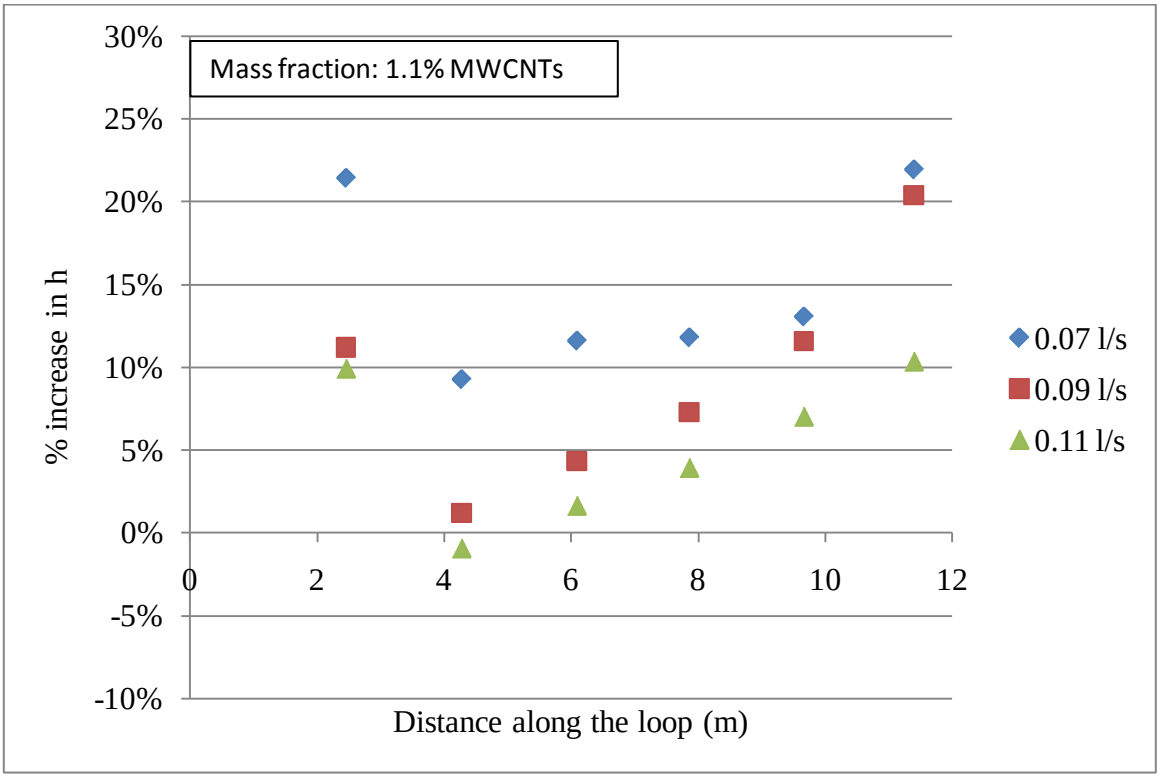

Figures 7.6: Comparison of % increase in *h* of 1.1% MWCNT fluid compared to water at q" = 13.4 kW/m^2 (165 V) and different flow rates

The maximum enhancement in the heat transfer coefficient for the case with 0.5% MWCNTs is 15% and the maximum enhancement for the case with 1.1% MWCNTs is 22.5%. In the first case, the enhancement decreases until one third of the

distance of the loop and then stabilizes to a constant value. In the second case, the enhancement decreases until one third of the distance of the loop and then increases again. The final enhancement reached at the end of the loop is lower in case of 0.5% CNTs and is higher in the case of 1.1% CNTs. % enhancement decreases with increase in flow rate.

c) Comparison of percentage increase heat transfer coefficients of MWCNT fluids (0.5% and 1.1% concentration by wt.) to that of water under similar heat flux and flow rate conditions

MWCNT fluid (0.5% concentration by wt.)

Figures 7.7 below compares the % increase in *h* of 0.5% MWCNT fluid compared to water at q" = 14.8 kW/m^2 (175 V) and flow rates = 0.07 l/s, 0.09 l/s and 0.11 l/s.

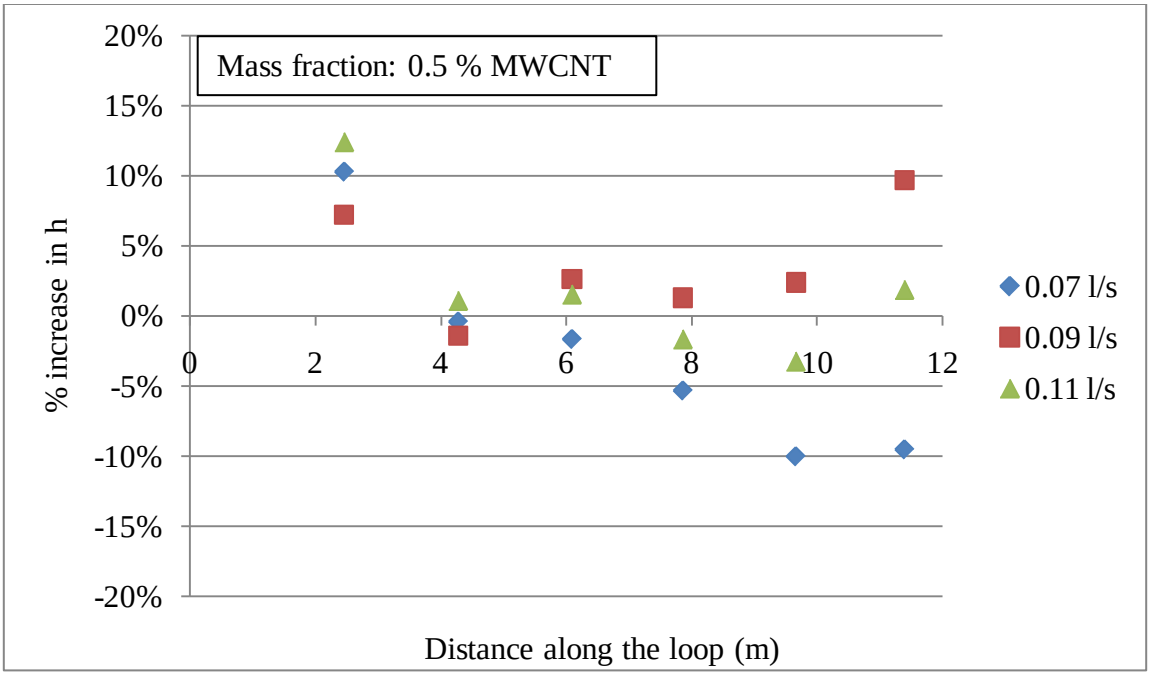

Figure 7.7: Comparison of % increase in *h* of 0.5% MWCNT fluid compared to water at q" = 14.8 kW/m^2 (175 V) and different flow rates

MWCNT fluid (1.1% concentration by wt.)

Figures 7.8 below compares the % increase in *h* of 1.1% MWCNT fluid compared to water at q" = 14.8 kW/m^2 (175 V) and flow rates = 0.07 l/s, 0.09 l/s and 0.11 l/s.

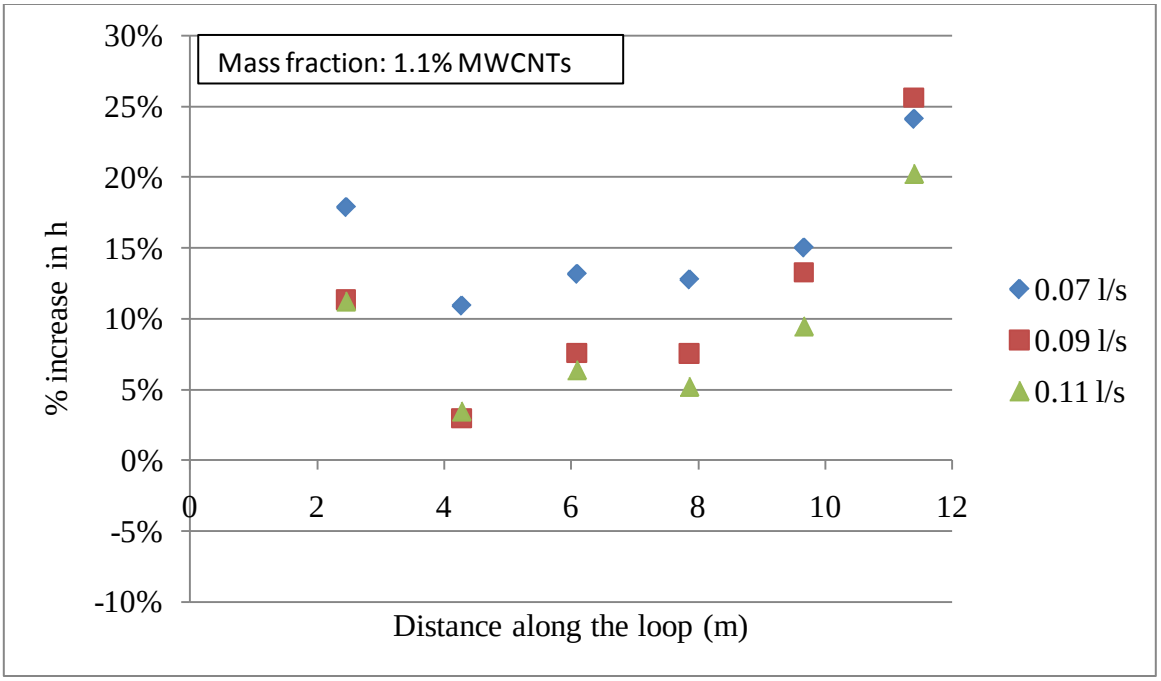

Figure 7.8: Comparison of % increase in *h* of 1.1% MWCNT fluid compared to water at q" = 14.8 kW/m^2 (175 V) and different flow rates

The maximum enhancement in the heat transfer coefficient for the case with 0.5% MWCNTs is 12.5% and the maximum enhancement for the case with 1.1% MWCNTs is 25%. In the first case, the enhancement decreases until about one third of the distance of the loop and then stabilizes to a constant value. In the second case, the enhancement decreases until one third of the distance of the loop and then increases again. The final enhancement reached at the end of the loop is slightly lower in case of 0.5% CNTs and is higher in the case of 1.1% CNTs. % enhancement decreases with increase in flow rate.

Observations from the above plots can be summarized as below:

1) For the MWCNT nanofluid (0.5% conc, by wt) the % enhancement of the maximum heat transfer coefficient value dropped from 20% to 12.5% as the heat flux value increased.

2) For the MWCNT fluid (1.1% conc. by wt) the % enhancement of the maximum heat transfer coefficient value remained more or less constant at 25%.

3) In all the plots, the heat transfer coefficient enhancement decreases with increase in flow rate. This could be due to the realignment of the clusters of MWCNTs in high turbulence conditions. Also, it appears that MWCNT stuck to the surfaces unevenly which could explain why the heat transfer coefficient changes along the heat transfer loop. Furthermore, MWCNT stuck to the surfaces seemed to affect the behavior of the hydrodynamic boundary layer at higher Reynolds number. It is suggested that aggregation or networking of nanotubes along with changes in flow structure may be a mechanism for heat transfer enhancement.

4) In all the plots, the enhancement in heat transfer coefficient decreases, reaches a minimum and then increases again. This suggests two possibilities a) the thermal entry length region may have been lengthened and this could be a probable reason for the high enhancement percentages observed in the starting of the loop. b) When the MWCNT fluid was filled in the heat transfer loop for the first time, a lot of MWCNTs may have stuck on the inner wall of the copper tube thus contributing to increase in heat transfer through enhancement in thermal conductivity.

d) Effect of CNTs on the copper pipes

To test for the effect of CNTs on the surface of copper pipes, two sets of experiments were conducted with 0.5% (by wt) CNT fluid under similar conditions. There was a gap of 15 days between the two sets of experiments. The first set of experiments was conducted when the CNT fluid was filled in the heat transfer loop for the first time and the copper pipe surfaces were wetted with CNT nanofluid for not more than an hour. The second test of experiments was conducted after a gap of 15 days and during that period the CNT fluid was in contact with the copper pipe surfaces all the time. The plots shown in Figure 7.9 and Figure 7.10 below suggest that the CNT fluid has very little effect on the surface of the copper pipes and almost similar trends and enhancements are seen in both sets of experimental results.

Figure 7.9 below compares the % increase in *h* of 0.5% MWCNT fluid compared to water at q" = 11.6 kW/m^2 (155 V) and flow rates = 0.07 l/s, 0.09 l/s and 0.11 l/s at the beginning of the 15 day test period.

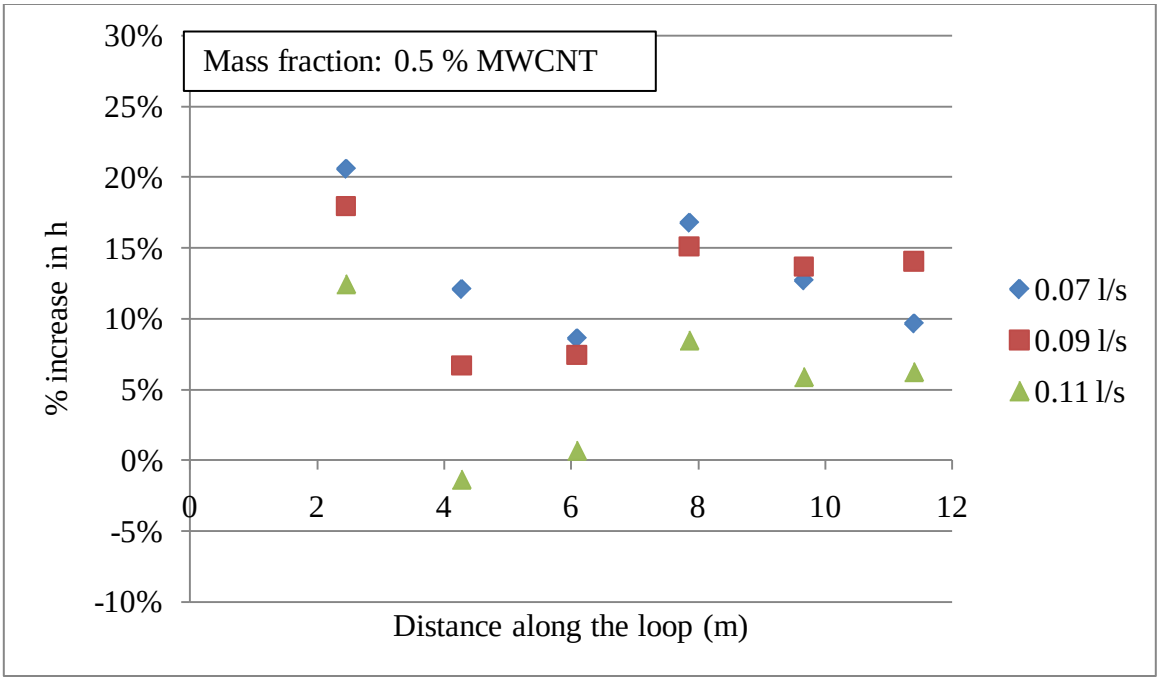

Figure 7.9: Comparison of % increase in *h* of 0.5% MWCNT fluid compared to water at q" = 11.6 kW/m^2 (155 V) and different flow rates at the beginning of the 15 day test period

Figure 7.10 below compares the % increase in *h* of 0.5% MWCNT fluid compared to water at q" = 11.6 kW/m^2 (155 V) and flow rates = 0.07 l/s, 0.09 l/s and 0.11 l/s at the end of the 15 day test period.

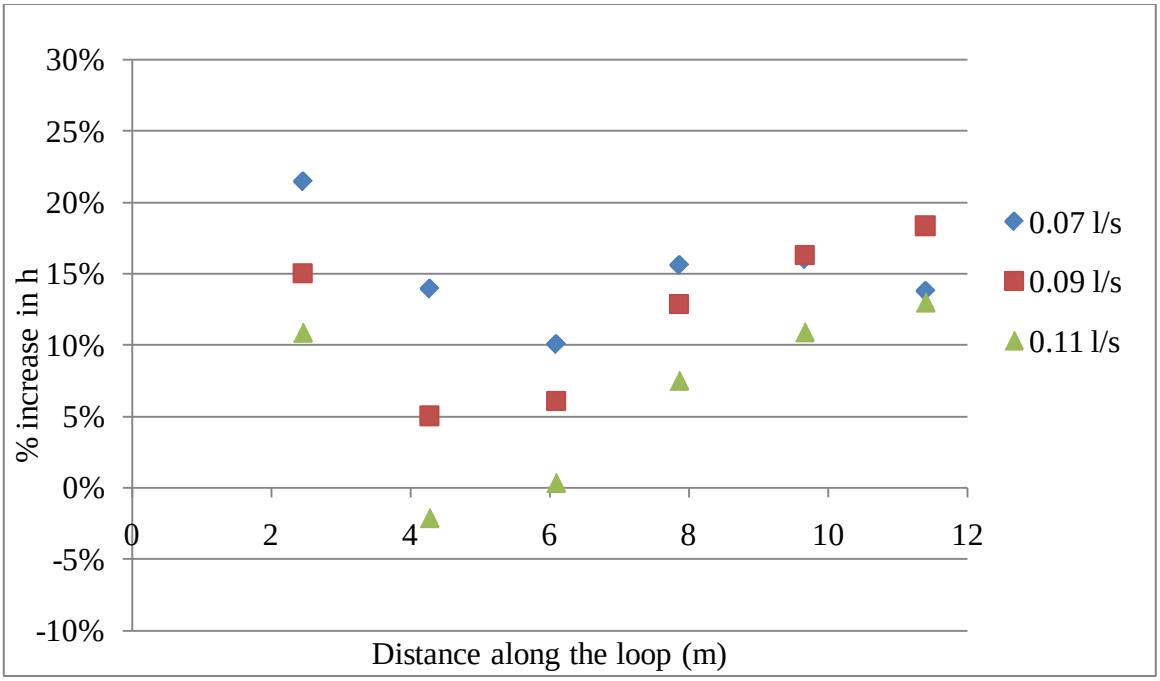

Figure 7.10: Comparison of % increase in *h* of 0.5% MWCNT fluid compared to water at q" = 11.6 kW/m^2 (155 V) and for different flow rates at the end of the 15 day test period

From the above test, it can be concluded that

1) No significant changes in the heat transfer coefficients of MWCNT fluid are observed.

2) The peaks and lows of both plots look similar.

3) The trend of decrease in heat transfer coefficient enhancement with increase in flow rate also remains the same in both cases. Thus we can conclude that the CNT fluid did not affect the inner wall of the copper tubing by means of MWCNT deposits.

e) Durability of CNTs under continuous pumping

The 0.5 % CNT fluid was subjected to 4 hours of continuous pumping under a heat flux of 13.4 kW/m^2 (165 V) and a flow rate of 0.09 l/sec. Data was collected at the start and the end of the test. The % enhancement in *h* at these two times was then compared.

Figure 7.11 below shows the comparison of % increase in *h* of 0.5% (by weight) MWCNT fluid at the start and end of long term tests at q"= 13.4 kW/m^2 and flow rate = 0.09 l/s.

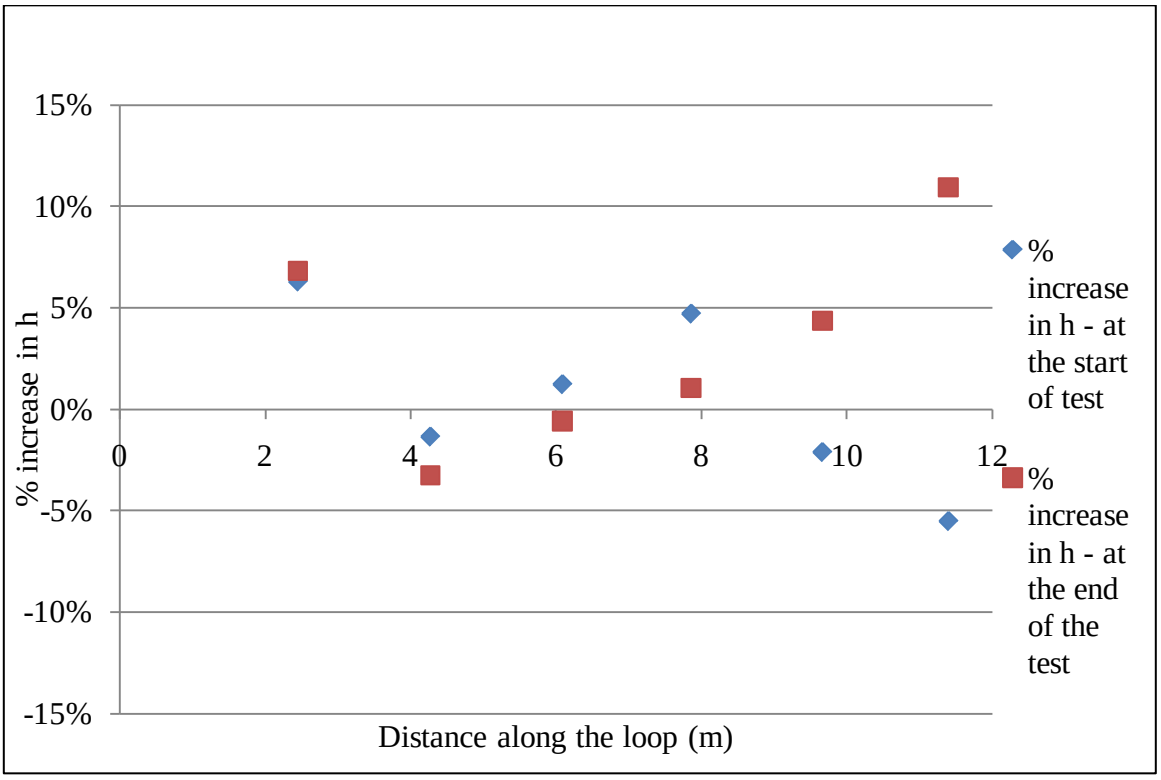

Figure 7.11: Comparison of % increase in *h* of 0.5% MWCNT fluid at the start and end of long term tests at q"= 13.4 kW/m^2 and flow rate = 0.09 l/s

The above plot shows that the enhancements at the start of the loop are similar but the enhancement seems to increase with time for the later sections of the loop. The % enhancement reaches a maximum of 11% for the end of test case. This could be possibly due to the redistribution of the CNTs on the tubing surfaces in the heat transfer loop along their longitudinal axis after such a long time of pumping. Since the thermal conductivity of CNTs is maximum along their longitudinal axis, this could have affected the heat transfer rate and possibly resulted in an enhancement which was observed at the end of the test.

Pressure drop of nanofluids

The pressure drop of MWCNT fluid (0.5% and 1.1% concentration by wt) is compared to that of water in as shown in Table 7.7.

Table 7.7: Pressure drop of MWCNT fluid (0.5% and 1.1% conc. by wt) compared with water

Velocity (m/s)	Water (kPa/m)	MWCNTs (0.5%) (kPa/m)	MWCNTs (1.1%) (kPa/m)
0.72	1.18	5.5	5.2
0.97	1.6	6.0	6.1
1.16	2.4	6.1	6.6

The pressure drop of MWCNT fluid is significantly higher than that of water under similar conditions. The pressure drop of 0.5% and 1.1% concentrated MWCNT fluids are almost similar. The increased pressure drop can be attributed to higher increase viscosity of the MWCNT fluid when compared to that of water, and greater (apparent) friction factor due to MWCNTs getting stuck on the tubing surfaces. In the turbulent flow region, roughness is a very important factor.

CHAPTER VIII

BLEND OF MICROENCAPSULATED PHASE CHANGE MATERIAL SLURRY AND MULTIWALLED CARBON NANOTUBE FLUID

A blend of microencapsulated phase change material slurry and multiwalled carbon nanotube fluid was prepared based on the results of a numerical simulation developed by Taherian and Alvarado [26]. The numerical simulation investigated the potential benefits of blending MPCMs with MWCNT nanofluid. A computer code was written which revealed that the best composition for a blend depended on the actual percentage of phase change that took place during the process. Simulations were performed on a concentric tube heat exchanger taking into account various thermal properties. The simulations results suggested that a 1% MWCNT and 10% MPCM slurry should be prepared to obtain optimal thermal performance.

Blend composition

Based on the simulation results, a blend was prepared containing the following constituents:

MPCMs – 10% by weight

MWCNTs – 1% by weight

Water - 89% by weight

Preparation of the blend

A blend of MPCMs and MWCNTs with the above mentioned composition was prepared. The existing MPCM slurry of 11% concentration was allowed to settle down for a few days after which water and MPCMs had separated out. The water was drained out using a hand pump. This process was repeated till the desired concentration of the MPCM slurry was obtained. MWCNT fluid containing 1% MWCNTs by wt. and 0.25% of gum Arabic was prepared in required quantities. After mixing the MPCM slurry with MWCNT fluid, some more water had to be removed to obtain the exact blend composition.

The MPCM slurry and the MWCNT fluid were mixed together and heated for 30 minutes with the average temperature of the fluid reaching 30°C after the heating process. The mixture was continuously stirred using a magnetic stirrer during this process. This process created some kind of bonding (absorption) between the MPCM particles and the MWCNTs where the MWCNTs and MPCM separated out of water together after the mixture was allowed to settle down. The final blend composition was MPCMs-12%, MWCNTs-1.3% and Water-86.7%. The concentrations of the components were increased slightly to ensure that at least 1% of MWCNT would remain in the slurry during testing.

Based on visual observations, MWCNTs were completely absorbed by MPCM. It is suggested that the MPCM encapsulant material (gelatin) has a very high affinity for MWCNTs. After preparing the blend, its viscosity was determined, as well as heat transfer performance and pressure drop.

Viscosity results of the blend

The viscosity of the blend was measured using the Brookfield viscometer. More details about the instrument and the measurement procedure are given in chapter VI- "Measurement of thermal conductivity and viscosity". Viscosity was measured at four different temperatures and at several spindle rates (shears rates). The plots of viscosity vs. shear rate, % Torque vs. spindle rate and viscosity vs. temperature are presented below. Figure 8.1 shows the viscosity vs. spindle speed plot of the blend.

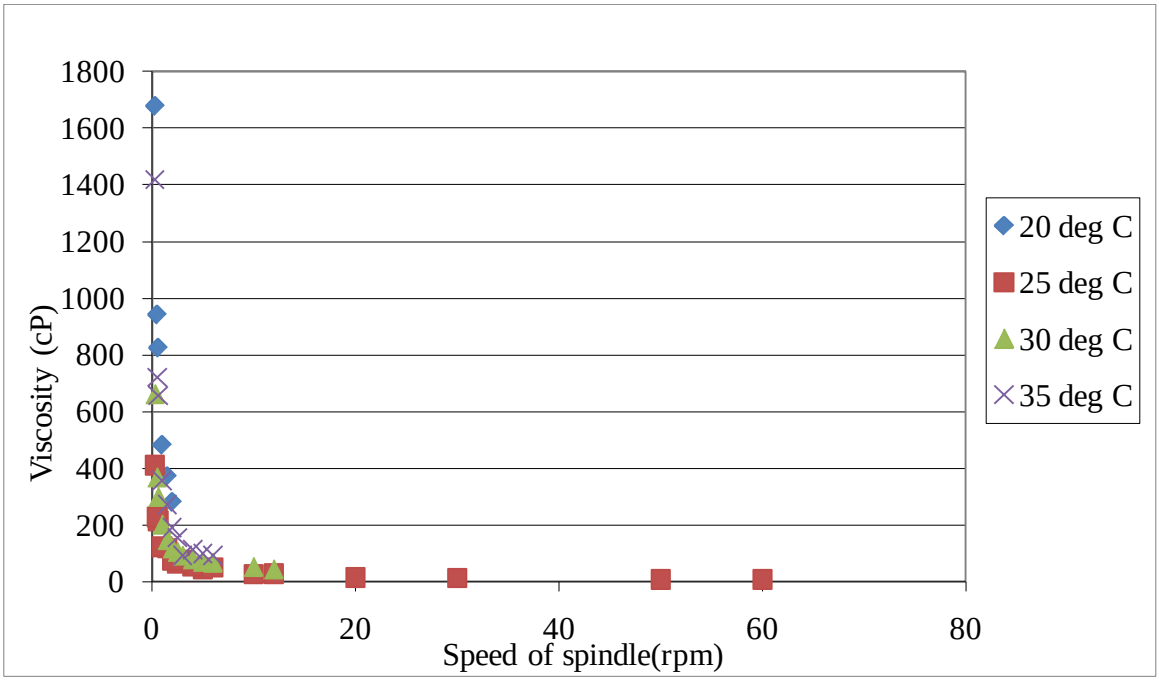

Figure 8.1: Viscosity vs. spindle speed of the MPCM and MWCNT blend

The blend exhibits a highly non-Newtonian behavior in the temperature range from 20 to 35 °C. A clear shear thinning behavior is exhibited by the blend. Viscosity vs. spindle speed plot has been plotted on the log-log chart to show the non-Newtonian

behavior more clearly. Figure 8.2 shows the log-log plot of viscosity vs. spindle speed of the blend, while Figure 8.3 shows the plot of % torque (shear stress) vs. spindle speed (shear rate).

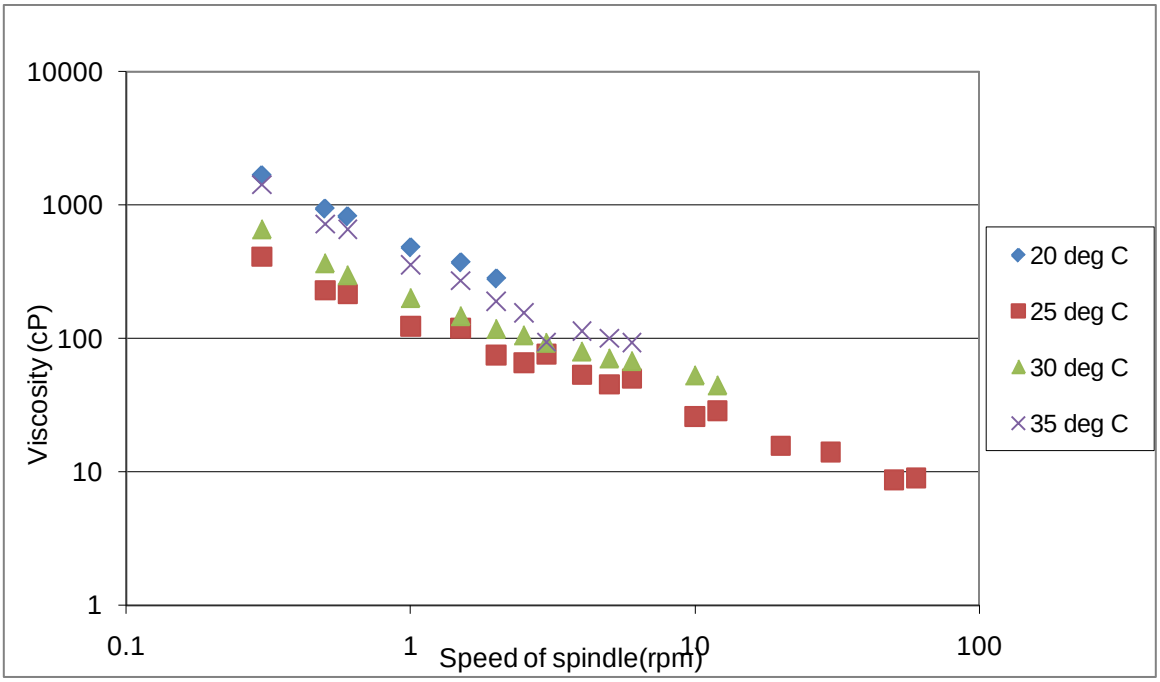

Figure 8.2: Log-log plot of viscosity vs. spindle speed of MPCM and MWCNT blend

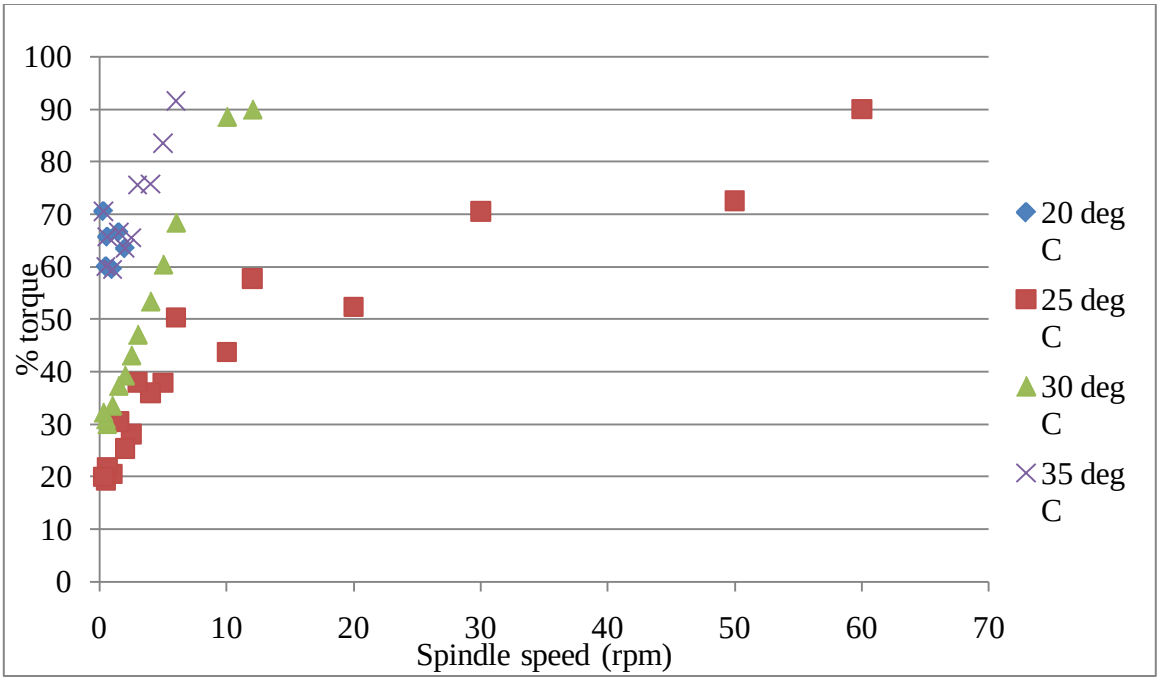

Figure 8.3: Plot of % torque vs. spindle speed of MPCM and MWCNT blend

a) Discussion of viscosity results

The blend of MPCMs (12%) and MWCNTs (1.3%) shows a strong shear thinning behavior. During the process of magnetic stirring, it is observed that the blend shows a thinning effect (similar to that of paint) while it appears as highly viscous slurry on standing. The viscosity of the blend reaches a minimum at the melting point of octadecane and increases thereafter as a function of temperature. This could be due to the reduced viscosity of MPCMs during the melting process. The increased viscosity of the blend at temperatures higher than the melting point could suggest some kind of bonding taking place between MPCM capsules and MWCNTs. The aggregation of

MPCMs and MWCNTs causes the viscosity to increase when the temperature is raised above that of the melting point of octadecane.

Heat transfer results of the blend

Heat transfer experiments were conducted at different heat flux values (different voltages) and different flow rates to study the heat transfer performance of the blend (MPCMs and MWCNTs). In order to compare the thermal performance of the blend with that of the MPCM slurry (11% concentration by weight), the maximum heat transfer coefficients obtained in each case are considered. These heat transfer coefficients are the maximum local heat transfer coefficients that are achieved due to phase change of MPCMs in each fluid. The value of the heat transfer coefficient of the blend reaches a maximum at the melting point of octadecane (26.09 °C) similar to that of the MPCM slurry. Irrespective of the operating conditions, maximum h was always achieved in the same temperature range of 25.5-26.5 °C.

Since the inlet temperatures were different for both MPCMs and the blend (the inlet temperatures had to be varied in order to achieve the phase change process in sections 4 and 5 which form the middle portion of the heat transfer loop), it became difficult to compare the heat transfer performance of the two fluids using the absolute values of their heat transfer coefficients at all the axial positions of the loop. Hence comparison is done based on the maximum local heat transfer coefficient value obtained in each case.

Figures 8.4, 8.5 and 8.6 compare the maximum value of heat transfer coefficient achieved for different flow rates of MPCM slurry (11% conc. by wt.) and the MPCM and MWCNT blend at heat flux values of q"=11.64 kW/m^2 (155 V), q" = 13.4 kW/m^2 and q" = 14.8 kW/m^2 respectively.

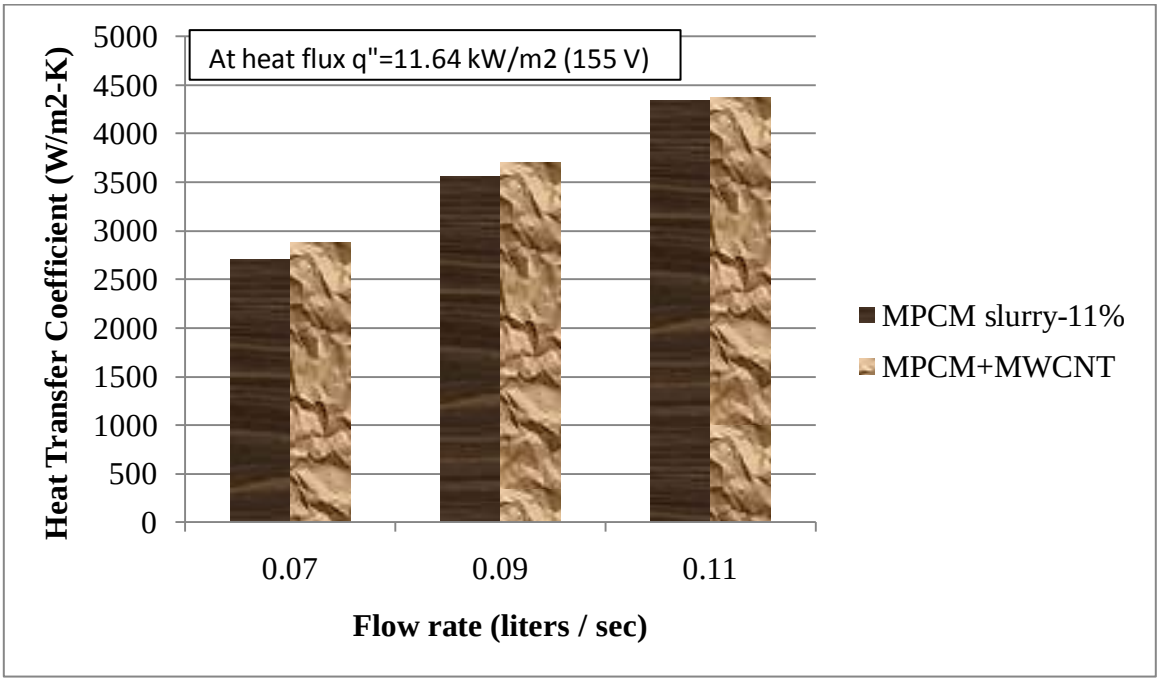

Figure 8.4: Comparison of maximum values of local heat transfer coefficient obtained in the case of MPCM slurry (11% conc. by wt.) and the blend for different flow rates at q"=11.64 kW/m^2

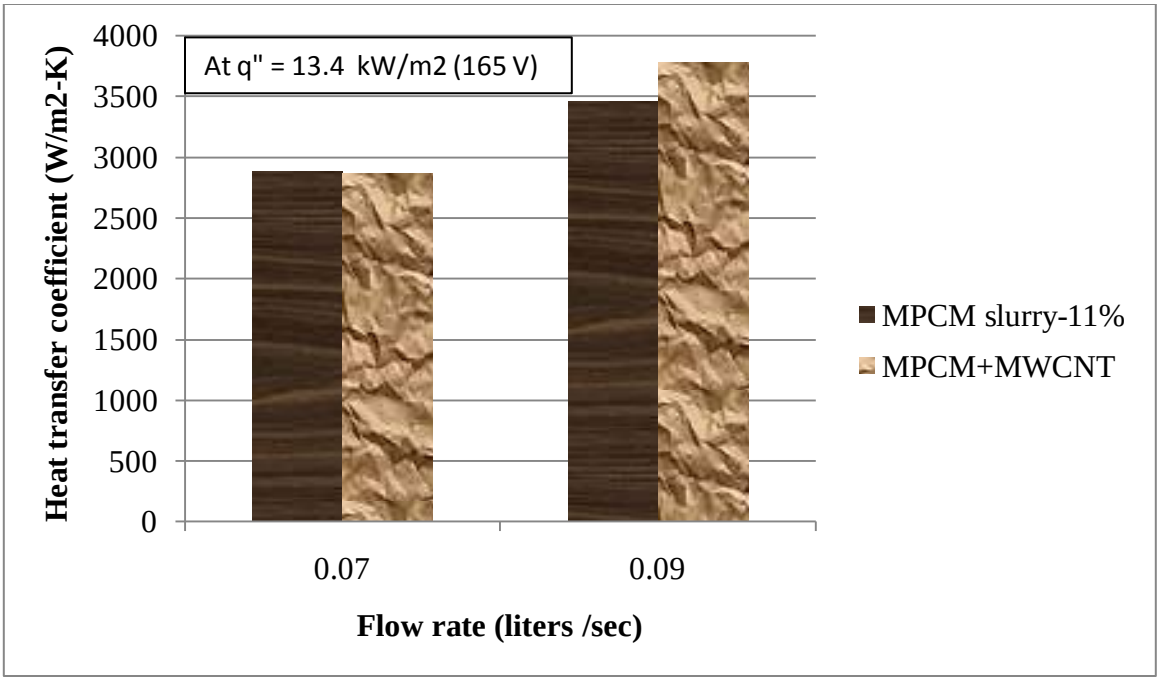

Figure 8.5: Comparison of maximum values of local heat transfer coefficient obtained in the case of MPCM slurry (11% conc. by wt.) and the blend for different flow rates at q"=13.4 kW/m^2

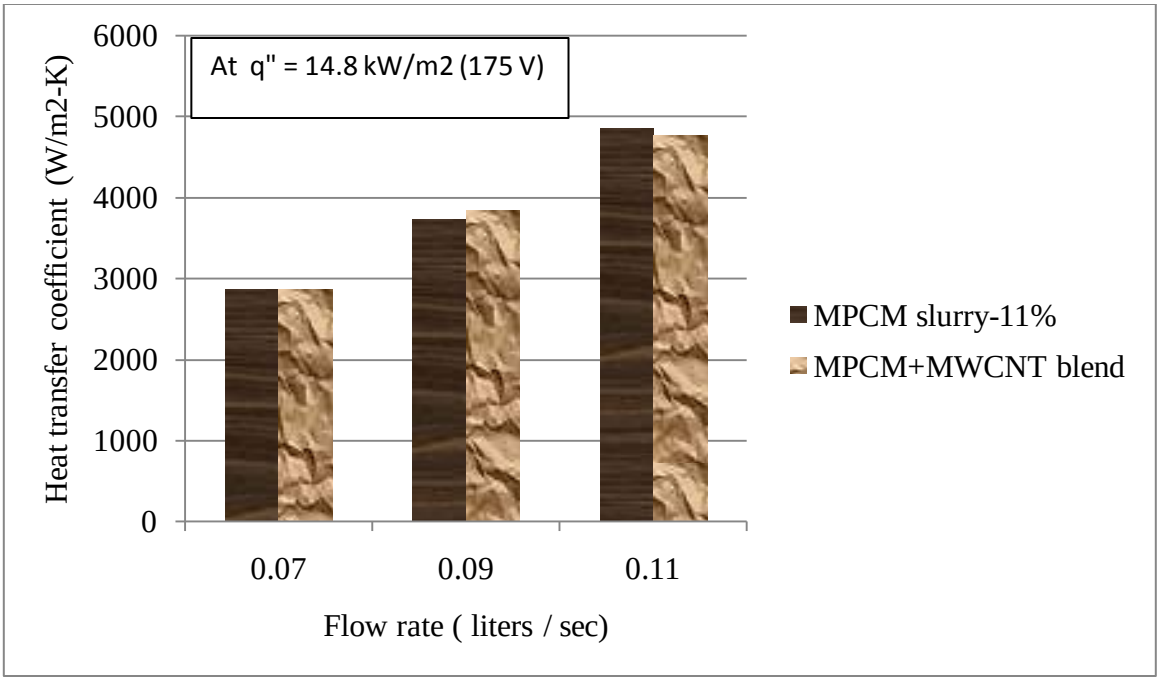

Figure 8.6: Comparison of maximum values of local heat transfer coefficient obtained in the case of MPCM slurry (11% conc. by wt.) and the blend for different flow rates at q"=14.8 kW/m^2

It can be observed from the above plots that:

1) at q"=11.4 kW/m^2, the maximum local heat transfer coefficient of the blend is always greater than that obtained in the case of MPCM slurry (11% conc. by wt) for all flow rates.

2) at q"=13.4 kW/m^2, the maximum local heat transfer coefficient value of the blend increases significantly when compared to that of MPCM slurry (11%) at the flow rate 0.09 l/s

3) at q"=14.8 kW/m^2, the maximum local heat transfer coefficient value is lower than that of the MPCM slurry at higher flow rates.

Figure 8.7 below plots the % enhancement in the maximum value of local heat transfer coefficient of the blend as compared to MPCM slurry (11% conc. by wt) at different heat flux values and different flow rates.

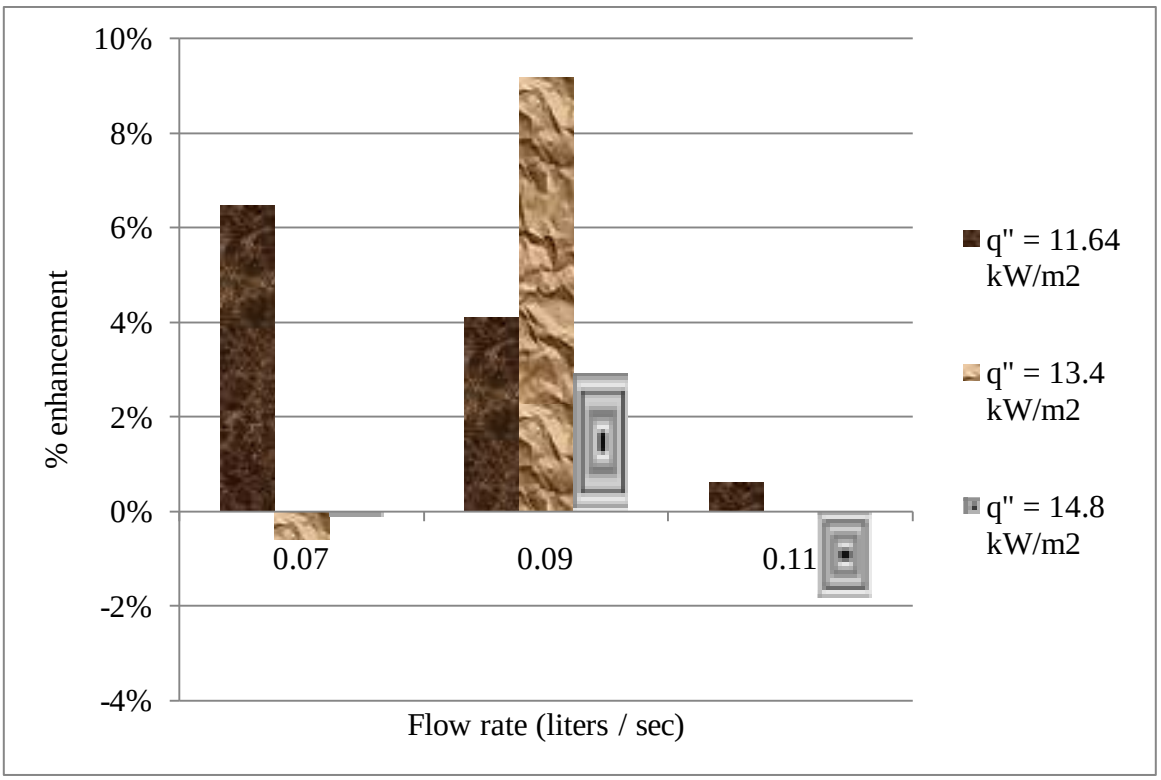

Figure 8.7: Percent enhancement in the maximum value of local heat transfer coefficient of the blend as compared to MPCM slurry (11% conc. by wt) at different heat flux values and different flow rates

From the above plot, we can conclude that

1) At lower flow rate, the percent increase decreases with increase in heat flux value

2) At a flow rate of 0.09 l/s, the percent increase varies from 3% to 9% at various heat flux values. This is the only flow rate, at which positive enhancement is seen for all the heat flux values.

3) At a higher flow rates, the percent increase is very small and becomes negative for increasing heat flux values.

Comparison of Reynolds number range for different heat transfer fluids

The Reynolds number ranges of different heat transfer fluids at a heat flux value of q"=15 kW/m^2 under different flow rates are compared in Table 8.1.

Table 8.1: Comparison of Reynolds number range for different heat transfer fluids

Flow rate (l/s)	Reynolds number range			
(q"=15.0 kW/m^2)	Water	MPCM slurry(11%)	MWCNTs (1.1%)	Blend of MPCMs and MWCNTs
0.07	8600-11600	3100-3700	~6300	~800
0.09	11000-14000	4000-4500	~8200	~1000
0.11	13000-16000	4800-5300	~10000	~1250

a) Conclusions from heat transfer tests

It is difficult to predict any particular trend in percentage enhancement of the maximum value of the local heat transfer coefficient of the blend. Looking at Table 8.1 which compares the Reynolds number range of different heat transfer fluids, it is clearly evident that the fluid flow structure of the blend of MPCMs and MWCNTs is no longer turbulent. The heat transfer results obtained for the blend are valid for the laminar flow regime of the blend.

Comparing the Re range of MPCM slurry and the blend, we can observe that while the blend flow is completely laminar, the MPCM slurry flow structure is turbulent. Though comparison of the maximum values of the local heat transfer coefficients of both the fluids may not yield accurate results, it is interesting to observe that the maximum values of the local heat transfer coefficient of the blend (laminar flow) is almost comparable to that of the MPCM slurry (turbulent) and in some cases, even exceeding the values for the MPCM slurry. The low enhancements in heat transfer coefficients of the blend are due to laminarization of the blend of MPCMs and MWCNTs by its highly viscous nature.

Pressure drop of the blend

The pressure drop of the blend was measured using pressure transducers during the heat transfer tests. The pressure drop data is tabulated in Table 8.2 below for different flow rates and heat flux values.

Table 8.2: Pressure drop data of the MPCM and MWCNT blend

Velocity (m/s)	Water (kPa/m)	MPCM slurry (11% by wt) (kPa/m)	MWCNTs (1% by wt.) kPa/m)	Blend (kPa/m)
0.75	0.9	1.0	5.2	3.7
0.97	1.3	1.5	6.1	4.2
1.16	1.8	2.1	6.6	5.0

The pressure drop of the blend increases with increase in velocity. The shear thinning behavior (i.e. lower viscosity at higher flow rate) has a direct effect on pressure drop when compared to the MWCNT fluid. The pressure drop is higher than that of water because of increased viscosity of the blend when compared to water. The pressure drop of the blend lies in between the values for MPCM slurry and MWCNT fluid. The high shear thinning behavior of the blend probably results in lower pressure drop when compared to MWCNT fluid which displays only slight shear thinning behavior.

CHAPTER IX

CONCLUSIONS AND RECOMMENDATIONS FOR FUTURE WORK

The conclusions for each heat transfer fluid are mentioned briefly below. Recommendations and scope for future work are also discussed later.

Microencapsulated phase change slurry

The heat transfer performance of the MPCM slurry investigated was in good agreement with the published literature. The MPCM capsules were durable and the super cooling was minimal. The MPCM slurry was Newtonian up to a concentration of 11%. Local heat transfer coefficients of the MPCM slurry increased due to the increase in apparent specific heat caused due to phase change. Effect of flow rate on the heat transfer coefficient was more significant than that of heat flux. Pressure drop of MPCM slurry was lower than that of water due to lower density in the former case.

Multiwalled carbon nanotube fluids

The thermal conductivity enhancement obtained for MWCNTs with diameter 60-100 nm and length (0.5-40μm) was 8.11%. The optimum time of ultrasonication was 10 minutes. The maximum % enhancement in heat transfer coefficient obtained reached a value of 20-25% (enhancement w.r.t. water). The CNT fluid showed a slight shear thinning behavior and the viscosity remained more or less constant in the selected

temperature range. The pressure drop of MWCNT fluid was significantly higher than that of water.

MPCM and MWCNT blend

The fluid flow structure of the blend of MPCMs and MWCNTs was no longer turbulent. The heat transfer results obtained for the blend are valid for the laminar flow regime of the blend. It is interesting to observe that the maximum values of the local heat transfer coefficient of the blend (laminar flow) is almost comparable to that of the MPCM slurry (turbulent) and in some cases, even exceeding the values for the MPCM slurry.

Due to the high viscosity of the blend, the flow structure has been laminarized completely. This resulted in lower heat transfer performance of the blend. The pressure drop of the blend lay in between the values for MPCM slurry and MWCNT fluid. The high shear thinning behavior of the blend probably resulted in lower pressure drop when compared to MWCNT fluid which displayed only slight shear thinning behavior.

Recommendations for future work

MPCMs with better durability characteristics and less super cooling behavior should be indentified for further research. The heat transfer potential of the MWCNT nanofluid looks promising. Further investigation needs to be taken up regarding the decrease in enhancement of heat transfer coefficient observed in the earlier sections of

the heat transfer loop. Also the mechanisms involved in heat transfer coefficient enhancement need to be understood more clearly.

For the blend of MPCMs and MWCNTs, future work must focus on improving the turbulence levels in the blend flow and determining the heat transfer performance under turbulent flow conditions. More experiments and analyses need to be done to determine the effect of variables such as Re, Pr, blend composition and viscosity on the heat transfer coefficient and pressure drop. Appropriate correlations should be developed after the effect of all the variables on the thermal performance of the blend has been studied and understood clearly. Future studies should also focus on the thermal performance of the MPCM-MWCNT blend in heat exchangers.

REFERENCES

[1] Alvarado, J.L., Marsh, C., Sohn, C., Phetteplace, G., and Newell, T. 2007. "Thermal Performance of Microencapsulated Phase Change Material Slurry in Turbulent Flow under Constant Heat Flux," International Journal of Heat and Mass Transfer, **50**(9)**,** pp. 1938–1952.

[2] Webb, R.L, and Eckert, E.R.G. 1972. "Application of Rough Surfaces to Heat Exchanger Design," International Journal of Heat and Mass Transfer, **15**(9), pp. 1647-1658.

[3] Winters, P.J., and Kooy, R.J. 1991. "Direct Freezing Ice Slurry District Cooling System Evaluation," International District Heating and Cooling Association, *Proceedings of 82nd Annual IDHCA Conference*, International District Energy Association, San Francisco, CA, pp. 381-398.

[4] Choi, S.U.S. 1995. "Enhancing Thermal Conductivity of Fluids with Nanoparticles," American Society of Mechanical Engineers, Fluids Engineering Division (FED) 231.

[5] Das, S K., Choi, S. U. S., and Patel, H.E. 2006. "Heat Transfer in Nanofluids—A Review," Heat Transfer Engineering, **27**(10), pp. 3-19.

[6] Wang, X.Q. and Mujumdar, A.S. 2008. "A Review on Nanofluids - Part II: Experiments and Applications," Brazilian Journal of Chemical Engineering **25**(4), pp. 631 – 648

[7] Buongiorno, J. and Zhou, S.Q. 2009. “A Benchmark Study on the Thermal Conductivity of Nanofluids,” Journal of Applied Physics, **106(**094312) pp. 1-14

[8] Garg, P, Alvarado, J.L., Marsh, C., Carlson, T.A., Kessler D.A., and Annamalai, K. 2009. “An Experimental Study on the Effect of Ultrasonication on Viscosity and Heat Transfer Performance of Multi-Wall Carbon Nanotube-Based Aqueous Nanofluids,” International Journal of Heat and Mass Transfer **52**, pp. 5090–5101

[9] Wen, D., and Ding, Y. 2004. “Effective Thermal Conductivity of Aqueous Suspensions of Carbon Nanotubes (Carbon Nanotube Nanofluids),” Journal of Thermophysics and Heat Transfer **18**(4), pp. 481-485.

[10] Zalba, B, Marín, J. M., Cabeza, L.F. and Mehling, H. 2002. “Review on Thermal Energy Storage with Phase Change: Materials, Heat Transfer Analysis and Applications,” Applied Thermal Engineering, **23**(3), pp. 251-283.

[11] Alvarado, J. L., Marsh, C., Sohn, C., Vilceus, M., Hock, V., Phetteplace, G., and Newell, T. 2006. “Characterization of Supercooling Suppression of Microencapsulated Phase Change Material by Using DSC,” Journal of Thermal Analysis and Calorimetry, **86**(2), pp. 505–509

[12] Yamagishi, Y., Takeuchi, H., Pyatenko, A.T. and Kayukawa, N.1999. “Characteristics of Microencapsulated PCM Slurry as a Heat-Transfer Fluid,” AIChE Journal **45**(4), pp. 696-707.

[13] Mulligan, J.C., Colvin, D.P. and Bryant, Y.G. 1996. “Microencapsulated Phase-Change Material Suspensions for Heat Transfer in Spacecraft Thermal Systems,” Journal of Spacecraft and Rockets **33**(2), pp. 278-284.

[14] Zeng, R, Wang, X., Chen, B, Zhang, Y, Niu, J, Wang, X, and Di, H .2009. "Heat Transfer Characteristics of Microencapsulated Phase Change Material Slurry in Laminar Flow under Constant Heat Flux," Applied Energy. Article in Press

[15] Roy, S.K., and Avanic, B.L. 2001. "Turbulent Heat Transfer with Phase Change Material Suspensions," International Journal of Heat and Mass Transfer **44**, pp. 2277-2285.

[16] Goel, M, Roy, S. K. and Sengupta, S. 1994. "Laminar Forced Convection Heat Transfer in Microencapsulated Phase Change Material Suspensions," International Journal of Heat and Mass Transfer, **37**(4), pp 593-604.

[17] Zhang, Y, Hu, X, and Wang, X. 2003. "Theoretical Analysis of Convective Heat Transfer Enhancement of Microencapsulated Phase Change Material Slurries," International Journal of Heat and Mass Transfer **40**, pp. 59-66.

[18] Inaba, H., Kim, M.J., and Horibe, A. 2004."Melting Heat Transfer Characteristics of Microencapsulated Phase Change Material Slurries with Plural Microcapsules Having Different Diameters," Transactions of the ASME. **126**, pp. 558-565.

[19] Assael, M. J., Chen, C.-F., Metaxa, I., and Wakeham, W. A. 2004. "Thermal Conductivity of Suspensions of Carbon Nanotubes in Water," International Journal of Thermophysics, **25**(4), pp. 971-985

[20] Xie, H., Lee, H., Youn, W., and Choi, M. 2003. "Nanofluids Containing Multiwalled Carbon Nanotubes and Their Enhanced Thermal Conductivities," Journal of Applied Physics. **94**(8), pp. 4967-4971.

[21] Ding, Y., Alias, H., Wen, D., and Williams, R.A. 2006. “Heat Transfer of Aqueous Suspensions of Carbon Nanotubes (CNT Nanofluids),” International Journal of Heat and Mass Transfer. **49**(1-2), pp. 240-250.

[22] Chen, L, Xie, H, Li, Y, and Yu, W. 2008. “Nanofluids Containing Carbon Nanotubes Treated by Mechanochemical Reaction,” Thermochimica Acta. **477**, pp. 21-24.

[23] Hwang, Y, Lee, J.K., Lee, C.H., Jung, Y.M., Cheong, S.I., Lee, C.G., Ku, B.C., and Jang, S.P. 2007. “Stability and Thermal Conductivity Characteristics of Nanofluids,” Thermochimica Acta. **455**, pp.70-74.

[24] Glory, J., Bonetti, M., Helezen, M., Mayne-L’Hermite, M., and Reynaud, C. 2008. “Thermal and Electrical Conductivities of Water Based Nanofluids Prepared with Long Multiwalled Carbon Nanotubes,” Journal of Applied Physics. **103**(094309) pp. 1-7.

[25] Wensel, J., Wright, B., Thomas, D., Douglas, W., Mannhalter, B., Cross, W., Hong, H., Kellar, J., Smith, P., and Roy, W. 2008. “Enhanced Thermal Conductivity by Aggregation in Heat Transfer Nanofluids Containing Metal Oxide Nanoparticles and Carbon Nanotubes,” Applied Physics Letters **92(**023110), pp. 1-3.

[26] Taherian, H., and Alvarado, J.L. 2010. “System Analysis of MPCM Slurry Enhanced with Carbon Nanotubes as Heat Transfer Fluid,” Submitted to ASHRAE Winter Meeting 2010, Orlando, FL.

[27] Wang, L., Lin, G., Chen, H. and Ding, Y. 2009. "Convective Heat Transfer Characters of Nanoparticle Enhanced Latent Functionally Thermal Fluid," Science in China Press. **52**(6), pp. 1744-1750.

[28] Moyno, Inc., 1996, *Moyno®500 Progressing Cavity Pumps::Bulletin 90 M*, Moyno, Inc, Springfield, OH.

[29] Wakeham, W.A., Nagashima, A. and Sengers, J.V., 1991, *Measurement of the Transport Properties of Fluids*, Blackwell Scientific Publications, Victoria, Australia.

[30] NIST Chemistry WebBook - NIST Standard Reference Database Number 69, 2009, U.S. Secretary of Commerce on behalf of the United States of America, http://webbook.nist.gov/chemistry

[31] Brookfield Engineering Labs, Inc., 2005, *More Solutions to Sticky Problems*, Brookfield, Middleboro, MA.

APPENDIX A

CALIBRATION OF THE HEAT TRANSFER LOOP

The heat transfer loop was calibrated using DI water under constant heat flux and turbulent flow conditions. Heat transfer experiments were conducted at different voltages and flow rates. Based on the data obtained from all the tests, correction factors for input power and heat transfer coefficient were determined. Surface thermocouples were also corrected based on the data gathered from the set of experiments. The bulk thermocouples were accurate enough and needed no correction. A detailed explanation of the experimental procedure and the calibration steps is explained below.

Resistance measurements

To achieve constant heat flux condition in each coil of the heat transfer loop, certain external resistances were added to each coil to compensate for the differences in the lengths and pipe resistances of each coil. This external resistances were needed only to achieve the constant heat flux condition and do not contribute to the heating of the fluid. Thus the total resistance of each coil is the sum of the pipe resistance and the external resistance. The total resistance and pipe resistance of each coil was measured using a digital multimeter. Instead of measuring the external resistance directly using a multimeter, we calculated it as a difference of the total and pipe resistances of the coil.

Since external resistances are quite small (close to the instrument's error range), measuring them indirectly introduces lesser amount of error into the calculation.

R_t– Total resistance of the pipe

R_p – Pipe resistance

$$R_e = R_t - R_p$$

where R_e - External resistance.

Current measurements

The voltage supplied to each set of pipe resistances and external resistances was fixed and can be read from the power meter. The power meter displays the total voltage, total current and total power supplied by each variable transformer. Since all the coils were connected in parallel, the voltage supplied to each of them was the same. The current to each coil can be calculated as below:

$$I = \frac{Volts}{R_t}$$

Power calculation

Though both external and pipe resistances were needed for achieving constant heat flux condition, it was only the pipe resistance that contributed towards heating of the fluid inside the heat transfer loop. Hence the power supplied to each coil can be calculated as follows:

$$P = I^2 R_p$$

The total power to each section is the sum of powers to each coil.

$$P_{section} = P_{coil,1} + P_{coil,2} + P_{coil,3}$$

Calculation of outer surface area

The length of each coil was measured using a measuring tape. The outer surface area of each coil was calculated as follows:

$$A_{coil} = \pi D_0 L_{coil}$$

where D_o is the outer diameter of the copper pipe of the heat transfer loop.

The length of each section was also measured using a measuring a tape. The outer surface area of each section was calculated as below.

$$A_{section} = \pi D_0 L_{section}$$

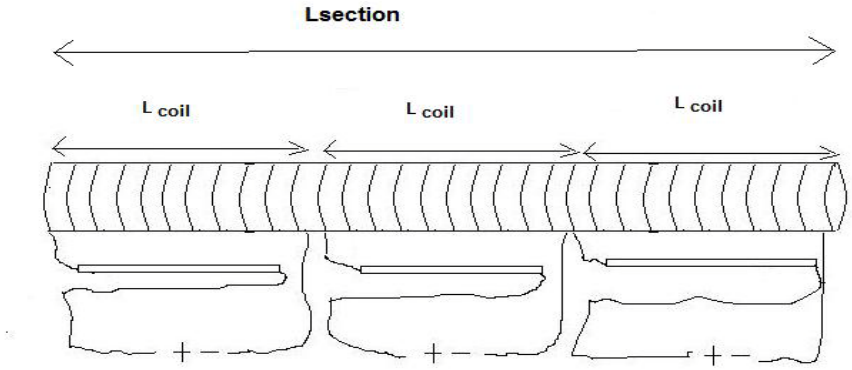

Figure A.1: Length of a coil and a section

Heat flux calculation

The heat flux of each coil was calculated by dividing the input power to each coil by the outer surface area of each coil.

$$q^{"} = \frac{P_{coil}}{A_{coil}}$$

Similarly the heat flux of each section is calculated as shown below.

$$q^{"} = \frac{P_{section}}{A_{section}}$$

Mass flow rate calculation

The mass flow rate of the heat transfer fluid was calculated by multiplying the volumetric flow rate (measured by the flow meter) by density of the fluid. All properties of fluid like density, specific heat, thermal conductivity and viscosity were measured at the average bulk temperature of the fluid. The average bulk temperature of the fluid was evaluated as follows:

$$T_{b,avg} = \frac{T_{b,inlet} + T_{b,outlet}}{2}$$

The properties of water were obtained from the NIST [30] tables at the bulk average temperature the fluid. The evaluation of properties for MPCMs, CNTs and the blend will be discussed in their respective chapters. Mass flow rate was calculated as follows:

$$\dot{M} = \dot{Q} \times \rho$$

$\dot{M}C_p\Delta T$ calculation

The specific heat value of water was looked up in the NIST [30] tables at the average bulk temperature of the fluid. The ΔT value was evaluated as follows:

$$\Delta T = T_{b,outlet} - T_{b,inlet}$$

$$\dot{M}C_p\Delta T = \dot{M} \times C_p \times \Delta T$$

Correction factors for input power

Not all the power input to each section actually contributed to the heating of the heat transfer fluid in the loop. There were always some heat losses that occurred in varying degrees in each section. To estimate the actual amount of power received by each section that went into heating the fluid inside, it was necessary to calculate the correction factors for input power.

$$Correction\ Factor_{section\ ,input\ \ power} = \frac{MC_p\Delta T}{P_{section}}$$

The correction factor for each section was found to be a value between 0.85 and 1.0. In order to compute the heat flux in each section, the total power to each section was multiplied by the correction factor and then divided by the outer surface area of the section. The correction factor was calculated for each section and not for every coil, since the bulk thermocouples were located at the start and end of every section, rather than for a coil.

For the case of DI water, the correction factors were computed for seven different cases involving two different voltages, 170 and 175 V and five different flow

rates, 0.06,0.07,0.08 0.09 and 0.1 liters per sec. Since the accuracy of the T type thermocouples was less than +/- 0.5 ℃, only those cases in which ΔT value was greater than 2 ℃ were considered. Thus seven cases were considered in total. The different cases and the values associated with each case are listed in Table A.1 below.

Table A.1: Correction factors for input power

Sno.	Case : 1	Case : 2	Case : 3	Case : 4	Case : 5	Case : 7	Case : 8	Average of all cases	Standard deviation	Relative deviation
Voltage:	170 V	170 V	170 V	170 V	175 V	175 V	175 V			
Flow rate:	0.1 l/s	0.09 l/s	0.08 l/s	0.07 l/s	0.09 l/s	0.07 l/s	0.06 l/s			
Correction Factors:										
Section 2	0.85	0.86	0.88	0.89	0.90	0.89	0.88	0.88	0.01	2%
Section 3	0.96	0.97	0.97	0.97	1.02	0.99	0.97	0.98	0.02	2%
Section 4	1.05	1.03	1.03	1.01	1.01	1.00	0.99	1.02	0.02	2%
Section 5	0.81	0.82	0.85	0.86	0.91	0.90	0.89	0.86	0.04	4%
Section 6	1.06	1.05	1.04	0.90	0.84	0.92	0.93	0.96	0.09	9%
Section 7	0.84	0.84	0.85	0.83	0.92	0.89	0.90	0.87	0.03	4%

The average of all the correction factors was taken for each section and they are summarized in Table A.2 below.

Table A.2: Average correction factors for input power

Section	**Average correction factor for input power (based on DI water data)**
2	0.88
3	0.98
4	1.02
5	0.86
6	0.96
7	0.87

Reynolds number

The Reynolds number of the heat transfer fluid is calculated as below:

$$Re = \frac{\rho \times V_{loop} \times D_i}{\mu}$$

where ρ is the density of the fluid (kg/m^3)

v_{loop} is the velocity of the fluid flowing in the loop which is calculated as follows.

v_{loop} = Volumetric flow rate/Inner cross sectional area of the pipe.

$$v_{loop} = \frac{\dot{Q}}{A_i}$$

D_i is the inner diameter of the copper pipe (m). Inner diameter of the pipe = 0.011 m

μ is the dynamic viscosity of the fluid (Pa.s)

Friction factor calculation

The friction factor for the copper pipe is calculated using the Colebrook equation which is given below.

$$f = \frac{0.25}{\left\{log\left(\frac{\varepsilon}{(3.7 \times D_i)}\right) + \left(\frac{5.74}{Re^{0.9}}\right)\right\}^2}$$

ε: Surface roughness

D_i: Inner diameter

Re: Reynolds number

Value of surface roughness is taken to be 3.2x10^{-6} m

Prandtl number

Prandtl number is the ratio of the thickness of hydrodynamic boundary layer to that of the thermal boundary layer. It represents the ratio of momentum transport to thermal transport.

$$Pr = \frac{\mu \times C_p}{k}$$

Nusselt number

The Nusselt number is calculated using the Gnielinski correlation for water:

$$Nu = \frac{\frac{f}{8}.(Re - 1000).Pr}{[1 + 12.7(f/8)^{1/2}(Pr^{2/3} - 1)]}$$

Correction factor for heat transfer coefficient

Although the correction factor for input power accounts for heat losses, there are several other factors to consider including the difference between the outer surface area where constant heat flux is applied, and inner surface area where convective heat transfer between the fluid and surface takes place. Other factors include, difference in surface roughness at different points of the copper pipe that contributed to errors in the heat transfer coefficient value. Hence a comparison was made between the experimental heat transfer coefficient value and the value obtained from the Gnielinski correlation and a correction factor was evaluated.

In the case of DI water, the correction factors were computed for seven different cases involving two different voltages, 170 and 175 V and five different flow rates, 0.06,

0.07, 0.08, 0.09 and 0.1 liters per second. The average of all the correction factors was taken for each section and they are summarized below. It is observed that the heat transfer coefficient obtained experimentally is under predicted when compared to the value obtained from the Gnielinski correlation because of the difference between inner and outer surface area, and friction factors. Thus the corrections were made accordingly for every section. The correction factors are shown in Table A.3 below.

Table A.3: Correction factors for heat transfer coefficient

Sno.	Case: 1	Case: 2	Case: 3	Case: 4	Case: 5	Case: 7	Case: 8	Average of all cases	Standard deviation	Relative devi--ation
Voltage:	170V	170 V	170V	170 V	175 V	175 V	175 V			
Flow rate:	0.1 l/s	0.09 l/s	0.08 l/s	0.07 l/s	0.09 l/s	0.07 l/s	0.06 l/s			
Section 2	0.71	0.73	0.76	0.78	0.75	0.78	0.81	0.76	0.03	5%
Section 3	0.78	0.80	0.81	0.83	0.80	0.83	0.85	0.81	0.02	3%
Section 4	0.85	0.85	0.86	0.87	0.83	0.85	0.87	0.85	0.01	2%
Section 5	0.65	0.67	0.71	0.74	0.75	0.77	0.79	0.73	0.05	7%
Section 6	0.85	0.86	0.87	0.77	0.67	0.78	0.81	0.80	0.07	9%
Section 7	0.69	0.71	0.72	0.73	0.77	0.77	0.78	0.74	0.03	5%

The average of all the correction factors for heat transfer coefficient in each section was computed and tabulated as shown in Table A.4 below:

Table A.4: Average correction factors for heat transfer coefficient

Section	Average Correction factor for heat transfer coefficient
2	0.76
3	0.81
4	0.85
5	0.73
6	0.80
7	0.74

Surface and bulk thermocouples calibration

Surface thermocouples were corrected based on the data gathered from heat transfer tests on water. The corrections were based on seven different tests involving two different voltages, 170 and 175 V and five different flow rates, 0.06, 0.07, 0.08, 0.09 and 0.1 liters per second. The surface temperatures were plotted and a linear trend was plotted for the temperatures using Excel. The differences between each surface thermocouple temperature and the corresponding temperature on the linear trend line were computed and tabulated as shown in Table A.5.

Table A.5: Surface thermocouple constants

Sno.	Case: 1	Case: 2	Case: 3	Case: 4	Case: 5	Case: 7	Case: 8	Average of all cases	Standard deviation of all cases
Voltage:	**170V**	**170 V**	**170 V**	**170 V**	**175 V**	**175 V**	**175 V**		
Flow rate:	**0.1 l/s**	**0.09 l/s**	**0.08 l/s**	**0.07 l/s**	**0.09 l/s**	**0.07 l/s**	**0.06 l/s**		
S12	0.57	0.58	0.62	0.76	0.71	0.74	0.79	0.68	0.09
S14	-0.10	-0.11	-0.11	-0.03	0.02	-0.06	-0.12	-0.07	0.05
S15	0.12	0.10	0.09	0.17	0.24	0.13	0.08	0.13	0.05
S21	-0.21	-0.22	-0.22	-0.16	-0.12	-0.19	-0.23	-0.19	0.04
S22	0.21	0.22	0.25	0.32	0.32	0.32	0.32	0.28	0.05
S23	-0.29	-0.31	-0.31	-0.28	-0.16	-0.25	-0.32	-0.28	0.05
S24	0.05	0.01	-0.02	0.00	0.09	0.01	-0.05	0.01	0.05
S25	0.55	0.53	0.58	0.56	0.66	0.63	0.58	0.58	0.05
S31	0.67	0.67	0.68	0.68	0.68	0.71	0.70	0.68	0.01
S32	0.22	0.22	0.24	0.23	0.13	0.20	0.22	0.21	0.04
S33	0.97	0.97	0.97	0.94	0.90	0.95	0.95	0.95	0.02
S34	-0.79	-0.77	-0.82	-0.86	-1.06	-0.98	-0.96	-0.89	0.11
S35	0.37	0.35	0.34	0.31	0.18	0.23	0.25	0.29	0.07
S41	-0.11	-0.08	-0.05	-0.09	-0.16	-0.08	-0.01	-0.08	0.05
S42	-0.82	-0.80	-0.79	-0.83	-0.88	-0.84	-0.76	-0.82	0.04
S43	-0.61	-0.59	-0.60	-0.67	-0.60	-0.62	-0.59	-0.61	0.03
S44	-0.48	-0.48	-0.50	-0.61	-0.50	-0.56	-0.56	-0.53	0.05
S45	-1.37	-1.36	-1.41	-1.51	-1.50	-1.52	-1.51	-1.45	0.07
S51	-1.45	-1.41	-1.41	-1.47	-1.65	-1.51	-1.42	-1.47	0.09
S52	0.17	0.19	0.19	0.08	0.10	0.17	0.24	0.16	0.06
S53	-0.10	-0.09	-0.12	-0.25	-0.25	-0.18	-0.15	-0.16	0.07
S54	0.43	0.44	0.40	0.29	0.36	0.40	0.44	0.39	0.05
S61	0.64	0.65	0.64	0.47	0.36	0.52	0.60	0.55	0.11
S62	0.64	0.66	0.66	0.49	0.34	0.54	0.65	0.57	0.12
S63	0.34	0.30	0.36	0.12	-0.05	0.08	0.14	0.18	0.15
S64	0.09	0.08	0.08	0.27	0.45	0.32	0.28	0.22	0.15
S65	-0.82	-0.82	-0.84	-0.68	-0.57	-0.70	-0.79	-0.75	0.10
S71	0.23	0.25	0.27	0.48	0.55	0.47	0.44	0.39	0.13
S72	0.19	0.21	0.19	0.39	0.53	0.37	0.30	0.31	0.13
S73	0.35	0.26	0.32	0.39	0.39	0.30	0.20	0.32	0.07
S74	0.33	0.34	0.33	0.50	0.51	0.38	0.30	0.38	0.08

After applying surface thermocouple constants to the thermocouple readings, the surface temperature readings follow the linear trend line quite accurately. Figure A.2 shows the surface thermocouple behavior before applying the surface thermocouple constants. Figure A.3 shows the behavior of thermocouples after applying the surface thermocouple constants.

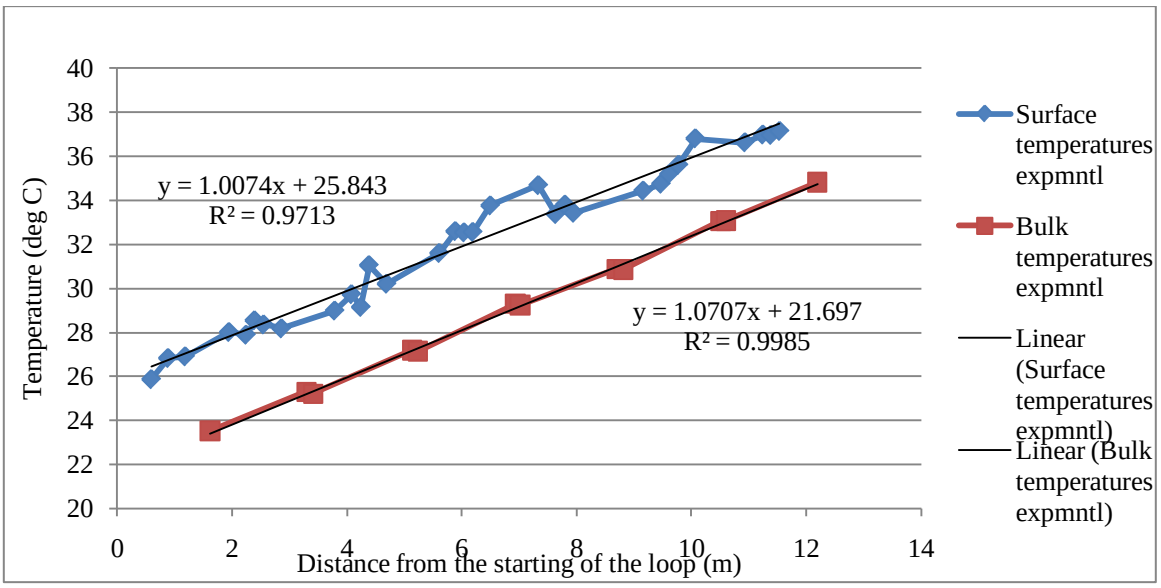

Figure A.2: Surface thermocouple behavior before applying surface thermocouple constants

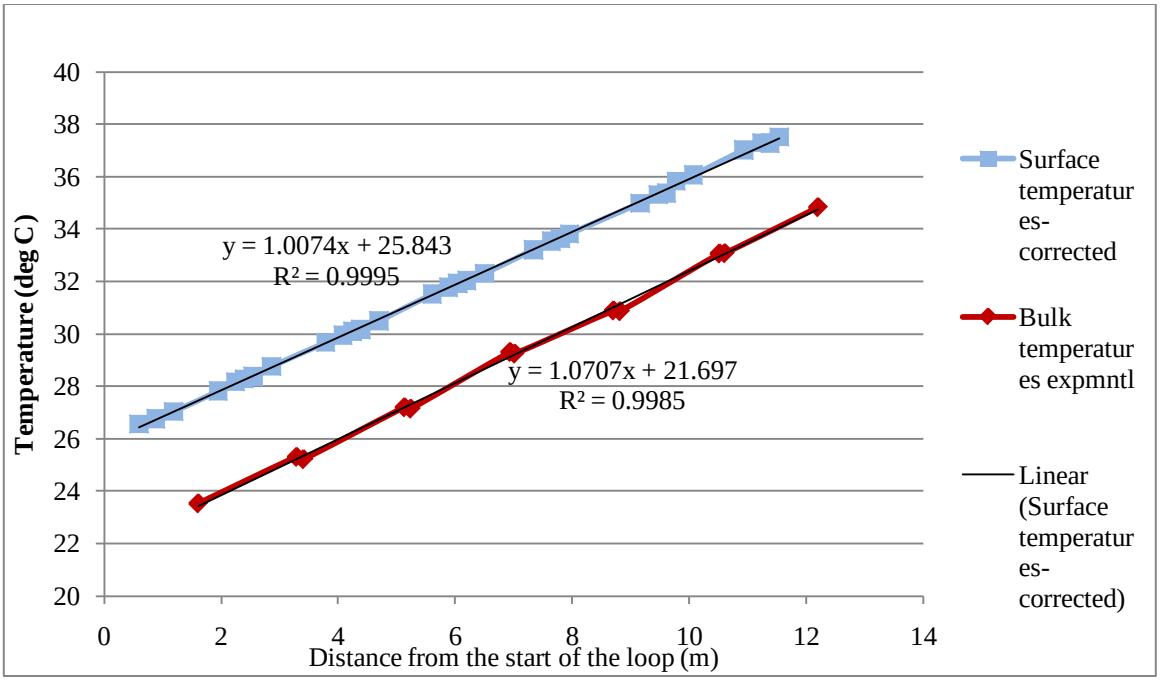

Figure A.3: Surface thermocouple behavior after applying surface thermocouple constants

The bulk thermocouples needed no correction since they followed the linear trend line quite closely. After the surface temperature corrections were made, heat transfer tests were conducted for water for different heat flux values and different flow rates. The deviation of the experimental heat transfer coefficient values from the values obtained from Gnielinski correlation are tabulated as shown in Table A.6 below:

Table A.6: Deviation of experimental heat transfer coefficient from the Gnielinski correlation value

Voltage (V)	**155**	**155**	**155**	**165**	**165**	**165**	**175**	**175**	**175**
Flow rate (l/s)	**0.07**	**0.09**	**0.11**	**0.07**	**0.09**	**0.11**	**0.07**	**0.09**	**0.11**
Section	**Deviation of experimental heat transfer coefficient from the Gnielinski correlation value**								
2	4%	-3%	-9%	3%	-4%	-8%	3%	-3%	-8%
3	7%	3%	0%	8%	3%	-1%	6%	2%	-4%
4	9%	4%	0%	3%	-1%	-3%	1%	-3%	-7%
5	2%	-3%	-8%	0%	-4%	-7%	0%	-3%	-8%
6	-1%	-5%	-8%	-1%	-4%	-7%	1%	-4%	-7%
7	-2%	-7%	-9%	-4%	-7%	-9%	-3%	-9%	-10%

The deviations of the experimental heat transfer coefficient values from the values obtained from Gnielinski correlation were within +/- 10 % for all the sections under all operating conditions.

Pressure transducer calibration

While conducting the calibration heat transfer tests on DI water, pressure drop data was also recorded simultaneously by the three pressure transducers installed on sections 2, 4 and 6. Based on the data gathered from the tests, the transducers were calibrated and correction constants were estimated for each transducer. The average correction constants are shown in Table A.7 below.

Table A.7: Pressure Transducer average correction constants

Pressure Transducer	**Pressure Transducer average correction constant (KPa/m)**
PT 1 (Installed on section 2)	-0.14
PT 2 (Installed on section 4)	-0.04
PT 3 (Installed on section 6)	-0.02

After applying the correction constants to the pressure drop readings, the pressure drop obtained was compared with the values obtained from the Darcy-Weisbach formula. Darcy-Weisbach formula for pressure drop is presented below.

$$\Delta P = f.\frac{L}{D}.\frac{\rho V^2}{2}$$

The deviations of pressure drop obtained experimentally from the pressure drop obtained from Darcy-Weisbach equation for different operating conditions are tabulated as shown below in Table A.8 below.

Table A.8: Percentage deviation of experimental value of pressure drop from the value obtained from Darcy-Weisbach equation

Velocity of fluid in the loop (m/s)	1.05	0.95	0.84	0.74
Pressure Transducer	% deviation of experimental value of pressure drop from the value obtained from Darcy-Weisbach equation			
PT 1	-2%	1%	-1%	4%
PT 2	-2%	1%	-1%	3%
PT 3	-1%	2%	-2%	1%

The above table shows that the deviation of the experimental pressure drop values from the values obtained from the Darcy-Weisbach equation is within +/- 5%.

APPENDIX B

Principle of transient method

As discussed earlier, in the case of transient methods, the temperature response of the fluid to an externally provided time dependent disturbance (in the form of heat flux) is measured. Generally, the heat flux to the fluid is provided by means of electrical dissipation in a long thin, cylindrical wire immersed in the fluid sample. The thin cylindrical wire represents an infinitely long, vertical line source of heat in the idealized case. The ideal line source of heat has zero heat capacity and infinite thermal conductivity. The fluid is assumed to be isotropic with the physical properties being independent of temperature and it is in thermodynamic equilibrium with the line source at time, t=0.

When a step wise heat flux, q per unit length is applied to the line source and if we assume that the transfer of energy from the line source to the fluid is entirely through conduction,

The temperature rise in the fluid at a distance r from the wire, at a time t can be given as:

$$\Delta T(r,t) = T(r,t) - T_o$$

Where T_o is the equilibrium temperature of the fluid. To obtain $\Delta T(r,t)$ we need a governing equation and a set of boundary conditions to solve for ΔT.

The governing equation is developed from the energy conservation equation as follows.

The energy conservation equation for a viscous, isotropic and incompressible fluid with temperature dependent properties can be written as follows:

$$\rho \frac{DU}{Dt} = -\nabla.\vec{Q} - P(\nabla.\vec{v}) - S:\nabla\vec{v}$$

Where U is the internal energy, t is the time, P the hydrostatic pressure, $\vec{v}$ is the hydrodynamic velocity of the fluid, S is the stress tensor, ρ is the density, and $\vec{Q}$ is the heat flux vector. The notation D/Dt represents the substantive derivative.

Assuming that the perturbation of the temperature is small and a local-equilibrium thermodynamic state exists, the above equation can be re written as:

$$\rho C_v \frac{DT}{Dt} - T\left(\frac{\alpha_P}{\kappa_T}\right)\left[-\alpha_P + \kappa_T \frac{DP}{DT}\right]\frac{DT}{Dt} = -\nabla.\vec{Q} + \varphi$$

Where C_v is the isochoric heat capacity, α_P is the isobaric expansion coefficient, κ_T is the isothermal compressibility and $\varphi = S:\nabla\vec{v}$ is the rate of internal energy increase owing to viscous dissipation. Transient techniques are operated so that $\kappa_T \frac{DP}{DT} << \alpha_P$. The equation is now re written as follows:

$$\rho C_P \frac{DT}{Dt} = -\nabla.\vec{Q} + \varphi$$

Further restrictions are applied to the above equation to bring it into a form for which a general solution is possible. They are as follows:

1) Temperature gradients should be small, so that a near equilibrium state is achieved.
2) Any fluid movement must be avoided so that $\vec{v}$ = 0 and hence $\varphi = 0$. It is very difficult to achieve this condition while applying temperature gradients, because

temperature gradients give rise to density variations in the fluid which in turn creates a state of motion in the fluid. This is natural convection. For this restriction to apply, the effect of convection should be reduced to a minimum if not eliminated completely. Under these conditions, the substantive derivative can be replaced by the partial derivative

$$\rho C_P \frac{\partial T}{\partial t} = -\nabla . \vec{Q} + \varphi$$

Heat flux vector can be written as

$$\vec{Q} = -\lambda \nabla T + \vec{Q}_r$$

where λ is the thermal conductivity and $\vec{Q}_r$ is the heat flux from radiation. Neglecting radiation effects,

$$\vec{Q} = -\lambda \nabla T$$

Therefore the governing equation that forms the basis of all transient methods of thermal conductivity measurement is as follows:

$$\rho C_P \frac{\partial T}{\partial t} = \lambda \nabla^2 T$$

To solve the above equation to get ΔT(r,t), a set of boundary conditions is developed which are as follows:

1) $\Delta T(r,t) = 0$ for $t <= 0$
2) $\lim_{r \to 0} \Delta T(r,t) = 0$ for $t > 0$
3) $\lim_{r \to 0} r \frac{\partial T}{\partial r} = -\frac{q}{2\pi\lambda} = \text{constant}$ for $t >= 0$
4) Thermal diffusivity $a = \lambda/\rho C_p$ is a constant

The solution of the governing equation is:

$$\Delta T_{id}(r,t) = -\frac{q}{2\pi\lambda} E_1\left(\frac{r^2}{4at}\right)$$

where $E_1(x) = \int_x^0 \frac{e^{-y}}{y} dy = -\gamma - ln + x + O(x^2)$

γ=0.5772157 …Euler's constant

For a cylindrical wire of radius r_o and for small values of $\frac{r^2}{4at}$ we get

$$\Delta T_{id}(r_o,t) = T(r_o,t) - T_o = \frac{q}{2\pi\lambda}\left[\ln\left(\frac{4at}{r_o^2 C}\right) + \frac{r_o^2}{4at} + \cdots\right]$$

C=exp(γ). If the wire radius is chosen such that the second term of the above equation is less than 0.01% of ΔT_{id} then the temperature rise of the wire can be given as:

$$\Delta T_{id}(r_o,t) = \frac{q}{4\pi\lambda}\ln\left(\frac{4at}{r_o^2 C}\right)$$

Where ΔT_{id} is the ideal temperature rise in the wire. The above equation is the fundamental working equation of the transient hot wire technique. Thermal conductivity of the fluid can be obtained from the slope of the line ΔT_{id} vs ln t and thermal diffusivity may be obtained from the intercept or from the absolute value of ΔT_{id} at a fixed time. There are many deviations in the actual transient hot wire when compared to that of an ideal one. Some of them are as follows:

1) A finite length metallic wire is used in an actual transient hot wire apparatus which also behaves as a resistance thermometer. Thus measured temperature rise of the wire departs from the ideal value even at the surface of the wire.

2) The wire used has a non zero radius, finite heat capacity and thermal conductivity
3) Finite outer boundaries exist for the fluid to be tested.
4) Radiative heat transfer effects
5) Variation of thermal conductivity and heat capacity per unit volume of ρCp of the fluid with temperature
6) Uncertainty in the measurement of resistance of the hot wire, resolution of the timing device, measurement of voltage to determine the heat flux in the wire all contribute to the error in the measurement of thermal conductivity of the fluid sample.
7) Tension in the wire and the end supports for the wire also form a source of error in the measurement of thermal conductivity.

All these factors can be corrected for by experimental means as well as by applying corrections to the results obtained. Experimental ways of correction include adjusting the length and thickness of the wire, measurement times and voltage adjustment for input heat flux.

KD2 Pro

For this research work, thermal conductivity of nanofluids was initially supposed to be measured by an instrument called KD2Pro Analyzer from Decagon Devices, Inc. The instrument works on the principle of the transient hot wire apparatus. The instrument has a probe of 60 mm length and 1.3 mm diameter. The KD2's sensor needle

contains both a heating element and a thermistor. The controller module contains a battery, a 16-bit microcontroller/AD converter, and power control circuitry. The instrument's accuracy is specified to be 5%. The algorithm for calculating the thermal conductivity is embedded in the microcontroller inside the probe. The data is measured continuously by the probe and the algorithm fits the data collected using a non linear least square procedure. The thermal conductivity values are displayed on the screen of the analyzer along with the correlation coefficient.

Working of KD2Pro

At the beginning of a measurement, the microcontroller waits for 30 seconds for temperature stability, and then applies a known amount of current for 30 seconds to a heater in the probe that has an accurately known resistance. The microprocessor calculates the amount of power supplied to the heater. The probe's thermistor measures the changing temperature for 30 seconds while the microprocessor stores the data. It then monitors the rate of cooling for 30 seconds. At the end of the reading, the controller computes the thermal conductivity using the change in temperature (ΔT) vs. time data. Thermal resistivity is computed as the reciprocal of thermal conductivity

Before measuring the thermal conductivity of the nanofluids, thermal conductivity of different fluids like water and propylene glycol aqueous solutions was measured using KD2Pro to verify its accuracy. Though the measured thermal conductivity values of water and propylene glycol solutions were in good agreement with the tabulated values at lower temperatures, the deviation increased significantly at

temperatures higher than 25 ° C. Different techniques were tried to improve the accuracy of the instrument at higher temperatures.

1) It was observed that the measurement with KD2Pro was extremely sensitive to the orientation of the needle inside the fluid. A slight inclination of the needle from its vertical position produced a large error. At higher temperatures, convective effects were also playing a role in producing errors in the measurement of thermal conductivity. To avoid convective effects and to hold the needle in its vertical position, a structure was designed out of Teflon disks supported with the help of plastic rods. The schematic of the structure designed is shown below:

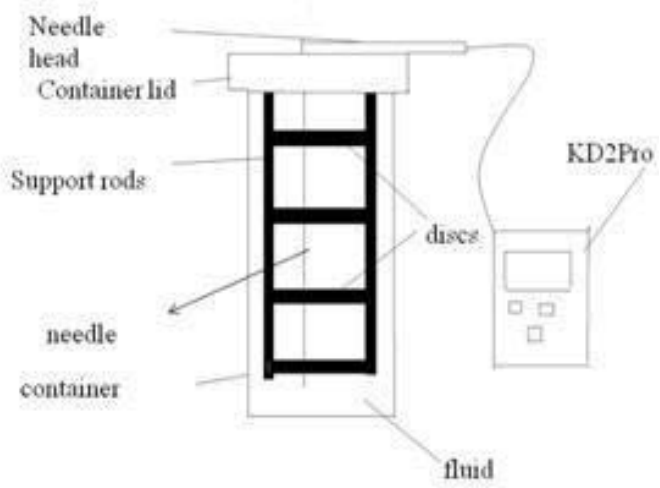

Figure B.1: Modification of KD2Pro

Though the accuracy of the instrument improved slightly, it was not sufficient to measure the thermal conductivity of nanofluids accurately.

2) Several other precautions were taken like avoiding vibrations during measurement by placing the instrument on an optical table and switching off the chiller during the measurement. But none of them yielded sufficient accuracy to KD2Pro to use it for measurement of thermal conductivity of carbon nanofluids. These findings are consistent with the observations outlined by Buongiorno et al.[7].

VITA

Kalpana Tumuluri received her Bachelor of Engineering degree in mechanical engineering from Osmania University in India. She entered the Master of Science program at Texas A& M University in August 2007. She received her master's degree in May 2010. Her research interests lie in areas of heat transfer and fluid mechanics.

Ms. Kalpana Tumuluri may be reached at Plot No: 41, Royal Enclave, Bowenpally, Secunderabad-500009. India. Her email id is: tumulurikalpana@yahoo.com